Utah State University
BINGHAM RESEARCH CENTER

BINGHAM RESEARCH CENTER

2025 TECHNICAL REPORT

Seth Lyman, PhD
Colleen Jones, PhD
John R. Lawson, PhD
Pamela Gardner, PhD
Trevor O'Neil
Loknath Dhar
Lisa Boyd
Justin Allred
KarLee Zager
Shalyn Drake
Michael Davies

Bingham Research Center
Utah State University
320 N Aggie Blvd
Vernal, UT 84078

DOCUMENT NUMBER: BRC_251112A
REVISION: ORIGINAL RELEASE
DATE: 21 NOVEMBER 2025

Acknowledgments

One of the main purposes of this document is to report on activities we have carried out with financial support from the Utah Legislature and Uintah Special Service District 1. We are grateful to these two entities for their ongoing support of our Uinta Basin air quality work. We have also received funding for our work from many other entities. In particular, we acknowledge Marc and Debbie Bingham, the namesakes of the Bingham Research Center, who provided initial funds to establish the Center and its facilities. We administer an endowment from Anadarko Petroleum Corporation that provides opportunities for students to research air quality in the Uinta Basin alongside full-time research scientists. Student recipients of those funds, as well as other students funded separately, were involved in the work presented here. Site access, electricity, and/or equipment at some of our monitoring stations were provided by the Utah Division of Air Quality, Scout Energy Partners, Koda Resources, and the Bureau of Land Management. Many energy companies have provided data and access to oil and gas facilities for our work. All funding sources are listed in the section entitled Performance Report, and funding sources for particular projects are acknowledged in the appropriate sections of this document.

Table of Contents

1. Introduction

1.1. Mission of the Bingham Research Center

The Bingham Research Center is a trusted leader in innovative research that advances science to serve our community through collaboration, education, and engagement.

1.2. Purpose of this Report

This report details the activities undertaken by the Bingham Research Center over the past twelve months. The report focuses on winter ozone research, as this is a core research area for the Center, and it serves as an annual report to the Utah Legislature and Uintah Special Service District 1, the primary funders of the Center's winter ozone research. The report also contains information about other projects funded by other entities, the Center's goals, and performance. This and past reports are available at https://www.usu.edu/binghamresearch/papers-and-reports.The Center's Management Plan is available at https://www.usu.edu/binghamresearch/files/UBAQR_management_plan.docx.

1.3. Background Information about Wintertime Ozone

Ozone negatively impacts respiratory health, especially for those with lung diseases. During wintertime temperature inversion episodes, ozone in the Uinta Basin sometimes increases to levels that exceed the standard of 70 ppb set by the U.S. Environmental Protection Agency (EPA). Because of this, portions of Uintah and Duchesne counties have been designated as federal ozone nonattainment areas.

The Uinta Basin is one of only two places in North America known to routinely experience wintertime ozone exceeding EPA standards (Wyoming's Upper Green River Basin is the other). Ozone forms in the atmosphere from reactions involving oxides of nitrogen (NO_X) and organic compounds, and the majority of NO_X and organic compound emissions in the Uinta Basin are from oil and gas development. Inversion conditions trap these pollutants near ground level, concentrating them and allowing them to generate ozone. The unique mix of pollutants during inversion episodes in the Uinta Basin leads to the formation of wintertime ozone, in contrast to the fine particulate matter ($PM_{2.5}$) pollution that is prevalent during winters on Utah's Wasatch Front.

The number of ozone exceedance days and concentrations of ozone that occur each year are closely tied to meteorology, though changes in emissions of organic compounds and NO_X also impact ozone levels. Years with persistent snow cover and high barometric pressure tend to have more days with strong winter inversions and high ozone. In the absence of snow cover and winter inversions, ozone concentrations in the Basin are similar to those in other rural, high-elevation locations around the western United States.

Because wintertime ozone is relatively new to science, some aspects of the meteorology, chemistry, and emissions that allow ozone to form during winter are still poorly understood. Federal and state agencies are required by law to promulgate regulations that reduce ozone-forming emissions in the Uinta Basin. These regulations will mostly target the local oil and gas industry, which contributes heavily to the Basin's economy. Scientific research to better elucidate the causes and characteristics of winter

ozone can help industry and regulators craft emissions reductions that maximize effectiveness and minimize costs to the local industry and economy. Since 2010, we (scientists at the Bingham Research Center) have conducted research to improve the understanding of winter ozone in the Uinta Basin.

A cumulative summary of all significant research findings that relate to Uinta Basin air quality from 2010 through the present is available here: https://www.usu.edu/binghamresearch/cumulative-research-summary.

2. Report of 2025 Performance

Author: Seth Lyman

This section provides information about our performance for 2025, including research outputs and achievement of goals and objectives as outlined in our management plan. Our management plan is available at https://www.usu.edu/binghamresearch/files/UBAQR_management_plan.docx.

2.1. Research Output

We report our research in presentations and academic publications, which make our findings available to other researchers, stakeholders, and the public. Listed below are our publications and presentations from November 2024 through October 2025. Not all are related to Uinta Basin Air Quality. All our peer-reviewed publications and significant technical reports are available on our website at: https://www.usu.edu/binghamresearch/papers-and-reports.

In the following lists, student authors are shown in **bold**.

2.1.1. Peer-reviewed Publications

1. Lawson J.R., Trujillo-Falcón J.E., Schultz D.M., Flora M.L., Goebbert K.H., Lyman S.N., Potvin C.K., and Stepanek A.J., 2025. Pixels and predictions: potential of GPT-4V in meteorological imagery analysis and forecast communication. Artificial Intelligence for the Earth Systems, 4, 240029.
2. Mansfield M.L. and Lyman S.N., 2025. Seasonal trends in the wintertime photochemical regime of the Uinta Basin, Utah, USA. Atmospheric Chemistry and Physics, 25, 11261-11274.
3. **Davies M.J.,** Lawson J.R., O'Neil T., Lyman S.N., **Zager K.**, and **Coxson T.D.**, 2025. Uinta Basin Snow Shadow: Impact of Snow-Depth Variation on Winter Ozone Formation. Air, 3, 22.
4. Jones C., O'Neil T., and Lyman S., 2025. Measurements of organic compound emissions from a produced water disposal vault. Journal of the Air & Waste Management Association, 75, 334-347.
5. **Lown L.**, Dunham-Cheatham S.M., Murray P., Lyman S.N., Carlson K.L., and Gustin M.S., 2025. Feasibility of Metal Oxide Glasses and Polymer Membranes as Sorbents for Gaseous Oxidized Mercury. ACS Omega. https://doi.org/10.1021/acsomega.5c05401.
6. Weiss-Penzias P.S., Lyman S.N., Elgiar T., Gratz L.E., Luke W.T., Quevedo G., Choma N., and Gustin M.S., 2025. The effect of precipitation on gaseous oxidized and elemental mercury concentrations as quantified by two types of atmospheric mercury measurement systems. Environmental Science: Atmospheres, 5, 204-219.
7. **Lown L.**, Dunham-Cheatham S.M., Lyman S.N., and Gustin M.S., 2024. Alternate materials for the capture and quantification of gaseous oxidized mercury in the atmosphere. *Atmospheric Measurement Techniques Discussions*, *2024*, pp.1-23.
8. **Flowerday C.E.**, Stanley R.S., Lawson J.R., Snow G.L., Brewster K., Goates S.R., Paxton W.F., and Hansen J.C., 2025. A ten-year historical analysis of urban PM10 and exceedance filters along the Northern Wasatch Front, UT, USA. Science of the Total Environment, 959, 178202.

2.1.2. Books, Reports, and Preprints

1. Lawson, J. R., 2025: A Probabilistic WxChallenge Proposal. arXiv [stat.AP], https://doi.org/10.48550/arXiv.2501.14139.
2. Lawson, J. R., 2024: Communicating risk with possibility, not probability. arXiv [stat.AP], https://doi.org/10.48550/arXiv.2410.21664.
3. Emery C., Tran H., Tran T., Lyman S., and Yarwood G., 2023, May. Comparing the Chemical Mechanisms CB6r5 and RACM2s21 for a Winter Ozone Episode in Utah. In International Technical Meeting on Air Pollution Modelling and its Application (pp. 137-145). Cham: Springer Nature Switzerland
4. Lyman S., Jones C., Lawson L., O'Neil T., Gardner P. (ed), 2024. 2024 Annual Report: Bingham Research Center. Utah State University, Vernal, Utah. https://www.usu.edu/binghamresearch/files/reports/2024AnnualReport.pdf
5. **Elgiar T.R.**, **Dhar L.**, Gratz L., Hallar A.G., Volkamer R., and Lyman, S.N., 2025. Underestimation of atmospheric oxidized mercury at a mountaintop site by the GEOS-Chem chemical transport model. EGUsphere, 2025, https://egusphere.copernicus.org/preprints/2025/egusphere-2025-977/.

2.1.3. Presentations

1. **Allred J.**, Cardon G., Jones C., November 2024. Wildfire Impacts on Erodibility and Soil Erosion Modeling. ASA-CSSA-SSSA Annual Meeting, San Antonio, Texas.
2. Lyman S.N, November 2024, March 2025, and August 2025. Uinta Basin Ozone Working Group update. Utah Division of Oil, Gas and Mining Collaborative Meeting, Duchesne, Utah.
3. **Davies M.J.**, Lawson J.R., January 2025. Snow Shadows, Data Sparsity, and AI Forecasts of Winter Ozone. 105th Annual American Meteorological Society Meeting, New Orleans, Louisiana.
4. Lawson J.R., January 2025. Communicating Hazard Risk as Possibility, not Probability. 105th Annual American Meteorological Society Meeting, New Orleans, Louisiana.
5. Lawson J.R., **Davies M.J.**, Lyman S.N., January 2025. Predicting Winter Ozone with Low-Complexity AI. 105th Annual American Meteorological Society Meeting, New Orleans, Louisiana.
6. **Zager K.**, Lyman S.N., O'Neil T., **Holmes B.**, **Holmes M.**, **Coxson T.**, March 2025. Effects of snow type, sunlight, and temperature on fluxes in organic air emissions and snow absorption. Air Quality: Science for Solutions, Logan, Utah.
7. Lawson J.R., March 2025. Clyfar: an unorthodox solution to unreliable Uinta Basin ozone forecasts. Air Quality: Science for Solutions, 9th Annual Conference, Logan, Utah.
8. **Dhar L.**, Lyman S.N., March 2025. Investigating the role of carbonyl compounds in winter ozone formation in Utah's Uinta Basin using box model simulations. Air Quality: Science for Solutions, Logan, Utah.
9. **Coxson T.**, Lyman S.N., March 2025. Methane emissions in the Uinta Basin: How do oil and gas production affect methane emissions? Air Quality: Science for Solutions, Logan, Utah.
10. **Davies M.**, Lawson J.R., March 2025. sensitivity of ozone formation to snowfall variations in the Uinta Basin, Utah. Air Quality: Science for Solutions, Logan, Utah.
11. O'Neil T., Lyman S., Jones C., March 2025. Building instrumentation for atmospheric mercury. Air Quality: Science for Solutions, Logan, Utah.
12. **Coley J.**, Haskins J., Lyman S., Jones C., Hansen J., Thalman R., March 2025. Verification of Atmospheric Mercury Redox Rates. Air Quality: Science for Solutions, Logan, Utah.

13. **Boyd L.**, Jones C. P., March 2025. A Cost-benefit Analysis of Cattail (Typha spp.) Treatments at Stewart Lake in Jensen, Utah. USU Spring Research Conference, Logan, Utah.
14. Lawson J.R., **Montague E.C.**, **Davies M.J.**, Lyman S.N., O'Neil T., March 2025. Updates to the USU UBAIR website: communicating forecast risk of elevated ozone. Air Quality: Science for Solutions, Logan, Utah.
15. **Allred J.**, Cardon G., Jones C., March 2025. Wildfire Impacts on Erodibility and Soil Erosion Modeling. CAAS Graduate Research Day, Utah State University, Logan, Utah.
16. **Davies M.J.**, Lawson J.R., April 2025. Sensitivity of Ozone Formation to Snowfall Variations in the Uinta Basin, Utah. Utah State University Statewide Student Research Symposium, Vernal, Utah.
17. **Zager K.**, **Davies M.J.**, April 2025. Clearing the Air: Evaluating the Impact of EPA Mobile Emission Standards on Carbon Monoxide Levels Across the United States. Utah State University Statewide Student Research Symposium, Vernal, Utah.
18. **Allred J.**, Cardon G., Jones C., April 2025. Wildfire Impacts on Erodibility and Soil Erosion Modeling. Plant, Soil, and Climate Annual Student Showcase. Logan, Utah.
19. Lyman S.N., May 2025. Stakeholder-engaged Air Quality Research in the Uinta Basin. The Utah Conference on Community Engagement, Price, Utah.
20. Lyman S.N., **Coxson T.**, June 2025. Trends in Uinta Basin-wide methane emissions. Uinta Basin Ozone Working Group, Vernal, Utah.
21. Lawson J., July 2025. Artificial Intelligence in the Uinta Basin. Vernal Area Chamber of Commerce, Vernal, Utah.
22. **Allred J.** et al., August 2025. QANR Graduate Student Orientation Panel. College of Agriculture and Natural Resources Orientation, Logan, Utah.
23. Lyman S.N., Colclasure, C., Vance S., Liang J., Natchees M., September 2025. Air quality panel at the Uintah Basin Energy Summit, Vernal, Utah.
24. Jones C.P., Drake S., September 2025. Drones in Ag Workshop – Stewart Lake State Waterfowl Management Area. Jensen, Utah.
25. Lyman S.N., September 2025. Invited Panelist for the Traditional Energy Landscape session of the 2025 Utah Energy Week Meeting, Salt Lake City, Utah.
26. Jones C.P., September 2025. Invited Panelist for the Geothermal Energy session of the 2025 Utah Energy Week Meeting, Salt Lake City, Utah.
27. Jones C.P., Drake S., October 2025. Drones in Research and flight simulation. STEAM Expo, USU-Uintah Basin, Roosevelt, Utah.

2.2. Media Appearances

The following are news articles from the reporting period that mention our work. A complete list of media mentions of our research is available at: https://usu.box.com/s/5s0busf524npd935mqfecsnvhn4cep52.

1. 2025. A change in EPA leadership might let Uinta Basin polluters off the hook. Utah Public Radio.
2. 2025. Despite ozone reductions, Uinta Basin air polluters still have work to do. Utah Public Radio.
3. 2025. Can Colorado Recycle Toxic Water from Oil and Gas Drilling Without Increasing Emissions? Inside Climate News.
4. 2025. USU Herbarium houses Uintah Basin's unique flora. USU Today.

5. 2025. USU Researcher Seth Lyman Named to Utah Air Quality Board. USU Today, BasinNow.com.
6. 2025. Statewide Campuses Students Present Research in Synchronized Symposium. USU Today.
7. 2024. Ozone Alert Program Underway For The Season; New Website To Replace UBAIR. BasinNow.com
8. 2024. USU's Science Unwrapped Asks 'AI Is Innovative, but Can We Trust It?' Friday, Nov. 15. USU Today.

2.3. Funding

2.3.1. Previous Twelve Months

The Bingham Research Center received $484,092 in grants and contracts, $47,000 in gifts, $400,000 in appropriations from the Utah Legislature, and $27,238 in endowment disbursements in the past 12 months, for a total of $958,330 (Table 2-1). Further, two grants from the U.S. Department of Energy are approved and pending funding. If these are funded, they will total an additional $1,181,039. The Uintah Special Service District provides $250,000 annually to support the air quality work of the Bingham Research Center.

Table 2-1. Funding received by the Bingham Research Center in the past twelve months.

Project	Funder	Type	Start	End	Amount
Uinta Basin Ozone Study	Uintah Special Service District 1	Contract	2025	2025	$250,000
Web tools to help land managers assess emissions from oil and gas wells	Utah Public Lands Initiative	Grant	2025	2026	$58,886
Precision Drone Technology for Sustainable Invasive Species Management and Herbicide Reduction at Stewart Lake	Utah Public Lands Initiative	Grant	2025	2027	$59,598
Formaldehyde analysis for air quality research in the Uinta Basin	Marriner S. Eccles Foundation	Gift	2025	2025	$47,000
Supplemental funding for: Verification of Atmospheric Mercury Redox Reaction Rates	U.S. National Science Foundation	Grant	2025	2027	$115,608
Uinta Basin Air Quality Study	Utah Legislature	Appropriation	2025	2026	$400,000
Anadarko student research endowment	Anadarko Petroleum	Endowment disbursement	2025	2026	$ 27,238
Methane Measurement and Mitigation—Subaward--IBM	Department of Energy	Grant (Approved, Pending funding)	2025	2028	$697,522
Carbon Management and Community Engagement—Subaward—University of Utah	Department of Energy	Grant (Approved, Pending Funding)	2025	2028	$482,517

2.3.2. All Funding to Date

We have received $15,909,414 in funding between 2011 and the present, including $11,855,039 in funding for research specifically related to Uinta Basin Air Quality. Figure 2-1 shows the funding we have received, organized by year and type of funding source. In the figure, funds are assigned to the year they were first awarded, not the years in which they were spent.

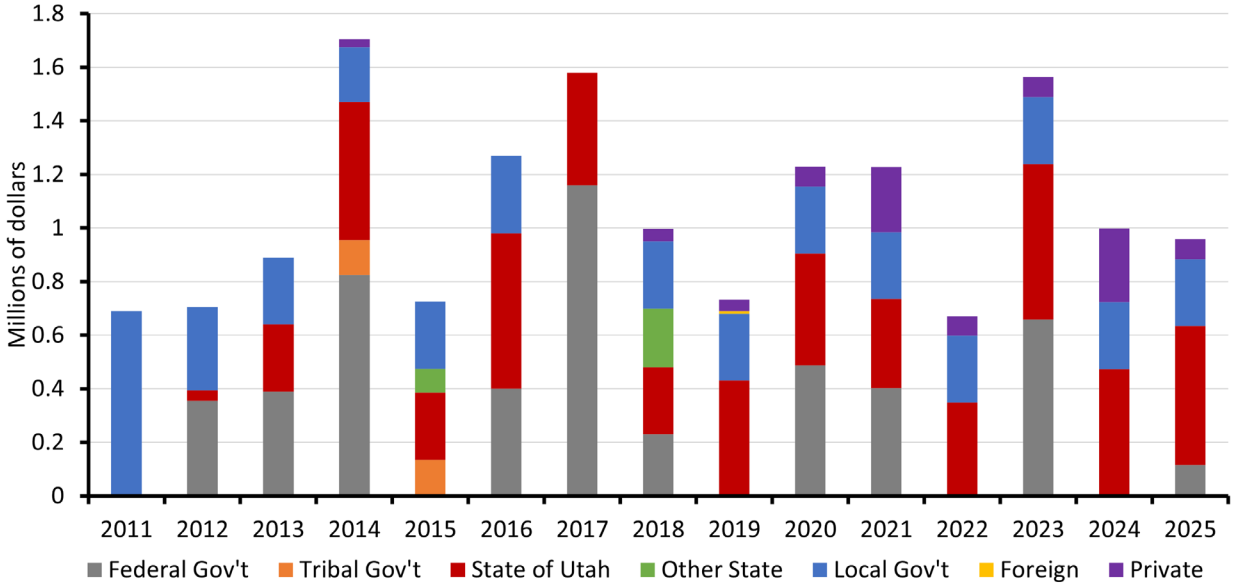

Figure 2-1. Funding awarded to our research group from 2011 to the present, categorized by type of funding source. For grants and contracts, the entire amount of funding awarded is shown in the first year of the award, even though funds may have been spent in subsequent years.

Figure 2-2 shows a breakdown of our team's total funding since 2011 by source type. 32% of our funding has come from federal government sources. 34% came from the state of Utah. 25% has come from local government (government entities within Uintah County). 2% and 2% have come from the Ute Indian Tribe and the State of Wyoming, respectively. 6% has come from private companies, and less than 0.1% has come from foreign entities.

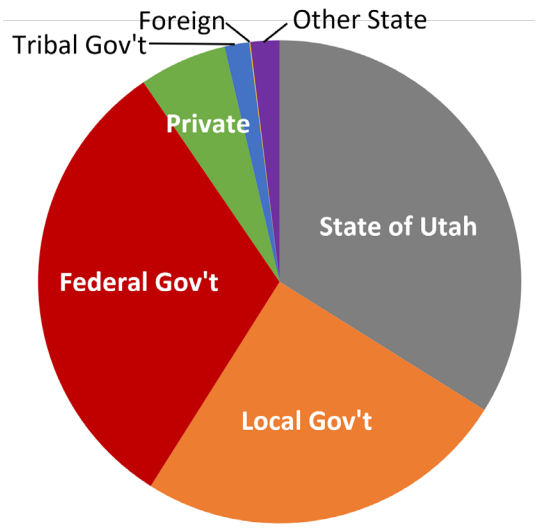

Figure 2-2. All funding sources for our research team from 2011 to the present.

Figure 2-3 shows a breakdown of funding for work specifically for projects related to Uinta Basin air quality. Compared to our research funding as a whole, a greater portion of our winter ozone-specific

research has come from the state of Utah (42%) and local government (34%), while less has come from federal government agencies (15%).

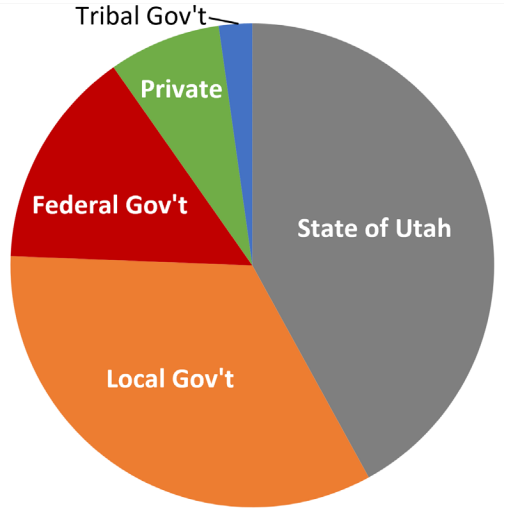

Figure 2-3. Sources of funding for our research team for Uinta Basin air quality projects from 2011 to the present.

Since our inception, we have received funding from the following entities, ranked in order of the total amount of funding received (endowment disbursement, rather than original endowment gift amount, is used in the case of Anadarko Petroleum:

- Uintah Special Service District 1
- Utah Legislature
- National Science Foundation
- Department of Energy
- USTAR
- Utah Division of Air Quality
- Department of Defense
- Bureau of Land Management
- State of Wyoming
- Ute Indian Tribe
- USTAR Energy Research Triangle
- Energy companies
- Anadarko Petroleum
- PacifiCorp
- Utah Division of Wildlife Resources
- Utah Public Lands Initiative
- Marriner S. Eccles Foundation
- National Oceanic and Atmospheric Administration
- SITLA
- Chevron Refinery
- Marc C. & Deborah H. Bingham Foundation

- Deseret Power
- Utah Governor's Office of Economic Development
- Environmental Protection Agency
- Dominion Energy
- UCAIR
- Mining company
- Big West Oil
- Nanjing University
- TriCounty Health
- Picoyune

2.4. Student Involvement and Training

A generous endowment from Anadarko Petroleum Corporation provides funds for students to participate in Uinta Basin air quality research (https://www.usu.edu/binghamresearch/student-fellowship). The following is a list of the students who have benefited from this program and other sources of funding for student research during the reporting period.

- Loknath Dhar has worked with us since May 2023. He is a PhD student in USU's Chemistry and Biochemistry Department in Logan. Loknath is researching the chemical pathways that lead to secondary formaldehyde formation during wintertime ozone episodes and how chemical mechanisms used in photochemical models represent those pathways. He is also working to improve 3D photochemical models of wintertime ozone.

- KarLee Zager has worked with us since August 2023. KarLee is pursuing a bachelor's degree at the USU Vernal Campus. She is involved in ozone measurement, characterizing organic

compound emissions from snow, and development and testing of atmospheric mercury instrumentation.

- Justin Allred worked with the Bingham Research Center as an undergraduate and is now pursuing a PhD in Soil Science with Colleen Jones. He is using drone-based multispectral imaging to evaluate the effectiveness of wildfire reclamation techniques.

- Lisa Boyd is pursuing a PhD in Ecology with Colleen Jones and is employed at the Vernal office of the Bureau of Land Management. She is studying the life cycle of endangered plants and ecological reclamation.

- Michael Davies has worked with us since 2024. He is an undergraduate student at the USU Vernal Campus and is working on meteorological data analysis.

- Tristan Coxson graduated in 2025 from Uintah High School. He started working with us in early 2024 on laboratory analysis and instrumentation.

- Myka Hansen is a junior at Uintah High School. She started working with us in early 2025 on laboratory analysis, instrumentation, and modeling.

- Luke Neilson is a senior at Uintah High School. He started working with us in early 2025 on data analysis and coding projects.

2.4.1. All Students and Postdoctoral Researchers

The following students and postdoctoral researchers have worked at the Bingham Research Center. Dates shown represent the first year of work at the Center.

1. Emily Smith, undergraduate, 2012
2. Chad Mangum, undergraduate, 2013
3. Cathy Crawford, undergraduate, 2013
4. Jordan Evans, undergraduate, 2013
5. Trevor O'Neil, undergraduate, 2013
6. Trang Tran, postdoctoral researcher, 2013
7. Huy Tran, postdoctoral researcher, 2014
8. Colleen Jones, postdoctoral researcher, 2015
9. Cody Watkins, master's student, 2014
10. Tate Shorthill, undergraduate, 2014
11. Tanner Allen, undergraduate, 2014
12. Lena Morgan, undergraduate, 2015
13. Felito Martinez, undergraduate, 2015
14. Sheree Meyer, graduate, 2015
15. Eric Hacking, undergraduate, 2016
16. Sandra Young, undergraduate, 2017
17. Justin Allred, undergraduate and graduate, 2017
18. Makenzie Holmes, undergraduate, 2018
19. Tyler Elgiar, undergraduate and graduate, 2018
20. Krystal White, undergraduate, 2019
21. Brant Holmes, undergraduate, 2020
22. Keirra Tolbert, undergraduate, 2021
23. Jackson Liesik, undergraduate, 2021
24. Davis Smuin, undergraduate, 2021
25. Lisa Boyd, graduate, 2022
26. Kristin Miller, undergraduate, 2023
27. Rachel Merrell, undergraduate, 2023

28. Loknath Dhar, graduate, 2023
29. KarLee Zager, undergraduate, 2023
30. Sam Dupaix, undergraduate, 2024
31. Michael Davies, undergraduate, 2024
32. Elspeth Montague, high school, 2024
33. Tristan Coxson, high school, 2024
34. Ambria Migliori, undergraduate, 2024
35. Myka Hansen, high school, 2025
36. Luke Neilson, high school, 2025

2.5. Data Management and Dissemination

2.5.1. Data Management

As described in our management plan, all measurement data and notes generated during the reporting period are stored on a cloud-based data storage server, with regular backups to local, removable hard drives. We stored all instrument maintenance, calibration, and repair information within this archival structure. We used established standard operating procedures for our work. These are publicly available at https://www.usu.edu/binghamresearch/team_pages/standard-operating-procedures.

2.5.2. Data Dissemination

We have uploaded the winter ozone dataset for the most recent winter and an updated air chemistry and meteorology dataset for the Roosevelt, Castle Peak, and Horsepool monitoring stations to the data access page of our website, https://www.usu.edu/binghamresearch/data-access. We have updated speciated organic compound data on the same web page.

During the year, we provided meteorological and chemical datasets to regulators, environmental consultants, and energy companies for use in their own analyses.

2.6. Outcomes from Annual Air Quality Project Objectives

We established project objectives for the current reporting period (November 2024 through October 2025) in 2024. They can be found at https://www.usu.edu/binghamresearch/files/annualplans/2025_SSD1_proposal.pdf. In Table 2-2, we report on progress toward those objectives and any discrepancies between planned work and actual outcomes.

Table 2-2. Outcomes of annual air quality project objectives for the current reporting period.

OBJECTIVE	OUTCOMES
Air Chemistry and Meteorology	
Operate air quality monitoring stations	We completed this objective for winter 2024-25. We will continue operation of these stations for the coming winter.
Continue Investigation of Carbonyl Fluxes at	Measurements for this objective are complete, and analysis of the data obtained is complete. This report contains a section highlighting key

OBJECTIVE	OUTCOMES
the Air-snow Interface	results from this project. We are currently preparing a peer-reviewed publication for this project.
Investigate Ozone Formation in Summertime Wildfire Smoke	We have developed an air chemistry box model to simulate ozone formation during smoke events at Roosevelt, but we have not yet completed analysis of the results or the model, and we believe we need additional field data before we can complete this project. We will continue this work in the coming year.
Air Quality Modeling	
Develop a System for Quantitative Winter Ozone Forecasts	The Clyfar winter ozone forecasting system was operational during winter 2024-25. We have made significant improvements, and will use the system again for the coming winter with our Ozone Alert program. Clyfar is able to provide quantitative forecasts, including likelihood and confidence information, so stakeholders who use Ozone Alert can make better decisions about how to reduce winter ozone when it matters most.
Study the Impact of Chemical Mechanisms on Simulations of Winter Ozone	Our box model study of winter ozone chemical mechanisms is complete and currently under review for publication. We are now developing a model using the WRF-SMOKE-CMAQ software system that we will use in the coming year to continue this work. Development of the WRF-SMOKE-CMAQ model has been slower than expected.
Develop a Winter Ozone 3D Photochemical Model	As discussed in the previous row, development of the model has been slower than expected. We have WRF meteorological model output ready, and we have finalized base model emissions with the SMOKE platform. We are currently working on using WRF and SMOKE outputs as inputs to run the CMAQ model. This work will continue in the coming year.
Emissions Characterization	
Determine changes to Basin-wide Pollutant Emissions over Time	We completed this objective. We used the Integrated Methane Inversion method to determine Basin-wide methane emissions from 2013 through 2024 and performed an analysis to determine the causes of emission changes. We are now working to publish these data and to create a web interface to share these data with stakeholders.
Analyze Emission Sources—Types and Spatial Distribution	We did not complete this objective.
Develop Methods to Determine Oil Storage Tank Emission Factors in the Uinta Basin	This project has been delayed because partners on the project have not completed their portion of the work. We have done everything we can and are waiting to receive data and analyses from partners so we can complete the work. We expect a manuscript to be complete and submitted for peer-reviewed publication in the first half of 2026.
Develop a Drone-based Measurement System for Emissions from Oil and Gas Sources	This is a multi-year objective. We are still working on development of software to convert the drone data into emission values. We expect to have that complete in early 2026, and then we will begin measurement of actual emission sources.
Stakeholder Engagement	

OBJECTIVE	OUTCOMES
Organize a New Stakeholder Guidance Committee	We completed this objective. We created a new stakeholder guidance committee, held meetings with them, and they are actively working with us to guide our research.
Operate a Website to Display Real-time Air Quality Information to the Public	We completed this objective for the reporting period. We also built a new website, basinwx.com, and the website is operational.
Operate the Ozone Alert program	We completed this objective for the reporting period.
Uinta Basin Ozone Working Group	We completed this objective for the reporting period. More about the working group can be found at https://www.usu.edu/basinozonegroup/.

3. Winter 2024-25 Air Quality and Meteorology

Authors: Seth Lyman and Trevor O'Neil

This section reports on air quality conditions that occurred during winter 2024-25 (1 December 2024 through 31 March 2025).

3.1. Methods

3.1.1. Ozone

During winter 2024-25, eleven monitoring stations that measured ozone operated in the Uinta Basin. Table 3-1 contains a list of all monitoring stations, including locations, elevations, and operators. We obtained data for stations operated by organizations other than USU from the U.S. Environmental Protection Agency (EPA)'s AQS database (https://aqs.epa.gov/api) and airnowtech.org. We utilized an Ecotech 9810 ozone analyzer at the Horsepool site, a 2B Technology 205 ozone monitor at the Seven Sisters site, and a Teledyne T400 at the Castle Peak site. We performed calibration checks at all USU stations at least every other week using NIST-traceable ozone standards. Calibration checks passed if monitors reported in the range of ±5 ppb when exposed to 0 ppb ozone and if monitors were within ±7% deviation from expected values when exposed to higher concentrations of ozone. We only included data bracketed by successful calibration checks in the final dataset.

Table 3-1. Air quality monitoring stations that operated during winter 2024-25. All stations measured ozone and basic meteorological parameters. Stations that measured organic compounds, NO_X, and/or $PM_{2.5}$ are indicated. NO_X* signifies NO_2 measured with a photolytic NO_2 (rather than molybdenum) converter. NPS is the National Park Service. UDAQ is the Utah Division of Air Quality. BLM is the Bureau of Land Management. AQS is the EPA AQS air quality database (https://aqs.epa.gov/api).

	Operator	Latitude	Longitude	Elev. (m)	Organics	NO_X, $PM_{2.5}$	Data Source
Seven Sisters	USU	39.981	-109.345	1618	N/A	N/A	USU
Castle Peak	USU	40.051	-110.020	1605	Yes	NO_X*	USU
Dinosaur N.M.	NPS	40.437	-109.305	1463	N/A	N/A	AQS
Red Wash	Ute Tribe	40.204	-109.352	1689	N/A	NO_X	AQS
Vernal	UDAQ	40.453	-109.510	1606	N/A	NO_X, $PM_{2.5}$	AQS
Whiterocks	Ute Tribe	40.484	-109.906	1893	N/A	NO_X	AQS
Ouray	Ute Tribe	40.055	-109.688	1464	N/A	NO_X	AQS
Roosevelt	DAQ/USU	40.294	-110.009	1587	Yes	NO_X*, $PM_{2.5}$	AQS/USU
Myton	Ute Tribe	40.217	-110.182	1610	N/A	NO_X	AQS
Horsepool	USU	40.144	-109.467	1569	Yes	NO_X*, $PM_{2.5}$	USU
Rangely	NPS/BLM	40.087	-108.762	1648	N/A	NO_X, $PM_{2.5}$	AQS

3.1.2. Reactive Nitrogen

We measured NO, true NO_2 (via a photolytic converter), and NO_Y at Roosevelt with a Teledyne-API NO_X analyzer. We measured NO, true NO_2, and NO_Y with a Thermo 42i with a photolytic converter at Horsepool, and we measured NO and true NO_2 with a Thermo 42i with a photolytic converter at Castle

Peak. All three photolytic converters were manufactured by Air Quality Design, Inc. NO_X is the sum of NO and NO_2. NO_Y is the sum of NO_X and other reactive nitrogen compounds in the gas and fine particulate phases. We calibrated the systems weekly with NO standards and for NO_2 and NO_Y via gas-phase titration using a dilution calibrator. Instruments were recalibrated throughout the season as needed, and, in some cases, data were adjusted after the season ended based on calibration data. Once during the season, we calibrated NO_Y instrumentation with nitric acid and isopropyl nitrate permeation tubes. All sites operated by other organizations measured NO and NO_2 via a molybdenum converter-based system, a method known to bias NO_2 and NO_X results high due to NO_Y interference (Jung et al., 2017; Mansfield and Lyman, 2021).

3.1.3. Methane and Total Non-methane Hydrocarbons

We measured methane and total non-methane hydrocarbons at Horsepool and Roosevelt with a Chromatotec ChromaTHC and a Thermo 55i, respectively. We calibrated these systems every week with certified gas standards (containing methane and propane) and a dilution calibrator. Instruments were recalibrated throughout the season as needed, and, in some cases, data were adjusted after the season ended based on calibration data.

3.1.4. Speciated Non-methane Hydrocarbons and Alcohols

To measure speciated non-methane hydrocarbons and alcohols, we collected whole-air samples with silonite-coated 6 L stainless steel canisters at Horsepool, Roosevelt, and Castle Peak. We collected at most one can per day via an automated sampling manifold (we filled some cans from 0:30 to 3:30 local standard time and the others from 12:30 to 15:30). We used stainless steel critical orifice-based flow regulators to regulate flow into the canisters, and we controlled sample collection with a nickel-plated brass manifold with inert solenoid valves (Clippard part number O-ET-2M-12). Tubing and fittings were all either PFA Teflon or stainless steel. A PTFE filter upstream of the sample line filtered particles (5 µm pore size). The filters and outdoor components of the inlet lines were heated to 30°C.

We analyzed the canisters for 54 hydrocarbons, methanol, ethanol, and isopropanol using a method similar to guidance provided by EPA for Photochemical Assessment Monitoring Stations (Epa, 1998). We used cold trap dehydration (Wang and Austin, 2006) with an Entech 7200 preconcentrator and a 7016D autosampler to preconcentrate samples. We analyzed samples with an Agilent 8890 gas chromatograph (GC), a flame ionization detector (FID; for C2 and C3 hydrocarbons), and an Agilent 5973 mass spectrometer (MS; for all other compounds). We used a Restek rtx1-ms column (all compounds; 60 m, 0.32 mm ID), a Restek Alumina BOND/Na_2SO_4 column (C2 and C3 hydrocarbons; 50 m,0.32 mm ID), and another Restek rtx1-ms column (all other compounds; 30 m, 0.25 mm ID) to separate compounds in the GCs.

We used 5-point curves to calibrate the flame ionization detector and mass spectrometer at least monthly. We analyzed at least one replicate sample, at least two blanks, and at least two calibration checks during each batch. We accepted data if calibration curves had r^2 values greater than 0.99, if all values for blanks were less than 1 ppb, if duplicate values for each compound averaged within 10% of each other, and if calibration checks for each compound were within 20% of expected values. We used blank values to correct sample results.

More information about our canister analysis protocols and results is available in Lyman et al. (2021) and Lyman et al. (2018). Table 3-2 lists the organic compounds measured.

Table 3-2. List of organic compounds measured, the compound group for each, and the analytical method used.

Compound	Group	Analytical method
Ethane	Alkane	GC/FID
Ethylene	Alkene	GC/FID
Propane	Alkane	GC/FID
Propylene	Alkene	GC/FID
Isobutane	Alkane	GC/MS
n-Butane	Alkane	GC/MS
Acetylene	Alkyne	GC/FID
Trans-2-butene	Alkene	GC/MS
1-Butene	Alkene	GC/MS
Cis-2-butene	Alkene	GC/MS
Isopentane	Alkene	GC/MS
N-Pentane	Alkane	GC/MS
Trans-2-pentene	Alkene	GC/MS
1-Pentene	Alkene	GC/MS
Cis-2-pentene	Alkene	GC/MS
2,2-Dimethylbutane	Alkane	GC/MS
Cyclopentane	Alkane	GC/MS
2,3-Dimethylbutane	Alkane	GC/MS
2-Methylpentane	Alkane	GC/MS
3-Methylpentane	Alkane	GC/MS
Isoprene	Alkene	GC/MS
1-Hexene	Alkene	GC/MS
n-Hexane	Alkane	GC/MS
Methylcyclopentane	Alkane	GC/MS
2,4-Dimethylpentane	Alkane	GC/MS
Benzene	Aromatic	GC/MS
Cyclohexane	Alkane	GC/MS
2-Methylhexane	Alkane	GC/MS
2,3-Dimethylpentane	Alkane	GC/MS
3-Methylhexane	Alkane	GC/MS
2,2,4-Trimethylpentane	Alkane	GC/MS
n-Heptane	Alkane	GC/MS
Methylcyclohexane	Alkane	GC/MS
2,3,4-Trimethylpentane	Alkane	GC/MS
Toluene	Aromatic	GC/MS
2-Methylheptane	Alkane	GC/MS

Compound	Group	Analytical method
3-Methylheptane	Alkane	GC/MS
n-Octane	Alkane	GC/MS
Ethylbenzene	Aromatic	GC/MS
m/p-Xylene	Aromatic	GC/MS
Styrene	Alkene	GC/MS
o-Xylene	Aromatic	GC/MS
n-Nonane	Alkane	GC/MS
Isopropylbenzene	Aromatic	GC/MS
n-Propylbenzene	Aromatic	GC/MS
1-Ethyl-3- methylbenzene	Aromatic	GC/MS
1-Ethyl-4-methylbenzene	Aromatic	GC/MS
1,3,5-Trimethylbenzene	Aromatic	GC/MS
1-Ethyl-2- methylbenzene	Aromatic	GC/MS
1,2,4-Trimethylbenzene	Aromatic	GC/MS
n-Decane	Alkane	GC/MS
1,2,3-Trimethylbenzene	Aromatic	GC/MS
1,3-Diethylbenzene	Aromatic	GC/MS
1,4-Diethylbenzene	Aromatic	GC/MS
Methanol	Alcohol	GC/MS
Ethanol	Alcohol	GC/MS
Isopropanol	Alcohol	GC/MS
Formaldehyde	Carbonyl	HPLC
Acetaldehyde	Carbonyl	HPLC
Acrolein	Carbonyl	HPLC
Acetone	Carbonyl	HPLC
Propionaldehyde	Carbonyl	HPLC
Crotonaldehyde	Carbonyl	HPLC
Butyraldehyde	Carbonyl	HPLC
Methacrolein	Carbonyl	HPLC
2-Butanone	Carbonyl	HPLC
Benzaldehyde	Carbonyl	HPLC
Valeraldehyde	Carbonyl	HPLC

3.1.5. Carbonyls

We collected samples on DNPH cartridges and eluted and analyzed them using modifications of the methods of Uchiyama et al. (2009), Anneken et al. (2015), Shimadzu method LAAN-J-LC-E090 (Shimadzu, 2011), and Restek Lit. Cat. # EVSS2393A-UNV (Restek, 2018). These techniques are somewhat different from U.S. EPA Method TO-11A (Epa, 1999), which has become outdated due to improved instrumentation capabilities and column separation technologies. The sample path upstream of the cartridges during field collection was composed entirely of PFA Teflon, with a PTFE filter upstream of the

sample line to filter particles (5 µm pore size). Sample collection times were the same as those for the canisters described above (3 hours). The filter and other outdoor components of the collection system were heated to 30°C.

We eluted cartridges within 14 days of sampling and analyzed the eluent within 30 days. To elute DNPH cartridge samples, we flushed cartridges with 5 mL of a solution of 75% acetonitrile and 25% dimethyl sulfoxide (percent by volume). We collected the solution into 5 mL volumetric flasks and brought the flasks to a volume of 5 mL using 0.5–1 mL of the acetonitrile/dimethyl sulfoxide solution. Finally, we pipetted a 1.6 mL aliquot from the 5 mL flask into two 2 mL autosampler vials for analysis by high-performance liquid chromatography (HPLC). The second vial was kept as a spare in case of contamination or equipment failure.

We used a commercial standard mixture (M-1004; AccuStandard, New Haven, CT, USA) of derivatized carbonyls in acetonitrile for calibration. We analyzed samples with a Shimadzu (Somerset, NJ, USA) Nexera-i LC-2040C 3d Plus HPLC and a Shimadzu Shim-Pack Velox C18 column. We used a mixture of acetonitrile, tetrahydrofuran, and water as the eluent. We calibrated the instrument on each analysis day with a 5-point calibration curve and ran at least one additional calibration standard at the beginning and end of each analysis batch to check for retention time drift or other errors.

Additional information about the methods used is available in Lyman et al. (2021). Table 3-2 lists the organic compounds that we measured.

3.1.6. Particulate Matter Measurements

We measured particulate matter with aerodynamic diameter smaller than 2.5 micrometers ($PM_{2.5}$) at Horsepool with a BAM 1020 monitor. We operated the instrument according to manufacturer protocols, with leak checks, flow and mass calibrations, detector calibrations, and cleanings performed at regular intervals. We obtained particulate matter values for other sites from the EPA AQS database (https://aqs.epa.gov/api).

3.1.7. Meteorological Measurements

We deployed solar radiation sensors at Horsepool (incoming and outgoing shortwave and longwave with a Hukseflux NR01 radiometer and UV-A and UV-B with Kipp and Zonen UV radiometers), Roosevelt (incoming and outgoing shortwave with a Kipp and Zonen CNR-4), and Castle Peak (incoming and outgoing shortwave and longwave with a Hukseflux NR01 radiometer). We checked these sensors against calculations of clear-sky radiation annually.

We operated a suite of comprehensive, research-grade meteorological instruments at all sites operated by USU. We checked wind speed and direction, temperature, humidity, and barometric pressure against a NIST-traceable standard once annually. We checked snow depth sensors against a height standard annually. We also obtained meteorological data from the EPA AQS database.

3.1.8. Data Quality

Table 3-3 shows a summary of data quality results for ambient air chemical measurements we collected during the reporting period. The maximum uptime possible for most measurements shown in the table is approximately 95% due to maintenance and calibration periods.

Table 3-3. Data quality summary for ozone, oxides of nitrogen (NO_X), carbon monoxide (CO), and organic compound data collected during 2024-25. Results are shown as averages ± 95% confidence intervals for all locations at which the indicated measurements were collected (confidence intervals are shown if the number of data points is three or more). Percent uptime indicates the percent of the measurement period for which valid measurements were obtained. NMHC indicates non-methane hydrocarbons. N/A means not applicable.

Measurement	Zero calib. (ppb)	Span calib. (% recov.)	Percent uptime
Ozone	-2.1 ± 0.5	100 ± 1	91 ± 31
NO	0.0 ± 0.0	100 ± 1	94 ± 5
NO_X (NO calib.)	0.1 ± 0.1	100 ± 1	94 ± 5
NO_Y (NO calib.)	-0.7 ± 0.3	99 ± 1	95
NO_X (GPT calib.)	N/A	101 ± 1	94 ± 5
NOy (GPT calib.)	N/A	99 ± 1	95
CO	0 ± 7	103 ± 3	46
Methane	33 ± 13	100 ± 1	66
Total NMHC	52 ± 25	103 ± 2	66
Speciated NMHC	0.1 ± 0.0	99 ± 0	86
Speciated Carbonyls	0.0 ± 0.0	96 ± 0	86
$PM_{2.5}$ (BAM)	N/A	N/A	97

Speciated NMHC and speciated carbonyl samples analyzed in duplicate were 3 ± 2% and 3 ± 1% different from each other (average ± 95% confidence interval).

In addition to the quality checks described in this section and above, we compared our ozone and NO_X instrumentation against calibration transfer standards made available by the Utah Division of Air Quality.

3.2. Results and Discussion

3.2.1. Ozone

Very little snow cover existed across the lower elevations of the Uinta Basin, keeping ozone well below the 70 ppb EPA standard throughout winter 2024-25 at Horsepool (Figure 3-1) and at sites across the Basin (Figure 3-2), except at the end of January and first of February, when temperature inversion conditions persisted for a few days. During those few days, ozone increased at several sites and exceeded the EPA standard for two days at the Castle Peak site, which is used for research purposes only and not for regulatory decision-making.

A general trend can be seen in Figure 3-2 that is distinct from the spike in ozone at the end of January and first of February, wherein ozone increases from December through March. Ozone production depends on solar radiation. Because of this, background ozone (i.e., ozone due to non-local and non-human-caused emission sources) is lowest at the winter solstice and increases until the summer solstice. The general trend in the figure can thus be attributed to the response of background ozone to seasonal changes in solar radiation.

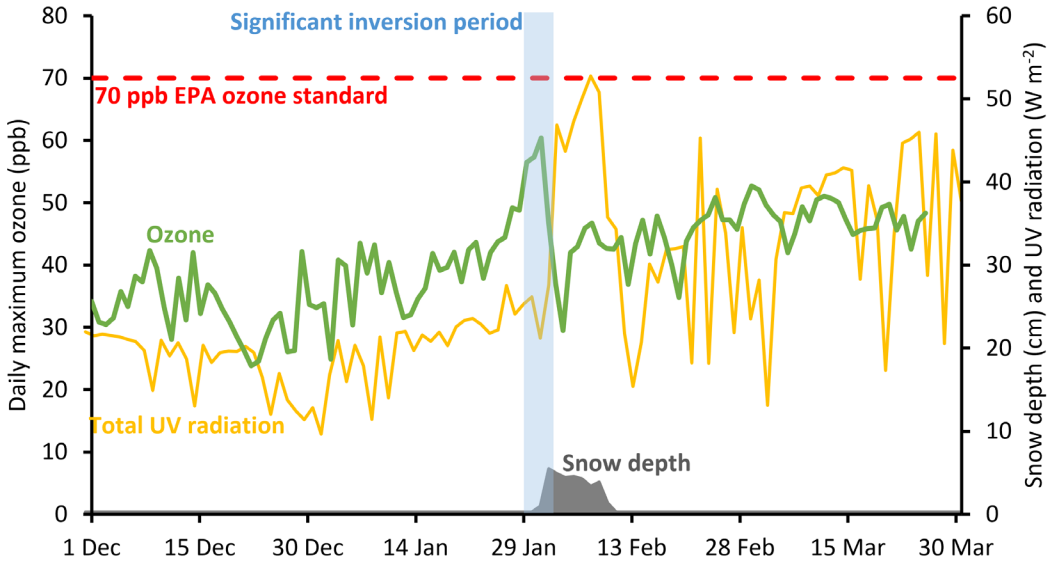

Figure 3-1. Horsepool daily maximum ozone, average snow depth, and daytime average total UV radiation. (incoming + reflected) during winter 2024-25. Inversion periods are shown as light blue boxes.

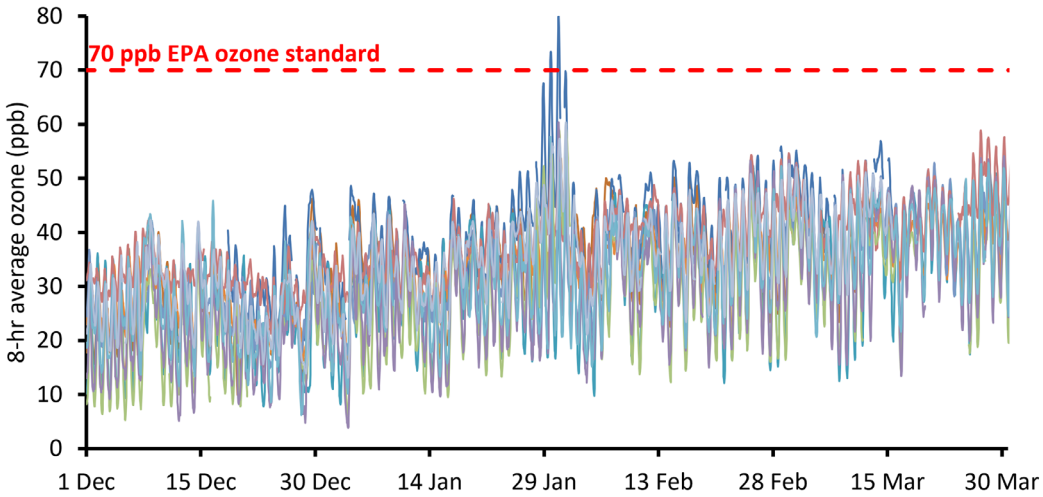

Figure 3-2. 8-hr average ozone from all sites listed in Table 2-1 during winter 2024-25.

Table 3-4 provides information about ozone observed at all monitoring stations in the Uinta Basin during winter 2024-25. Only the non-regulatory Castle Peak monitoring station experienced exceedances of the EPA ozone standard during the winter. An exceedance occurs when the daily maximum 8-hr average ozone value at a station is greater than the EPA standard of 70 ppb. The average of the fourth-highest daily maximum 8-hr average ozone value over three consecutive calendar years is used to determine regulatory compliance with the standard.

Table 3-4. Eight-hour average ozone concentrations around the Uinta Basin during winter 2024-25.

	Mean	Maximum	Minimum	4th Highest Daily Maximum	Number of Exceedances
Seven Sisters	33.2	58.3	10.0	51.4	0
Castle Peak	39.7	79.9	16.8	67.6	2
Dinosaur N.M.	29.7	53.3	7.8	51.7	0
Red Wash	32.8	48.4	16.3	46.4	0
Vernal	32.2	54.5	14.4	51.8	0
Whiterocks	37.1	54.6	21.3	53.3	0
Ouray	26.8	59.4	5.3	52.3	0
Roosevelt	27.7	60.4	3.9	52.8	0
Myton	30.9	57.7	6.3	50.4	0
Horsepool	34.1	60.4	13.1	52.0	0
Rangely	33.2	58.3	10.0	51.4	0

Figure 3-3 shows the spatial distribution of the highest daily maximum 8-hr average ozone concentration around the Uinta Basin during winter 2024-25. Ozone was higher in the southwest Uinta Basin and was lower for sites in the north and east. While snow cover existed across a broad swath of the Basin during the inversion episode that occurred at the end of January and first of February (Figure 3-4), snow cover was deeper at the Castle Peak site than at other locations where snow depth was measured (Figure 3-4), and this may have led to stronger inversion conditions and higher ozone at the Castle Peak site. Castle Peak also had higher organic compound concentrations than other sites in the Uinta Basin during winter 2024-25 (Figure 3-19).

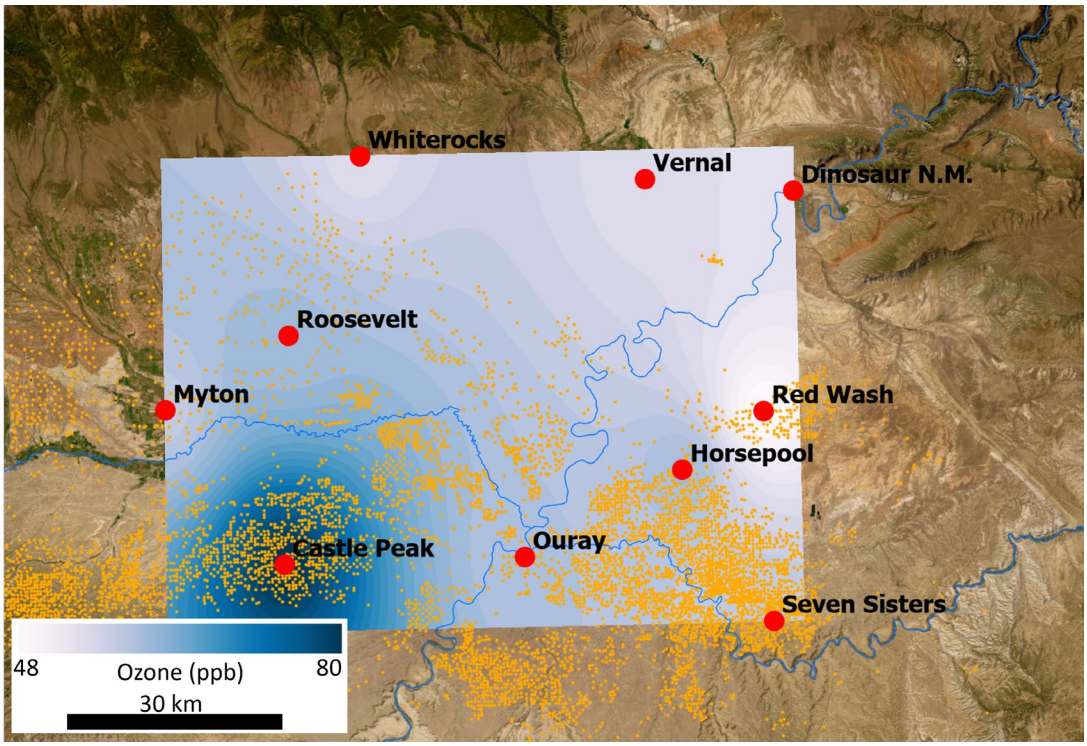

Figure 3-3. Highest daily maximum 8-hr average ozone in the Uinta Basin during winter 2024-25. The background color indicates ozone concentration and was interpolated using the inverse distance weighting method in ArcGIS Pro.

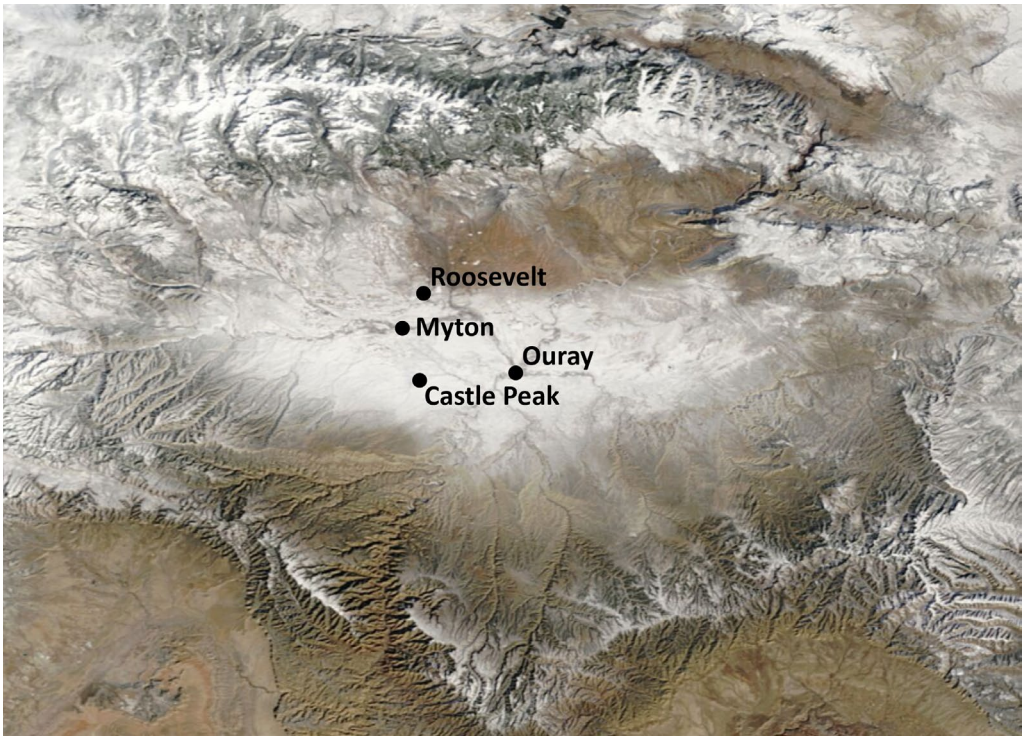

Figure 3-4. Satellite image of the Uinta Basin on 31 January 2025. White areas are covered with snow.

3.2.2. Particulate Matter

$PM_{2.5}$ concentrations stayed at or below the EPA standard of 35 µg m^{-3} during winter 2024-25 at Vernal, Roosevelt, and Horsepool (Figure 3-5). As is typical of previous winters in the Uinta Basin, $PM_{2.5}$ was lower at Horsepool than at the other stations (Figure 3-6), where urban sources of particulate pollution dominate $PM_{2.5}$. Roosevelt reached the EPA standard during the inversion episode that occurred at the end of January and first of February.

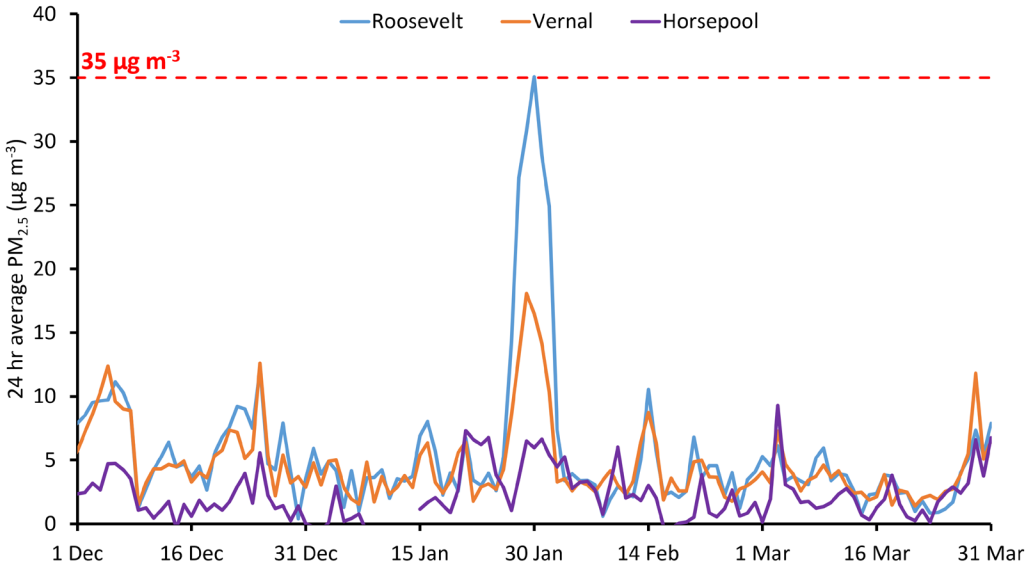

Figure 3-5. 24-hr average $PM_{2.5}$ at monitoring stations around the Uinta Basin during winter 2024-25. The red dashed line indicates the EPA $PM_{2.5}$ standard.

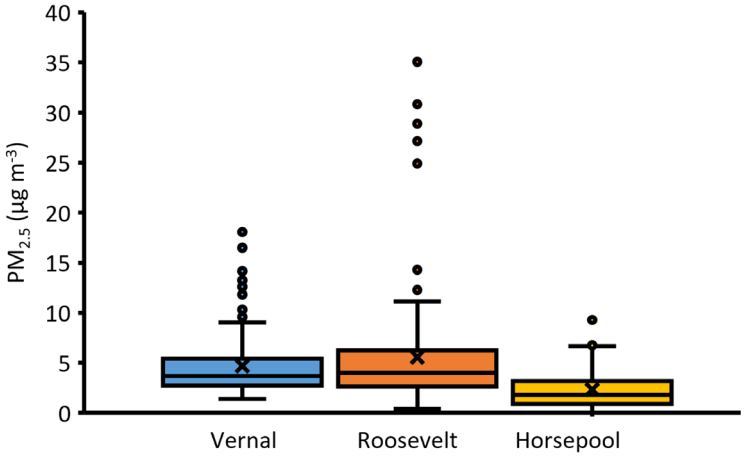

Figure 3-6. Box-and-whisker plots of 24-hr average $PM_{2.5}$ at four monitoring stations during winter 2024-25. X's indicate average values. Lines within the boxes indicate medians. Tops and bottoms of boxes indicate the third and first quartiles. Top and bottom whiskers indicate maximum and minimum values. Circles indicate outliers.

Comparison of Roosevelt, Horsepool, Castle Peak, and Seven Sisters Data

The Horsepool and Roosevelt monitoring stations began operating in winter 2011-12 and were designed to contain nearly identical suites of instrumentation. At both stations, for example, we measure NO_X

with instrumentation that doesn't bias NO_2 during winter inversion episodes, whereas all regulatory monitoring stations in the Uinta Basin use alternative, biased instrumentation (See Methods section for more information). The areas surrounding the Horsepool and Roosevelt stations are different from one another. The Horsepool station is on the northern edge of an area of dense oil and gas development (mostly gas), whereas the Roosevelt station is within a small city. Oil and gas development exists within and near the city of Roosevelt (mostly oil). The two stations are at very similar elevations (Table 3-1).

In 2017, Utah DAQ donated a NO_X analyzer that we upgraded with a photolytic converter and installed at our Castle Peak monitoring station, and we also collect some organic compound data at Castle Peak. Castle Peak is in an area of dense oil development, and its elevation is less than 100 meters higher than the Roosevelt and Horsepool stations. We also include ozone and snow depth data from the Seven Sisters station in a few of the analyses below.

Figure 3-7 shows NO_X measured at Roosevelt, Horsepool, and Castle Peak during winter 2024-25, and Figure 3-8 shows NO_Z at Roosevelt and Horsepool. NO_X is the sum of NO and NO_2, which are important precursors to ozone production. NO_Y (not shown in the figures) is the sum of NO_X and all other reactive nitrogen compounds (e.g., nitric and nitrous acids, organic nitrates, and particulate-bound nitrogen compounds). NO_Z is the sum of all reactive nitrogen compounds except NO_X (in other words, it is NO_Y minus NO_X). While NO_X is an ozone precursor, the compounds that comprise NO_Z are mostly generated along with ozone as a result of photochemical reactions and are byproducts and indicators of atmospheric photochemical activity.

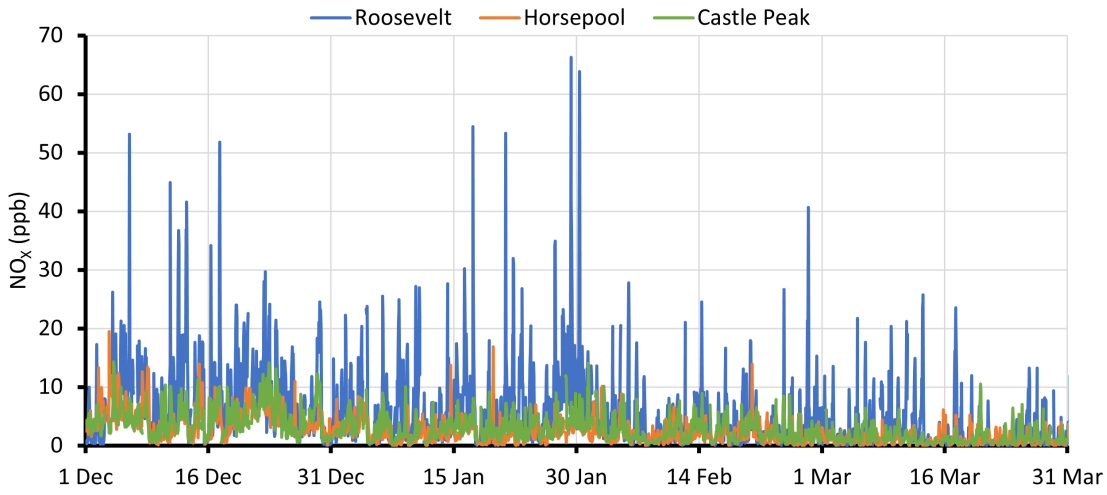

Figure 3-7. Hourly average NO_X measured at Roosevelt, Horsepool, and Castle Peak during winter 2024-25.

During winter 2024-25, as in previous winters, NO_X was higher in Roosevelt than at Horsepool and Castle Peak (Figure 3-7) and was 2.3 times higher than Horsepool on average. NO_X in Roosevelt is emitted from urban sources like cars and home heating, as well as from oil and gas sources, while NO_X in the vicinity of Horsepool and Castle Peak originates almost entirely from oil and gas activity. NO_X at Castle Peak was 21% higher than Horsepool (p-value for a t-test of difference was <0.01). NO_Z was 57% higher at Horsepool than at Rosevelt, indicating greater photochemical activity at Horsepool (Figure 3-8).

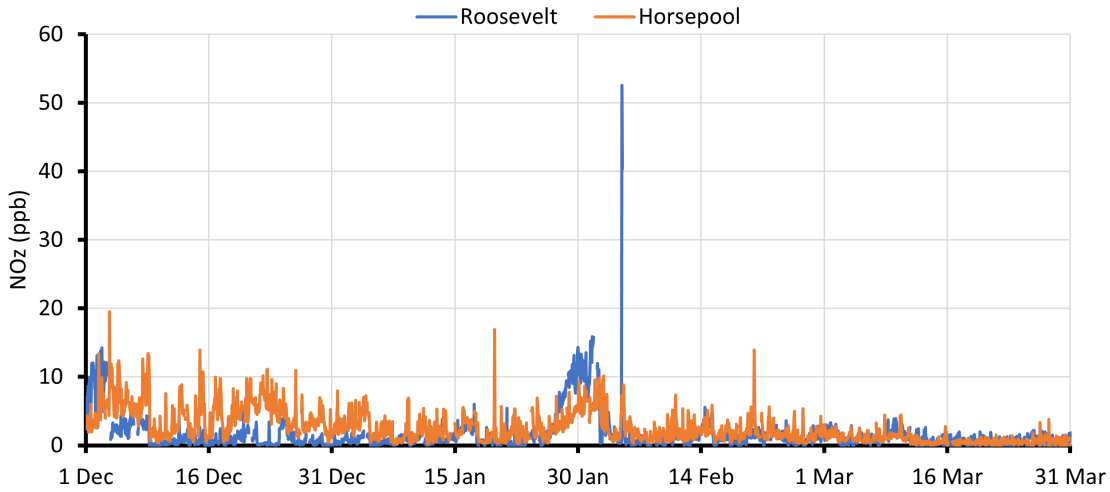

Figure 3-8. Hourly average NO_Z measured at Roosevelt and Horsepool during winter 2024-25.

NO_X at Roosevelt exhibited a pronounced peak in the morning and a lesser peak in the late afternoon and early evening, probably due to morning and afternoon peaks in local traffic (Figure 3-9). Horsepool and Castle Peak did not show a pronounced peak, probably because the majority of NO_X emissions at the site was due to stationary, continuous sources rather than traffic-related sources.

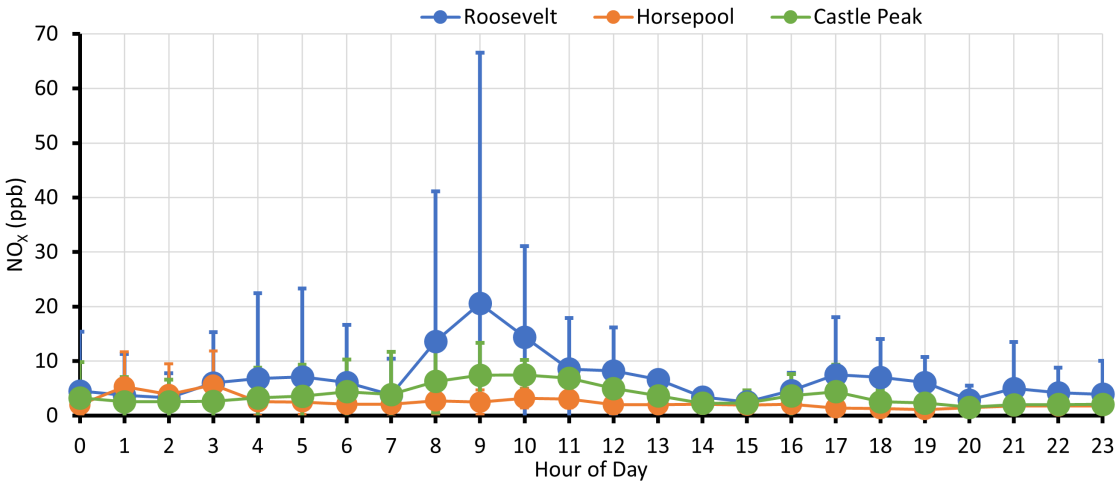

Figure 3-9. Average NO_X at Roosevelt, Horsepool, and Castle Peak during each hour of the day during inversion episodes that occurred during winter 2024-25. Whiskers represent 95% confidence intervals.

Methane at Horsepool and Roosevelt were similar ($p = 0.55$ for a t-test; Figure 3-10), but average total non-methane hydrocarbons (TNMHC; measured as a single group of compounds with an in-situ hydrocarbon GC) were 82% higher at Horsepool ($p < 0.01$; Figure 3-11).

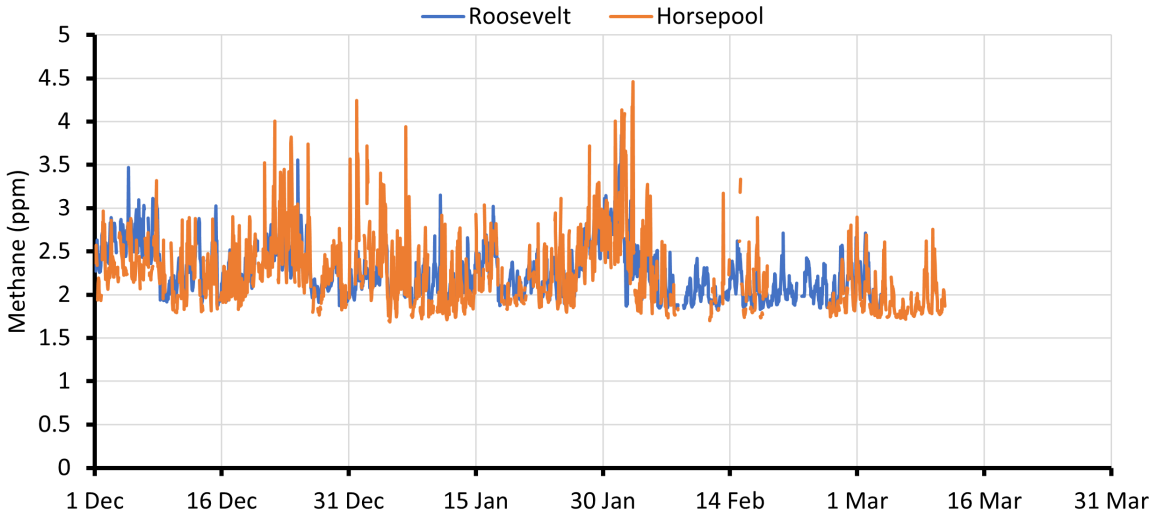

Figure 3-10. Hourly average methane measured at Roosevelt and Horsepool during winter 2024-25.

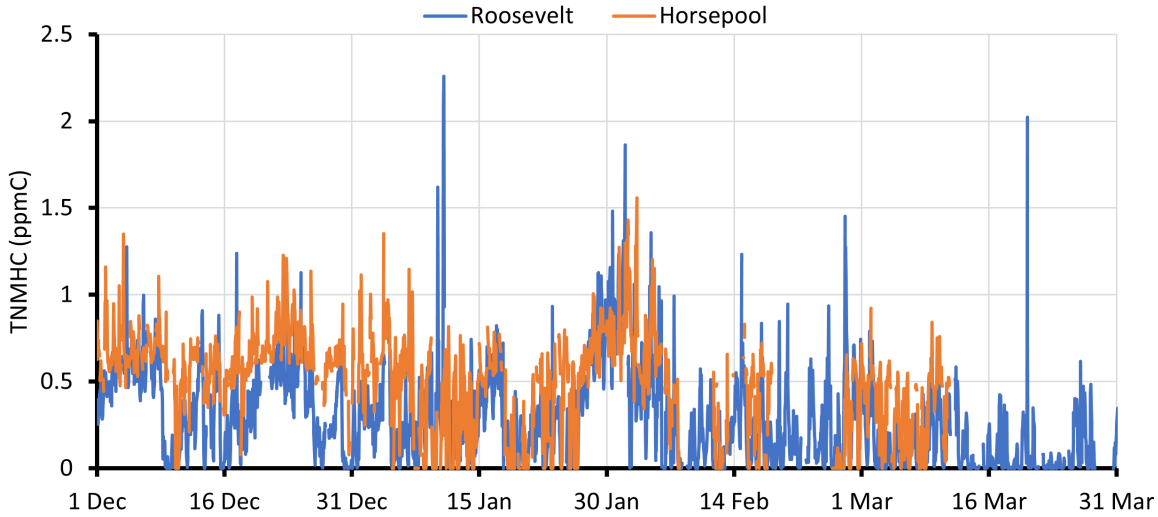

Figure 3-11. Hourly average total non-methane hydrocarbons (TNMHC) measured at Roosevelt and Horsepool during winter 2024-25. ppmC is parts-per-million of carbon atoms.

Little or no snow was present during winter 2024-25, except around the end of January and first of February (Figure 3-12), keeping albedo (i.e., reflectivity of solar radiation from the ground surface) low (Figure 3-13).

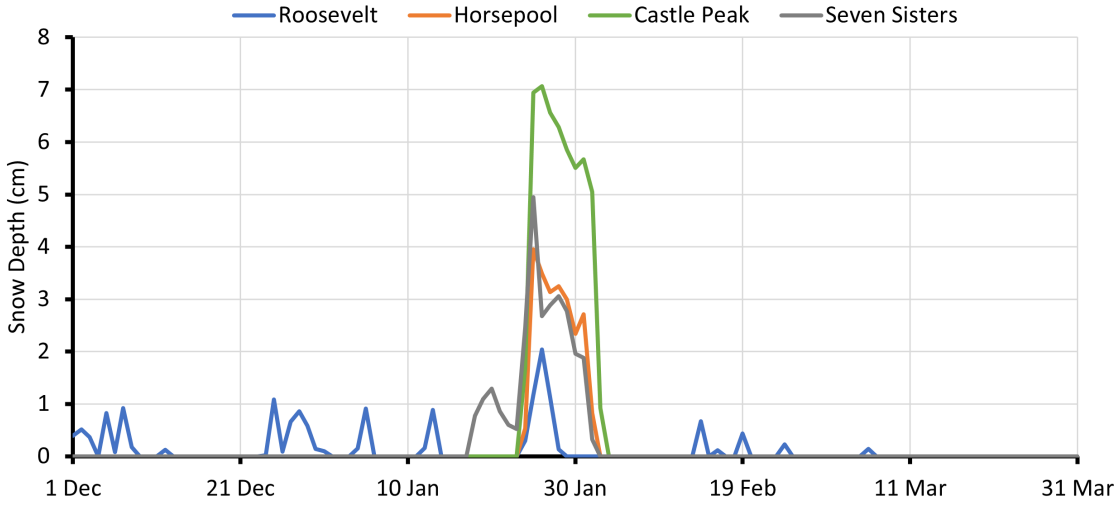

Figure 3-12. Snow depth at the Roosevelt, Horsepool, and Castle Peak stations during winter 2024-25.

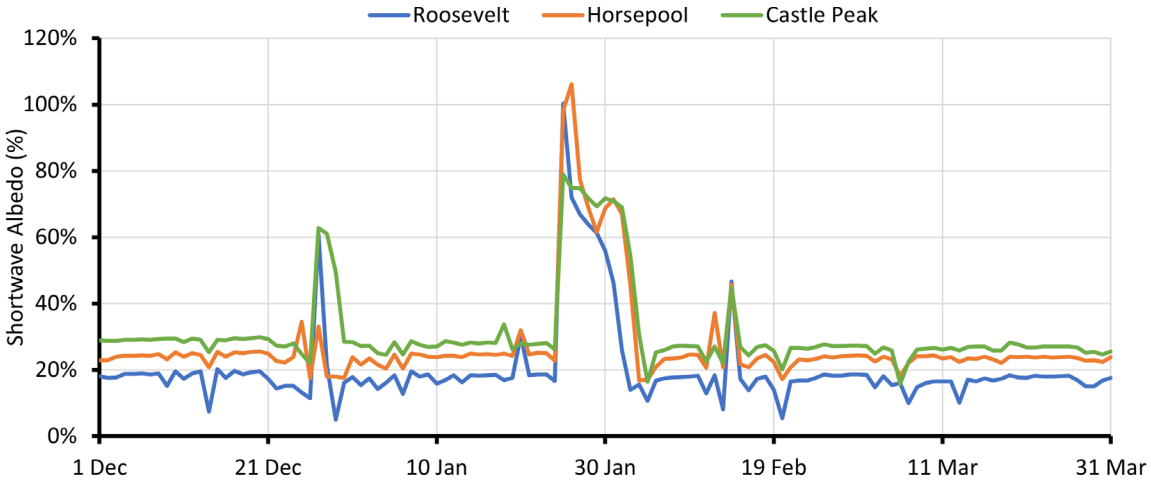

Figure 3-13. Shortwave albedo at the Roosevelt and Castle Peak stations during winter 2024-25. Shortwave radiation is visible light from the sun. Albedo is the percentage of radiation that is reflected by the earth's surface.

Ozone at Castle Peak was higher than at the other stations during the second half of winter 2024-25 (Figure 3-14). When snow cover existed at the end of January and the first of February, Castle Peak was the only site with ozone above 70 ppb, which could be because it had higher average organic compound concentrations than the other sites (Figure 3-19). Roosevelt ozone tended to be lower than at Horsepool and Castle Peak, especially at night (Figure 3-15). This was the case even though NO_X and non-methane hydrocarbons were both higher at Roosevelt than at Horsepool, and even though snow depth and albedo were similarly low at all sites. We expect that this occurred because the atmosphere at Roosevelt has more NO_X than is needed for ozone production. Too much NO_X can allow NO_X to react with and destroy ozone, suppressing ozone concentrations. At night, when no photochemistry occurs, ozone is not formed, but NO_X can still react with and destroy ozone, leading to the larger NO_X reduction at night in Roosevelt compared to the other locations.

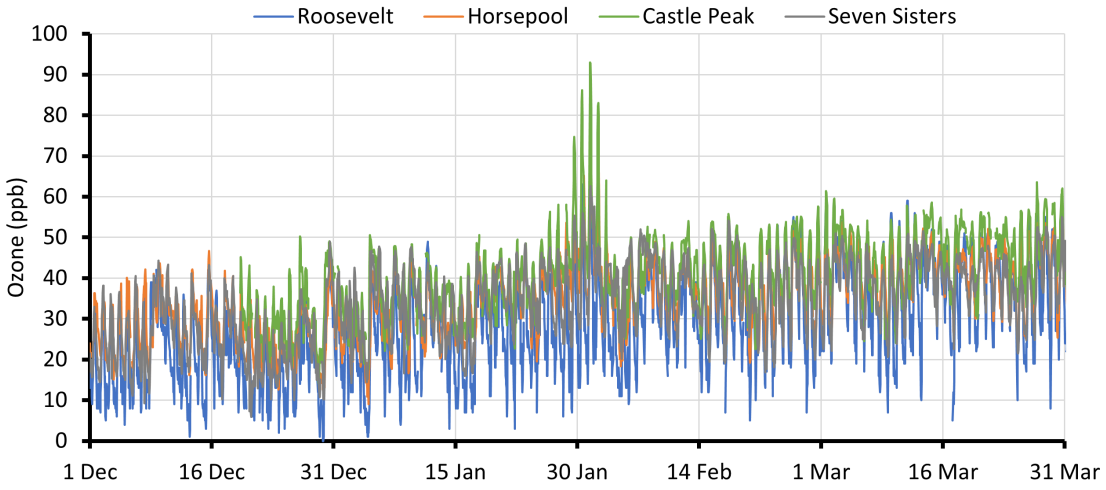

Figure 3-14. Hourly average ozone measured at Roosevelt, Horsepool, Castle Peak, and Seven Sisters during winter 2024-25.

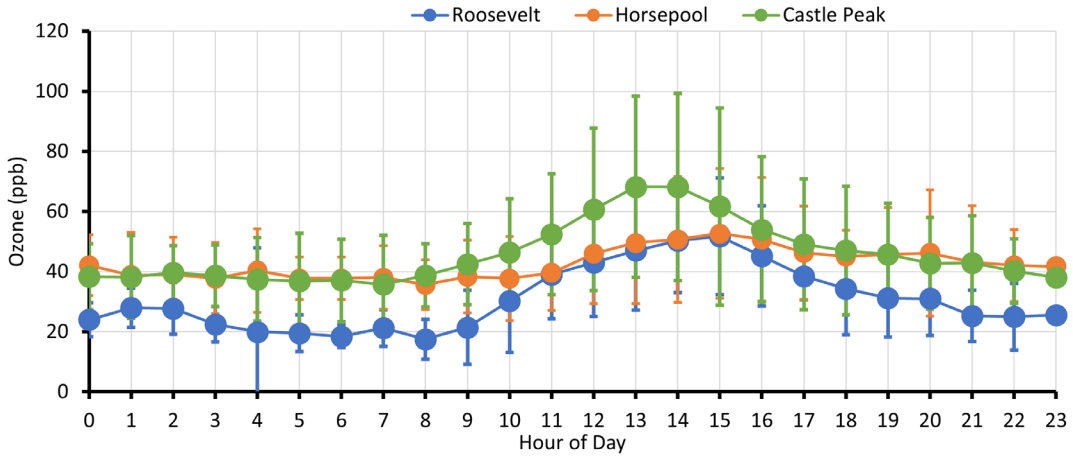

Figure 3-15. Average ozone at Roosevelt, Horsepool, and Castle Peak during each hour of the day during inversion episodes that occurred during winter 2024-25. Whiskers represent 95% confidence intervals.

3.2.4. Speciated Volatile Organic Compounds

This section focuses on measurements of individual organic compounds measured from whole air canister samples (Section 3.1.4) and DNPH cartridge samples (Section 3.1.5).

As in previous years, organic compounds in the atmosphere at field sites were dominated by alkanes, especially lighter alkanes (Figure 3-16 and Figure 3-17). Benzene, toluene, xylenes, and other aromatics were relatively low, and C8 and larger aromatics were at very low levels when observed. The organic compound speciation at all sites was similar, indicating that the locations were all influenced by the same general source type (oil and natural gas production).

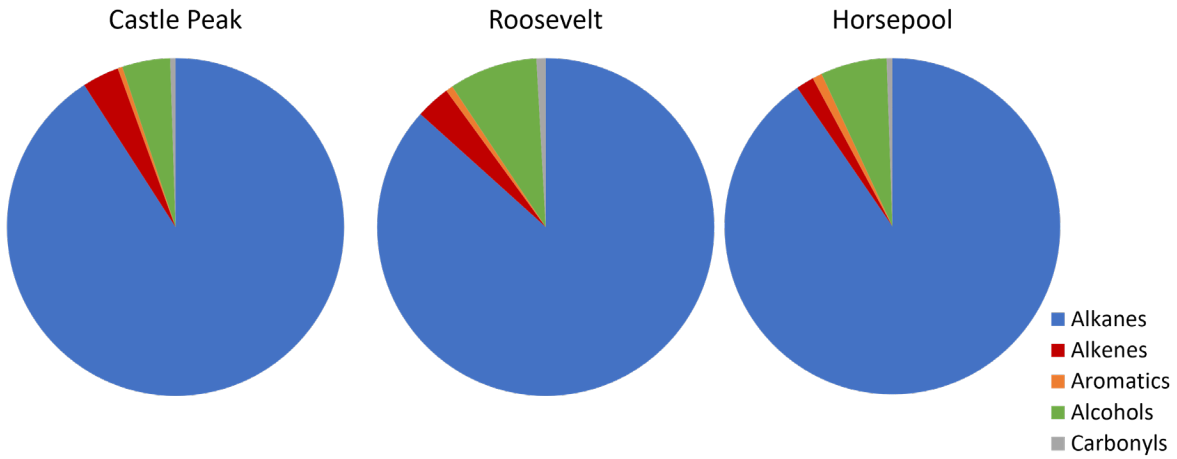

Figure 3-16. Percent by volume of measured organics at Castle Peak, Horsepool, and Roosevelt during winter 2024-25 comprised of alkanes, alkenes, aromatics, alcohols, and carbonyls.

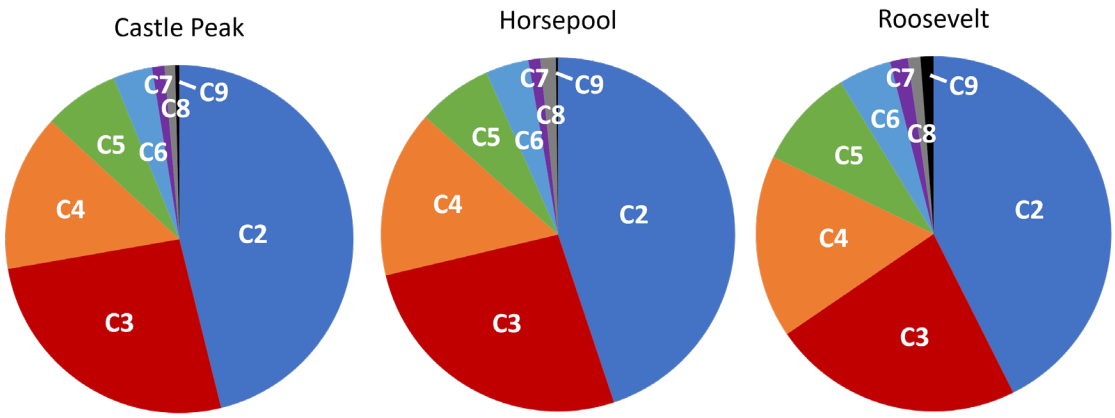

Figure 3-17. Percent by volume of measured non-methane hydrocarbons at Castle Peak, Horsepool, and Roosevelt during winter 2024-25 comprised by compounds containing 2-9 carbon atoms (i.e., C2-C9; excludes alcohols and carbonyls).

Total hydrocarbon concentrations at Roosevelt, Horsepool, and Castle Peak generally tracked each other and tended to be higher in early winter when atmospheric mixing was lower (Figure 3-18), and at the end of January and first of February, when inversion conditions existed. Total hydrocarbons were higher in canister samples than in real-time total hydrocarbon analyzer data during inversion conditions, probably because the canisters measure compounds that are missed or undersampled with the real-time analyzers. Average total non-methane hydrocarbons, measured as the sum of individual compounds in units of ppbC, were not statistically different among the sites ($p > 0.34$ for t-tests; Figure 3-19), but Castle Peak had higher average total non-methane hydrocarbons than the other sites, and it had the highest total non-methane hydrocarbons during the inversion episode at the end of January and first of February (Figure 3-18).

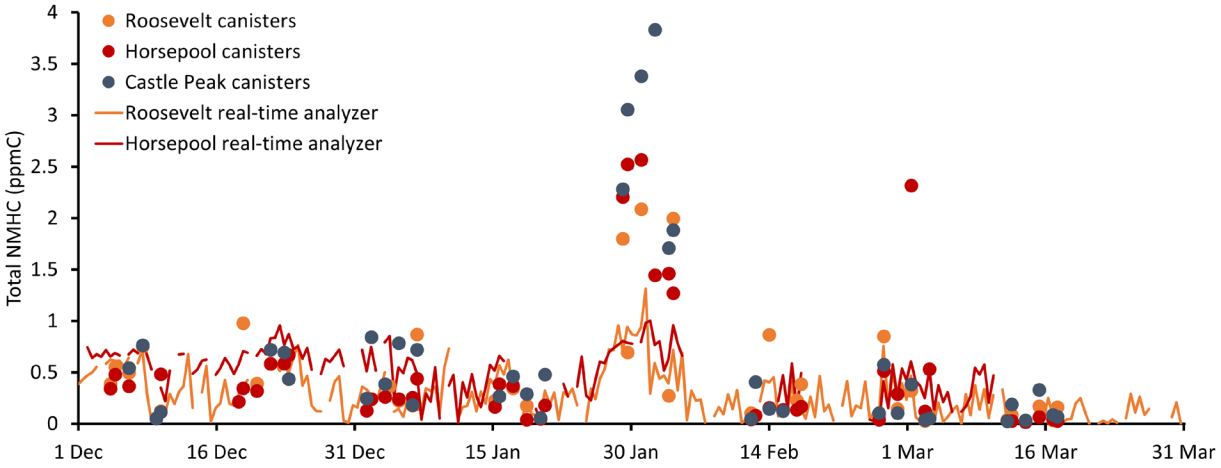

Figure 3-18. Time series of total non-methane hydrocarbons (NMHC) at Roosevelt, Horsepool, and Castle Peak during winter 2024-25. Units are parts per million of carbon atoms. Circles show the sum of speciated organic compounds derived from 3-hr canister measurements. Lines show 12-hour averages from continuously operating gas chromatographs.

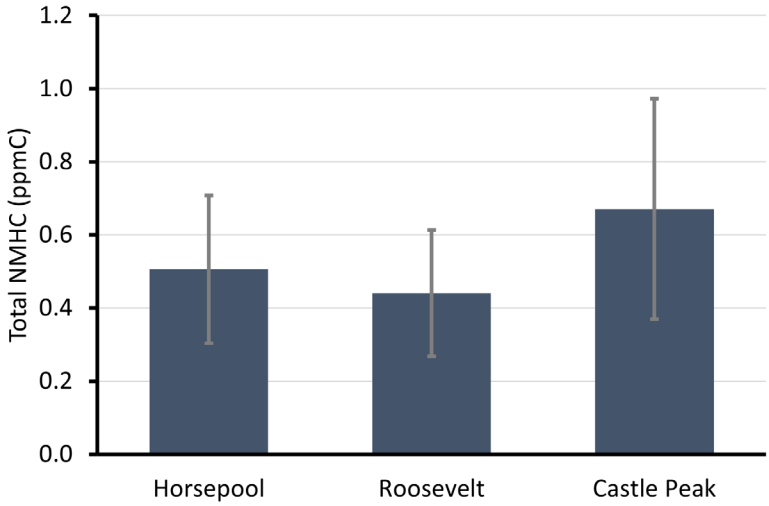

Figure 3-19. Average total NMHC at Horsepool, Roosevelt, and Castle Peak. Values are the sum of individual compounds measured from canister samples in units of parts per million of carbon atoms. Whiskers show 95% confidence intervals.

3.3. Data Access

All the data presented here, as well as data collected in previous years, are available at https://www.usu.edu/binghamresearch/data-access.

3.4. Acknowledgments

This work was funded by the Utah Legislature and Uintah Special Service District 1. Site access for USU monitoring stations was provided by Koda Energy, Scout Energy, the U.S. Bureau of Land Management,

and the Utah Division of Air Quality. We also thank Braden Cluster, Bo Call, and others at the Utah Division of Air Quality for providing calibration support, data access, and equipment. The Marriner S. Eccles Foundation provided funds for a gas chromatograph-mass spectrometer that is used for analysis of organic compounds in canister samples. Chevron provided funds for a high-performance liquid chromatograph that is used for analysis of carbonyls collected on DNPH cartridges.

4. Summertime Air Quality

Author: Seth Lyman

Five exceedances of the U.S. Environmental Protection Agency (EPA) ozone standard of 70 ppb occurred during the spring and summer seasons in 2025 (1 April through 30 September). The maximum ozone during spring and summer occurred in Whiterocks (78 ppb on 31 May). Figure 4-1 shows a time series of ozone in the Basin during this period, and Table 4-1 shows a list of ozone values on exceedance days for the same stations. Some of these data are from EPA's real-time AirNowTech database, are not final, and may change.

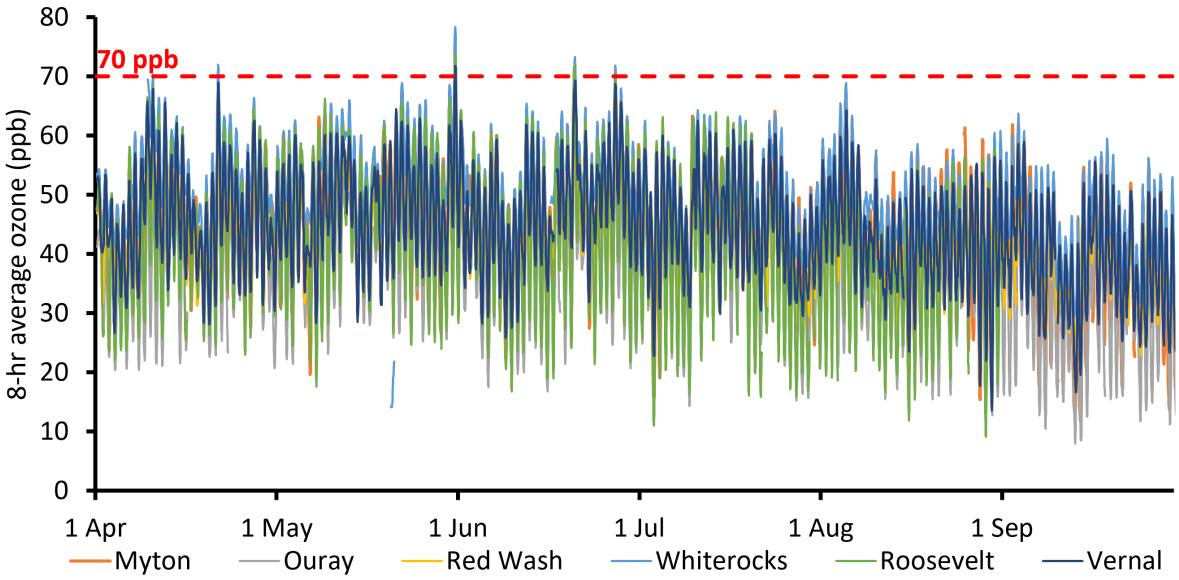

Figure 4-1. 8-hr moving average ozone at monitoring stations in the Uinta Basin during summer 2025. The red dashed line shows the EPA ozone standard of 70 ppb.

Table 4-1. Daily maximum 8-hour average ozone for days during which ozone at at least one station exceeded the EPA standard for the period of 1 April through 30 September 2025.

	21 Apr	31 May	20 Jun	21 Jun	27 Jun
Myton	63	69	71	65	68
Ouray	54	60	58	54	56
Red Wash	58	64	61	60	--
Whiterocks	72	78	73	71	71
Roosevelt	66	74	71	61	70
Vernal	69	71	69	69	68

Figure 4-2 shows a time series of basin-wide daily maximum 8-hr average ozone along with basin-wide daily maximum 8-hr average $PM_{2.5}$ for 1 April through 30 September 2025. Smoke emitted from fires is rich in $PM_{2.5}$ (visible smoke *is* mostly $PM_{2.5}$). Figure 4-2 shows that $PM_{2.5}$ did not increase above the 35 $\mu g\ m^{-3}$ standard during the period (the standard is for a 24-hr average, but 8-hr averages are used here for consistency with ozone data). High $PM_{2.5}$ days were sometimes (but not always) high ozone days.

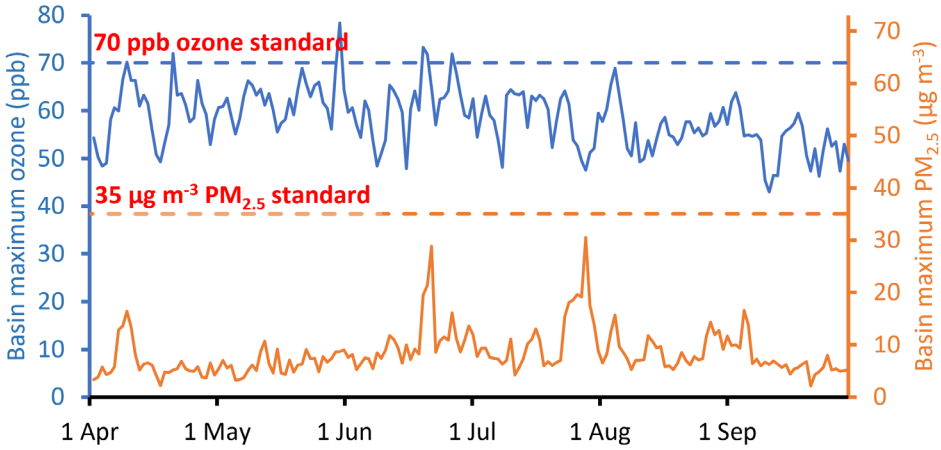

Figure 4-2. Maximum ozone measured at any site in the Uinta Basin and Basin-maximum $PM_{2.5}$ for 1 April through 30 September 2025. All values are 8-hr moving averages. The EPA ozone standard of 70 ppb and the EPA $PM_{2.5}$ standard of 35 µg m^{-3} are also shown. The EPA $PM_{2.5}$ standard is for a 24-hr average.

Wildfire smoke can lead to ozone exceedances, but high $PM_{2.5}$ from wildfire smoke does not always mean that ozone will also be high. High $PM_{2.5}$ in late July was associated with relatively low ozone, for example (Figure 4-2). Ozone can also be high in summer because of intrusion of ozone-rich air from the stratosphere, and this may have been the cause of ozone exceedances on 21 April and 31 May. More work would be needed to confirm the cause of ozone exceedances on these days.

4.1. Acknowledgments

This work was funded by the Utah Legislature and Uintah Special Service District 1.

5. Uinta Basin Air Quality Trends

Author: Seth Lyman

5.1. Introduction

The purpose of this section is to track changes in Uinta Basin air quality and the reasons for those changes. We seek to answer:

1. Are levels of ozone and its precursors changing over time?
2. What are the causes of any changes that occur?

In general, temporal trends in ozone and its precursors, if they exist, can be expected to be caused by changes in meteorology or changes in pollutant emissions. In this section, we use statistical methods to attempt to separate the two.

5.2. Ozone

Figure 5-1 shows a time series of ozone concentrations in the Uinta Basin from winter 2010-11 through the most recent winter. The figure shows the 4th-highest 8-hr average ozone concentration (the ozone metric used by EPA) of the monitoring station with the highest value for each winter season. The figure shows that the 4th-highest 8-hour average ozone exceeded the EPA standard of 70 ppb in 7 of the past 15 winters (47%). Of the past six winters, however, only one had a site with 4th-highest 8-hour average ozone above the EPA standard, indicating that ozone exceeding the EPA standard is becoming less common during Uinta Basin winters.

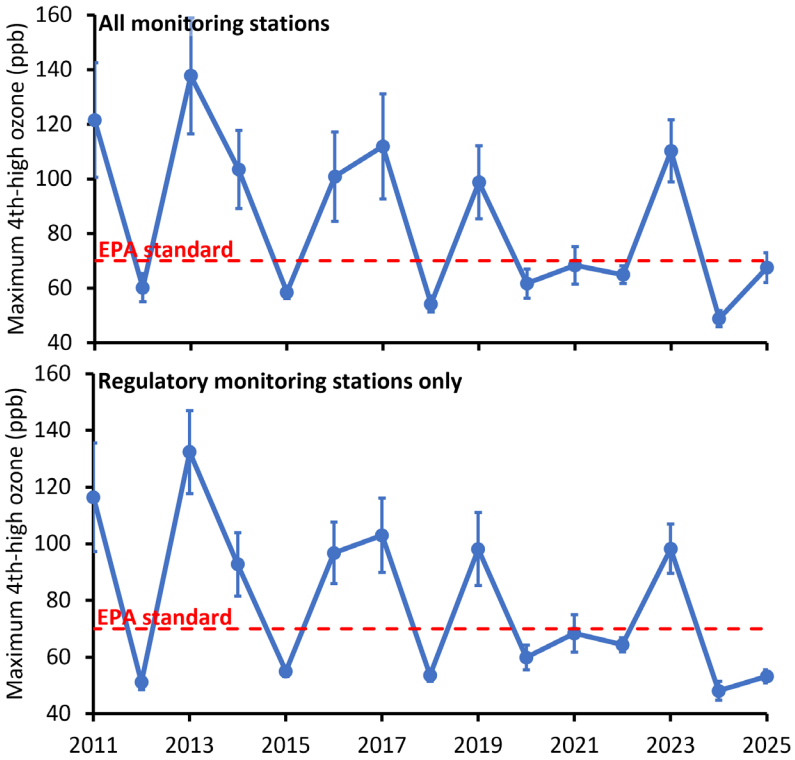

Figure 5-1. Time series of the maximum wintertime 4th-highest daily maximum 8-hr average ozone concentration observed at any monitoring station in the Uinta Basin (top) or at regulatory monitoring stations only (bottom) from winter 2010-11 through the most recent winter. The red dashed lines show 70 ppb, the EPA standard for ozone. The year shown on the X axis is for January of each winter season, so 2011 on the X axis indicates winter 2010-11.

Figure 5-2 shows the maximum number of ozone exceedances experienced at any monitoring station in the Uinta Basin for each winter (i.e., the number of days with 8-hr average ozone above the EPA standard of 70 ppb). The highest number of exceedances (41) occurred during winter 2012-13, but the number for winter 2022-23 was similar (39), even though the 4th-highest daily maximum ozone value for any site was much lower in winter 2022-23 (110 ppb) compared to winter 2012-13 (138 ppb; Figure 5-1).

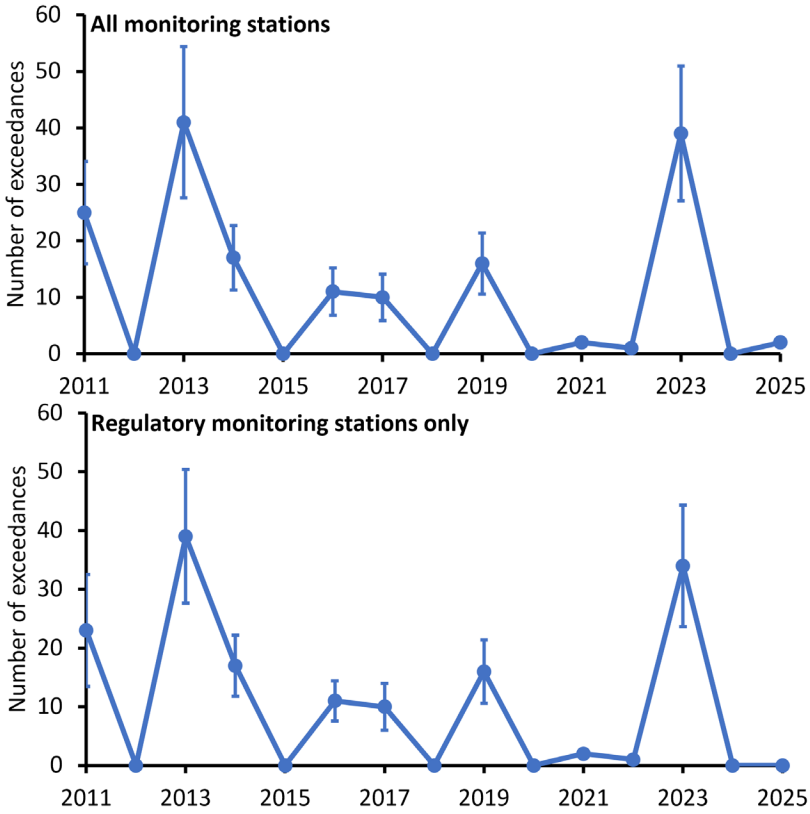

Figure 5-2. Time series of the maximum number of days with 8-hour average ozone above the EPA standard of 70 ppb observed at any monitoring station in the Uinta Basin (top) or at regulatory monitoring stations only (bottom) from winter 2010-11 through the most recent winter. The year shown on the X axis is for January of each winter season, so 2011 on the X axis indicates winter 2010-11.

The Ouray and Red Wash monitoring stations operated during winter 2009-10 and experienced multiple exceedances of the EPA ozone standard in that year, but those data are not shown in the figures because those were the only two sites in operation, whereas all other years have data from 10 or more sites. Also, Utah DAQ measured ozone in Vernal during 2006 and 2007, but those data are not publicly available and are not included here. No wintertime exceedances of the ozone standard were measured in Vernal during that period. Summertime exceedances are not considered in this section.

The three-year average of annual fourth-highest daily maximum 8-hr averages for a given monitoring station (using calendar years) is referred to as that station's design value. The design value is the value EPA uses to determine whether an airshed is in attainment of the 70 ppb ozone standard (design values of 71 and above are out of attainment). EPA used the 2014-16 period in their 2018 decision to designate the Uinta Basin as a nonattainment area for ozone. Table 5-1 shows the ozone design value for past three-year periods. EPA uses the regulatory monitoring station with the highest design value as the design value for the entire nonattainment area, and the table follows that protocol. Note that the table includes summertime data, and summertime exceedances also occur in the Uinta Basin. Many summertime ozone exceedances may be due to wildfires, intrusions of ozone-rich air from the stratosphere, or other events that can be excluded from regulatory consideration.

Table 5-1. Average of the fourth-highest daily maximum 8-hr average ozone during three consecutive calendar years for the regulatory monitoring station in the Uinta Basin with the highest value for each period (a.k.a. the ozone design value for the Uinta Basin). Values in exceedance of the EPA standard are in bold font. Values shown may include summertime ozone events that could be excluded from regulatory consideration. Data are from https://www.epa.gov/air-trends/air-quality-design-values.

3-year period	Design value
2010-2012	**101**
2011-2013	**106**
2012-2014	**94**
2013-2015	**79**
2014-2016	**80**
2015-2017	**88**
2016-2018	**88**
2017-2019	**89**
2018-2020	**76**
2019-2021	**78**
2020-2022	67
2021-2023	**77**
2022-2024	**76**

Figure 5-3 shows the same data from the table, but as a time series. The figure shows that the Uinta Basin ozone design value has decreased since measurements began.

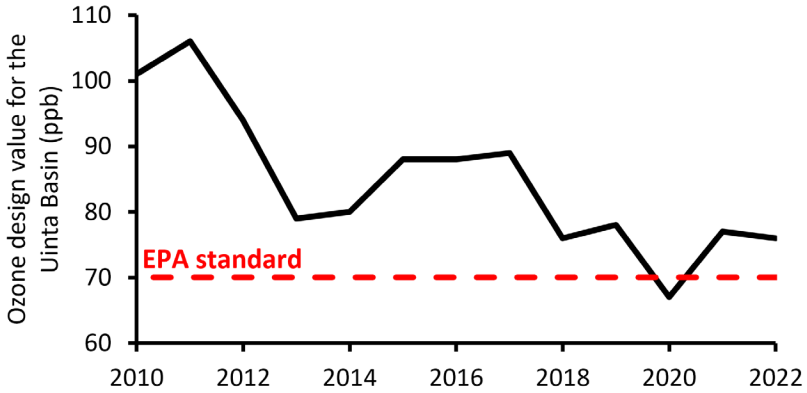

Figure 5-3. Time series of the average of the fourth-highest daily maximum 8-hr average ozone during three consecutive calendar years for the regulatory monitoring station in the Uinta Basin with the highest value for each period (a.k.a. the ozone design value for the Uinta Basin). Values shown may include summertime ozone events that could be excluded from regulatory consideration. The X axis in the figure is the start of each three-calendar year period, so 2010 indicates the period from January 2010 through December 2012. Data are from https://www.epa.gov/air-trends/air-quality-design-values.

5.3. Particulate Matter

Figure 5-4 shows the annual 98th percentile of 24-hour average particulate matter smaller than 2.5 microns in aerodynamic diameter ($PM_{2.5}$) for each calendar year in Roosevelt, Vernal, and Horsepool. This is the metric used by EPA to determine compliance with the EPA 24-hour standard for $PM_{2.5}$ of 35 µg m^{-3}. Roosevelt, Vernal, and Horsepool are the only stations in the Uinta Basin with long-term

measurements of $PM_{2.5}$, and Horsepool only has measurements for the months of December, January, February, and March. Figure 5-5 shows three-calendar year averages for the 98th percentile values at each station, which EPA uses as its "design value" to determine regulatory compliance. The Uinta Basin is currently in attainment of the EPA 24-hour standard for $PM_{2.5}$. The figures show that $PM_{2.5}$ has declined over time at Vernal and Horsepool, but the declining trend is less clear for Roosevelt.

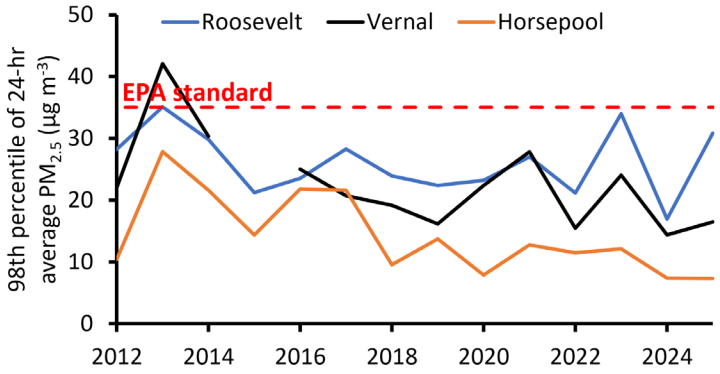

Figure 5-4. Time series of 98th percentile of daily 24-hr average $PM_{2.5}$ concentrations for each calendar year at the Roosevelt, Vernal, and Horsepool monitoring stations. The red dashed line shows 35 µg m^{-3}, the EPA 24-hour standard for $PM_{2.5}$.

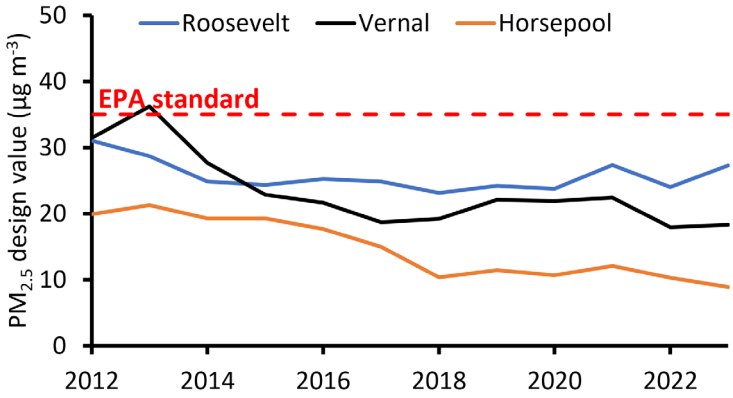

Figure 5-5. Time series of the average of the annual 98th percentile of daily 24-hr average $PM_{2.5}$ concentrations over three calendar years at the Roosevelt, Vernal, and Horsepool monitoring stations. The red dashed line shows 35 µg m^{-3}, the EPA 24-hour standard for $PM_{2.5}$. The X axis in the figure is the start of each three-calendar year period, so 2012 indicates the period from January 2012 through December 2014.

5.4. Trends in the Capacity of Winter Inversion Episodes to Produce Ozone

5.4.1. Ozone Exceedance Days

The number of exceedances of the EPA ozone standard exhibited a decreasing trend from 2010 through 2022 (Mansfield and Lyman, 2021). Mansfield and Lyman (2021) showed that NO_X emissions also decreased over the same period, and Lin et al. (2021) showed that methane emissions also decreased over the same period. Mansfield and Lyman (2021) attributed the decline in ozone and its precursors to (1) a decline in energy production (which was driven mostly by a decline in natural gas production) and (2) regulatory and voluntary action by the oil and gas industry to reduce emissions.

Figure 5-6 shows that the declining trend in winter ozone reversed sharply in 2023 when deep snow cover and many strong inversions allowed for many exceedance days. The figure shows that oil and gas production have also increased, and increased emissions likely also contributed to increased ozone in 2023, though subsequent sections provide evidence that emissions have begun to decline again, even as production has continued to increase.

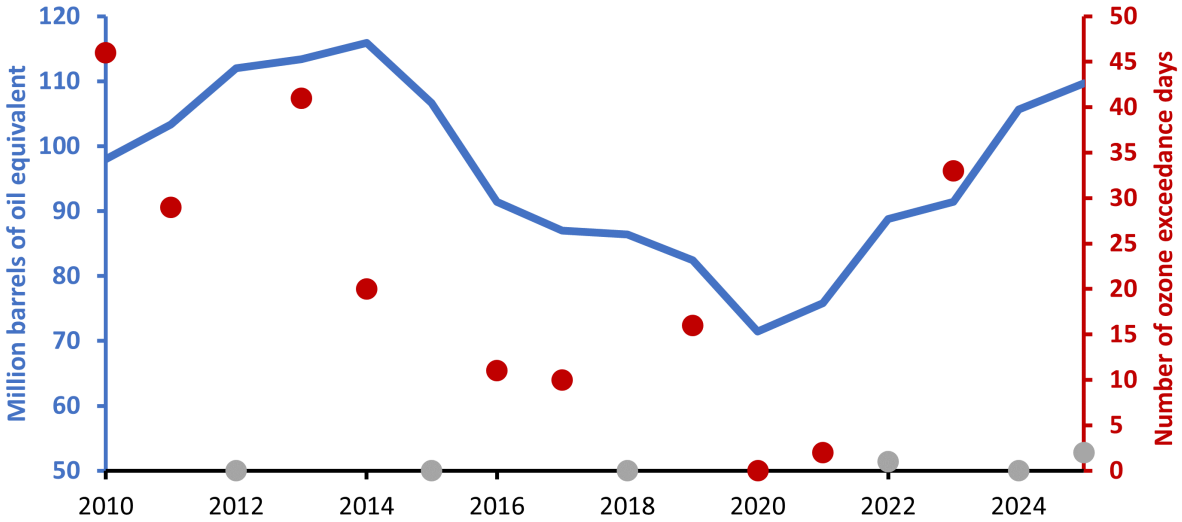

Figure 5-6. Number of ozone exceedance days (8-hr average ozone in excess of 70 ppb at any site) per winter season and total energy production per year in units of barrels of oil equivalent (i.e., sum of oil production and gas production scaled to equivalent amount of energy). Winters with at least 15 days of snow depth greater than 5 cm are shown in red, and other years are shown in grey.

5.4.2. Dependence on Meteorological Conditions

As Figure 5-6 shows, significant local production of wintertime ozone has never occurred and cannot occur without significant snow cover across the Uinta Basin (Oltmans et al., 2014). Indeed, winter ozone levels are positively correlated with snow depth (r^2 = 0.50 for the Horsepool site). The number of winter exceedance days is more strongly correlated with the season-average inversion strength, however (Figure 5-7), since snow cover sometimes exists in stormy or windy conditions that don't allow for strong winter inversion episodes, but strong winter inversion episodes almost never occur without snow cover, and winter ozone needs inversions *and* snow to form (Mansfield, 2018).

Figure 5-7 plots the number of ozone exceedance days per season against the seasonal average pseudo-lapse rate. The lapse rate is the inverse of the change in temperature with altitude. The lower the lapse rate, the stronger the inversion. Typically, lapse rates are measured by releasing temperature sensors attached to helium balloons, but these measurements are expensive and have rarely been performed in the Uinta Basin. As an alternative, Mansfield (2018) used temperature measurements from surface stations at different elevations to approximate the lapse rate (a "pseudo" lapse rate). We follow Mansfield's method of determining pseudo-lapse rates in this section. In Figure 5-7, the number of ozone exceedances is correlated with pseudo-lapse rate as long as the seasonal average pseudo-lapse rate is less than 2 -K km^{-1}. Winter seasons with a seasonal average pseudo-lapse rate above that value generally don't have strong enough or long enough temperature inversions to lead to many days with high winter ozone.

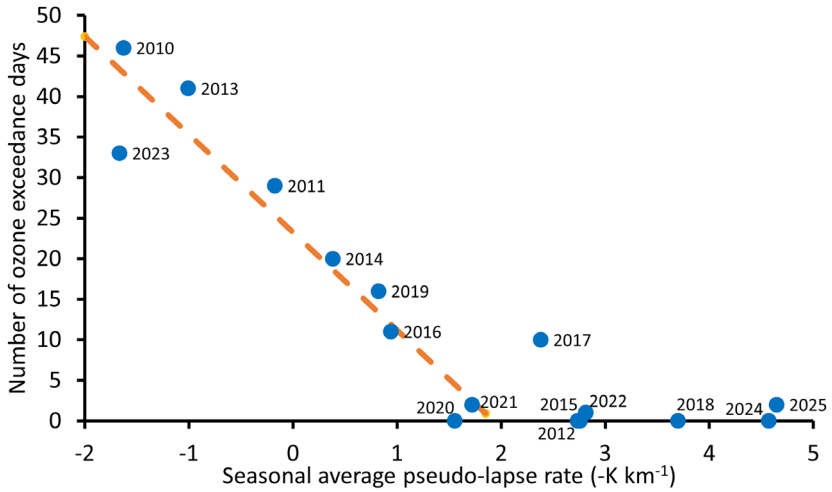

Figure 5-7. Number of ozone exceedance days per winter season versus seasonal average pseudo-lapse rate. Pseudo-lapse rate is a measure of inversion strength (a more negative value indicates stronger inversion) and is discussed at length by Mansfield (2018). The orange dashed line is a linear regression that only includes seasonal average pseudo-lapse rates less than 2 -K km^{-1}. The r^2 value for this line is 0.89.

Figure 5-8 shows the difference between actual ozone exceedance days per winter season and the number of exceedance days expected from the relationship shown by the dashed orange line in Figure 5-7. Figure 5-8 shows an apparent decreasing trend over time, meaning that fewer exceedance days than expected have occurred in recent years. This could indicate that, for similar seasonal conditions, the capacity of the Uinta Basin atmosphere to produce ozone has decreased.

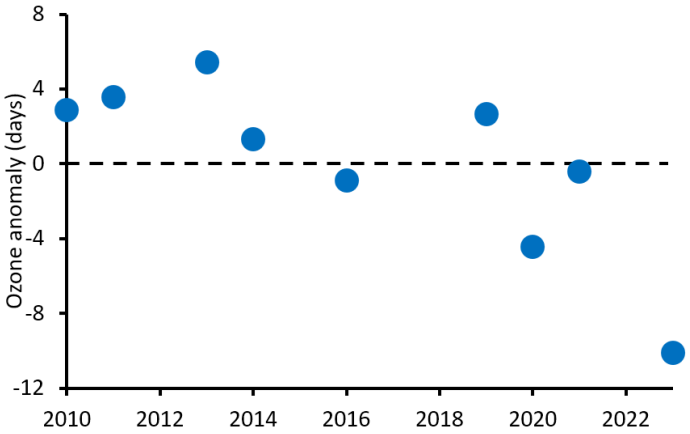

Figure 5-8. Number of excess ozone exceedance days per winter season relative to the amount expected from the relationship shown in Figure 5-7. Only years with seasonal average pseudo-lapse rates less than 2 -K km^{-1} are shown.

5.4.3. Site-level Trends in Ozone Precursors

Mansfield and Lyman (2021) used a linear regression of daily maximum 8-hr average ozone against daily pseudo-lapse rate to "correct" ozone for inversion strength. Mansfield and Lyman (2021) found that the daily pseudo-lapse rate and the daily maximum 8-hr average ozone for most winter seasons were correlated. They used the linear regression for each season to calculate the daily maximum 8-hr average

ozone value that would be expected for a pseudo-lapse rate of -15 K km^{-1}in that season, and they called this metric $\langle[O_3]\rangle_{-15}$. Since the $\langle[O_3]\rangle_{-15}$ value normalizes for the influence of inversion strength on ozone production, they assumed that year-to-year differences in $\langle[O_3]\rangle_{-15}$ were due to differences in ozone-forming emissions, not differences in meteorology. Mansfield and Lyman showed that $\langle[O_3]\rangle_{-15}$ declined from 2010 to 2020, and they attributed this decline to declines in NO_X and organic compound emissions.

We applied the method of Mansfield and Lyman (2021) to methane, NO_X, and non-methane hydrocarbon emissions in an attempt to separate emission trends from meteorological variability. We calculated linear regressions of the pseudo-lapse rate versus daily average methane, NO_Y (as a proxy for NO_X, since NO_Y is the sum of NO_X and its photochemical degradation products), and total non-methane hydrocarbons measured at Horsepool and Roosevelt. We calculated separate regression equations for each site for each year for which data were available. We omitted days with relatively uncertain pseudo-lapse rates ($r^2 < 0.3$ for the relationship between temperature and elevation).

The pseudo-lapse rate was predictive of the majority of the variability in methane, NO_Y, and non-methane hydrocarbons (r^2 or 0.56 ± 0.26, 0.60 ± 0.24, and 0.51 ± 0.25, respectively; average ± standard deviation). We determined residuals by subtracting predicted daily concentrations from measured concentrations. Daily average concentrations of methane, NO_Y, and non-methane organics were significantly correlated with temperature, wind speed, the number of consecutive inversion days, and the number of days since the winter solstice. The residuals, however, were not significantly correlated with any of these variables, which indicates that regression against the pseudo-lapse rate was adequate to account for the influence of these other variables on daily average concentrations.

Following Mansfield and Lyman (2021), we applied site-and-year-specific regression equations to determine daily average concentrations that would be expected in each winter season at a pseudo-lapse rate of -15 K km^{-1}. The results are shown in Figure 5-9 through Figure 5-11. Since this method takes into account the propensity of methane, NO_Y, and non-methane hydrocarbon concentrations to increase under inversion conditions, and since no other significant meteorological correlations existed after inversion strength was taken into account in this way, we attribute the temporal trends in the figures to changes in emissions. We acknowledge that the trends shown in the figures may be local and may not hold true for the Uinta Basin as a whole.

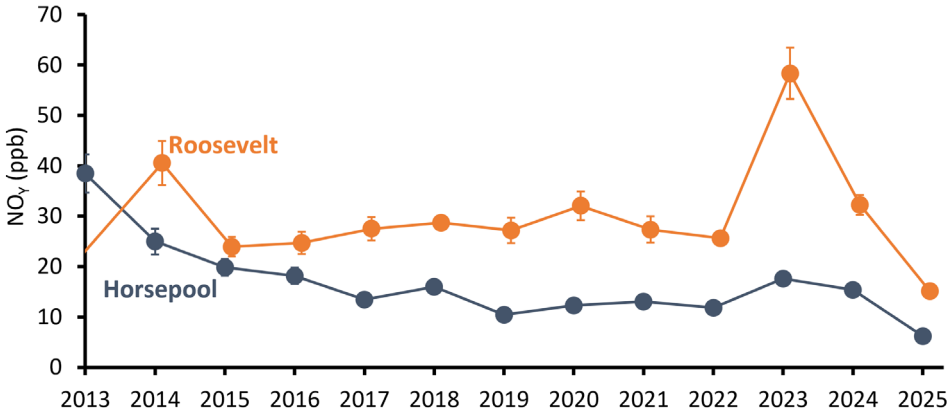

Figure 5-9. Daily average NO_Y (a proxy for NO_X) at a pseudo-lapse rate of -15 K km^{-1}, as predicted from year- and site-specific linear regressions of NO_Y against the pseudo-lapse rate. Whiskers show the combined uncertainty of

the pseudo-lapse rate calculation and the NO_Y measurement. The year shown on the X axis is for January of each winter season, so 2013 on the X axis indicates winter 2012-13.

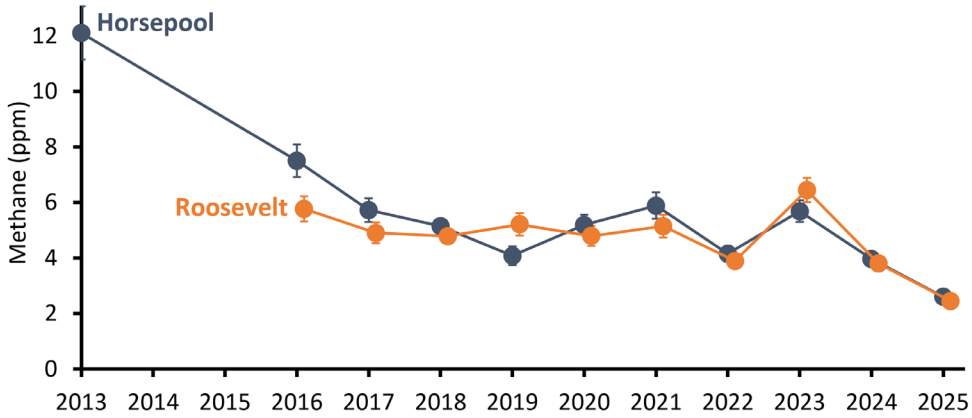

Figure 5-10. Daily average methane at a pseudo-lapse rate of -15 K km^{-1}, as predicted from year- and site-specific linear regressions of methane against the pseudo-lapse rate. Whiskers show the combined uncertainty of the pseudo-lapse rate calculation and the methane measurement. The year shown on the X axis is for January of each winter season, so 2013 on the X axis indicates winter 2012-13.

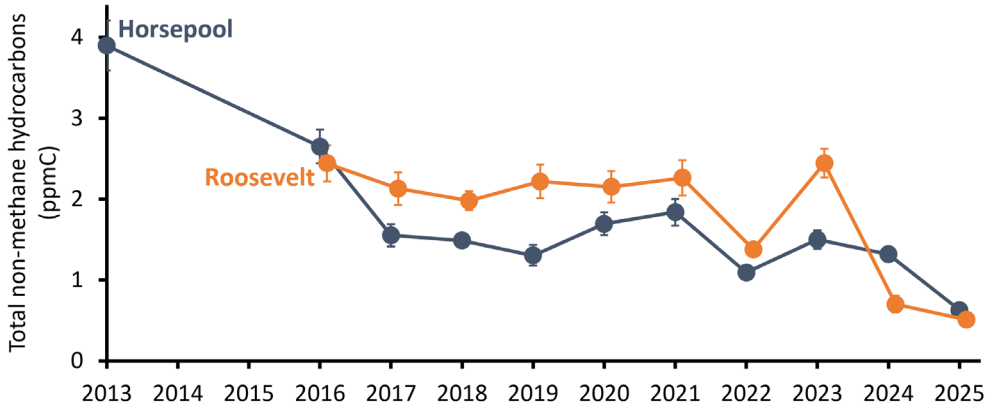

Figure 5-11. Daily average total non-methane hydrocarbons at a pseudo-lapse rate of -15 K km^{-1}, as predicted from year- and site-specific linear regressions of non-methane hydrocarbons against the pseudo-lapse rate. Whiskers show the combined uncertainty of the pseudo-lapse rate calculation and the non-methane hydrocarbons measurement. The year shown on the X axis is for January of each winter season, so 2013 on the X axis indicates winter 2012-13.

The results for Horsepool are similar to the findings of Mansfield and Lyman (2021) and Lin et al. (2021), which all show that emissions of methane, NO_X, and non-methane hydrocarbons have declined since 2013. No clear trend exists for methane and non-methane hydrocarbons at Roosevelt except for the most recent two years, when methane and non-methane hydrocarbons declined. The NO_Y trend at Roosevelt is dominated by a strong upswing in winters 2014 and 2023, and a notable decline in 2025.

5.4.4. Basin-wide Methane Emissions Trends

We have used two methods to assess methane emissions at the Basin scale. The first method is detailed in a final technical report to the Utah Division of Air Quality (Lyman et al., 2024b), which builds upon a

method pioneered by Lin et al. (2021). The Lin et al. method calculates top-down, Basin-wide methane emissions estimates from observed enhancements of methane at Horsepool relative to Fruitland, an upwind baseline site with little influence from local emission sources. The residence time of air parcels measured at Horsepool, and the resulting sensitivity of Horsepool methane enhancements to Basin emissions, are calculated using the Stochastic Time-Inverted Lagrangian Transport (STILT) atmospheric model, which simulates air parcel transport 24 hours backward in time from the measurement site. The STILT model is used to calculate expected emissions from oil and gas facilities, based on the methane enhancement at Horsepool. Details of this method are available in the cited references. In the final technical report, we also estimated emissions of NOx and non-methane organics based on their measured ratio to methane in ambient air.

The second method we used was the Integrated Methane Inversion, which uses methane concentration data from the TROPOMI satellite instrument (Figure 5-12) with the GEOS-Chem photochemical transport model in inverse mode to estimate the emissions required to achieve the methane concentrations observed with TROPOMI (Figure 5-13). Details of the Integrated Methane Inversion method are given in Varon et al. (2022) and Varon et al. (2023). We carried out inversion estimates for Uintah and Duchesne Counties for each two-month period from January 2019 (the first full year that TROPOMI data are available) through December 2024. We used two-month averaging periods to increase the statistical power of the method. Each calendar year was run separately, with a 6-month spin-up period prior to the start of each year, and default emissions from the U.S. EPA greenhouse gas emissions inventory were used to initiate each spin-up period. For this method and the Lin et al. method, only data for spring and summer were used in final analyses because of uncertainty in the models used to generate the meteorological datasets for wintertime conditions in the Uinta Basin.

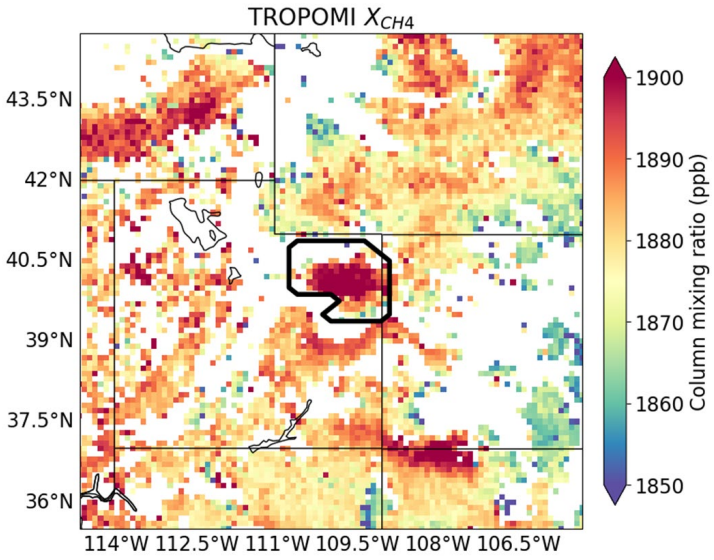

Figure 5-12. Average column mixing ratio of methane for November and December 2021, determined by the TROPOMI satellite methane sensor. The black line shows Uintah and Duchesne Counties at the 25 km resolution of the GEOS-Chem model used for the Integrated Methane Inversion.

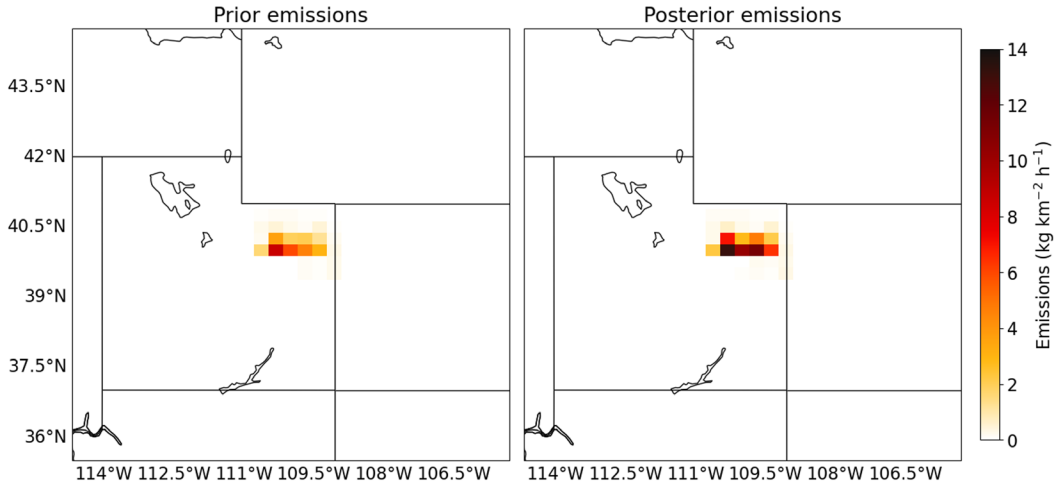

Figure 5-13. Emissions of methane within Uintah and Duchesne Counties determined by the Integrated Methane Inversion method for November and December 2021. Prior emissions are the emissions assumed by the model at the outset, and posterior emissions are those determined by comparing GEOS-Chem model results to TROPOMI satellite-based methane measurements.

The results for the two methods are shown in Figure 5-14. The two methods gave similar results, except for year 2021, during which the estimate from the Lin et al. method was anomalously high. The Lin et al. method relies on measurements from a ground-based measurement station in an oil and gas-producing area (Horsepool) and could have been biased high by one or more local emission sources. An exhaustive exploration of this possibility is available in Lyman et al. (2024b). We assume the satellite-based Integrated Methane Inversion method provides a more representative estimate of emissions for the Uinta Basin as a whole.

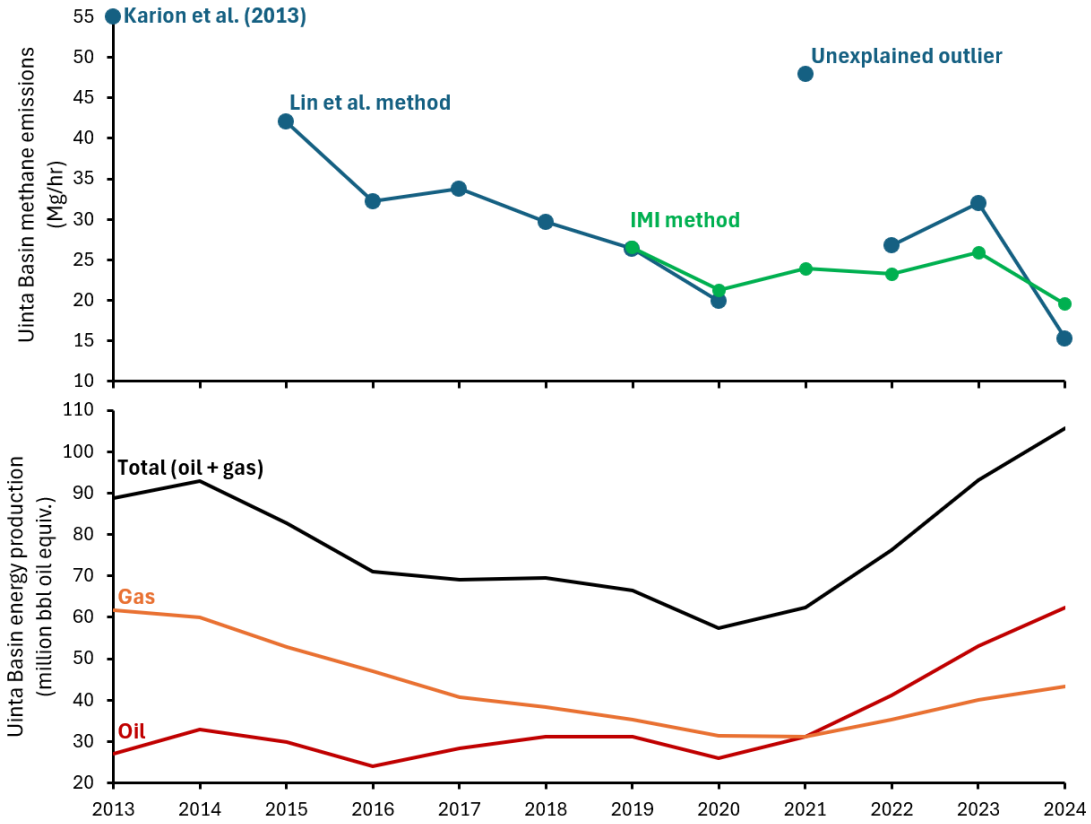

Figure 5-14. Top panel: annual Uinta Basin methane emissions estimated using the Lin et al. and Integrated Methane Inversion (IMI) methods. The 2013 estimate is from Karion et al. (2013). Bottom panel: total annual oil, gas, and combined oil+gas production for Uintah and Duchesne Counties (Udogm, 2023).

Figure 5-14 also shows that Basin-wide methane emissions tracked total fossil energy and natural gas production in the Uinta Basin, declining from 2013 through 2020, and then increasing thereafter as production increased. This is true for all years except 2024, when methane emissions dropped markedly while oil and gas production continued to increase.

One way of tracking methane emissions from oil and gas infrastructure is as a percentage of energy produced. In the Uinta Basin, the percentage of fossil energy produced that was lost to the atmosphere as methane has declined almost continuously over the study period (Figure 5-15). In 2013, for a given amount of oil and gas produced, 5% of that energy was lost to the atmosphere as methane. In 2024, only 1.5% was lost as methane. This shows that oil and gas production in the Basin has become more efficient over time.

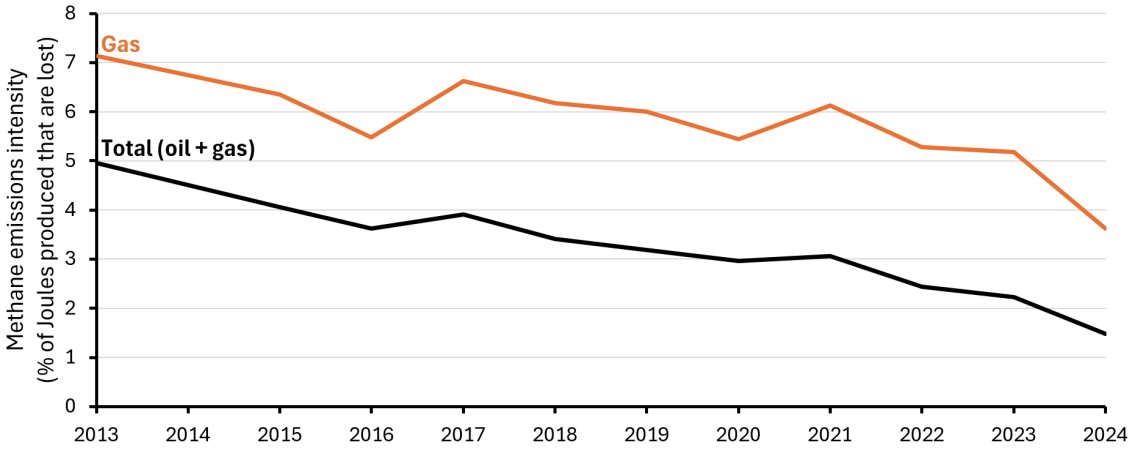

Figure 5-15. Annual time series of the percentage of natural gas or total energy (oil+gas) produced in the Uinta Basin that was lost to the atmosphere as methane. Uinta Basin methane emissions data from the Lin et al. method were used through 2018, and data from the Integrated Methane Inversion method were used from 2019 through the most recent year.

5.5. Acknowledgments

This work was funded by the Utah Legislature and Uintah Special Service District 1.

6. Ozone Alert Program

Authors: John R. Lawson and Seth Lyman

At the request of oil and gas industry representatives and with input from the Utah Division of Air Quality, TriCounty Health, and several oil and gas companies, we created a program in 2017 to alert oil and gas companies when high winter ozone is expected. The program includes a web page (https://www.usu.edu/binghamresearch/ozone-alert) to describe the program and allow individuals to sign up to receive alerts. When individuals sign up, we collect their name, company name, and email. We have also created a comprehensive real-time weather and forecasting page, https://basinwx.com/.

We send everyone on the list an email when local ozone formation is expected, if an ozone episode extends longer than expected, and when episodes end or are expected to end. We attempt to forecast ozone episodes up to two weeks in advance, but we acknowledge increasing uncertainty with more distance into the future. The purpose of this program is to provide users with information that allows them to reduce ozone-forming pollution when it matters most.

Winter 2024-25 had two days with ozone exceeding the EPA standard of 70 ppb, which occurred during a snow event that led to snow accumulation throughout much of the Basin. Periods during which we alerted subscribers that high ozone was likely are indicated in Figure 6-1. Alerts given are color-coded in the figure by risk severity.

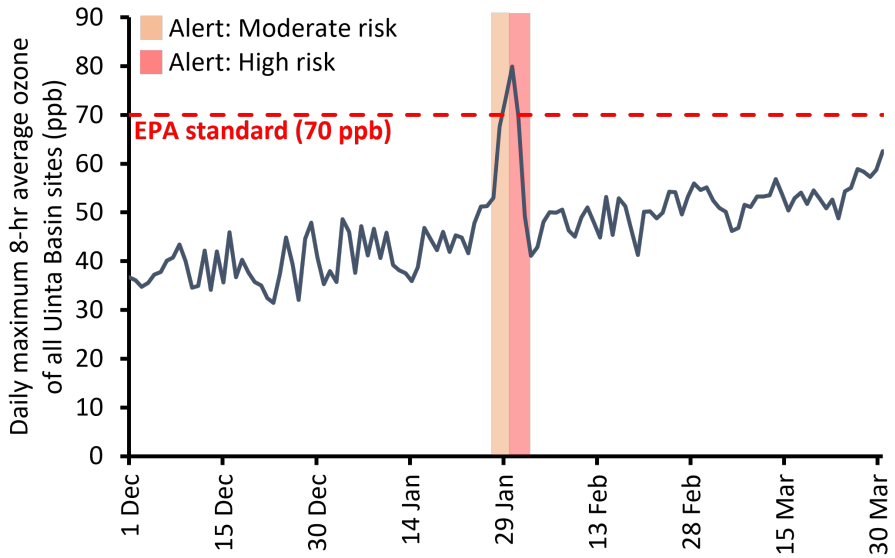

Figure 6-1. Time series of the highest daily maximum 8-hr average ozone the site observed at any monitoring site in the Uinta Basin during winter 2024-25. The EPA ozone standard is shown as a red dashed line. Periods during which USU issued ozone alerts are shown as colored shading.

The program currently has 192 subscribers, among whom 42% represent the energy industry, 23% are affiliated with government entities, 19% are members of the local public, 11% are academics, 2% are representatives of the media, and 1% are from environmental groups.

7. Clyfar: Wintertime Ozone Forecasting System

Author: John R. Lawson

7.1. Executive Summary

Winter 2024-25 marked the first winter in which Ozone Alert was supported by an experimental ozone prediction system, Clyfar, in the Uinta Basin. The Bingham Research Center (hereby "Center") combined two initiatives: the Clyfar ozone forecasting system discussed herein, and the Ozone Alert early warning program. Further work has led to the BasinWx.com website to display interactive products undergoing active development. After completing its first quasi-operational season serving Basin stakeholders, Clyfar version 1.0 will be deployed operationally on 1 December 2025 to support Ozone Alert 2025-26.

This project continues to fill the gap between math theory, cutting-edge machine learning and artificial intelligence, and the practical needs of stakeholders. By translating complex, uncertain weather forecasts into accessible visual products and plain language summaries, we are demonstrating that advanced forecasting can, despite some needed tuning, serve diverse audiences from researchers to industrial operations to members of the public.

During the reporting period, we completed the following with regard to Clyfar and ozone forecasting:

- Successful detection of temperature inversion (cold pool) potential during winter 2024-25.
- First signal of inversion conditions over 10 days out, enabling Ozone Alert forecasters to monitor the evolution of forecasts over long periods
- Real-time experience forecasting gave an intuitive sense of where, when, and why Clyfar has performed poorly, informing further development
- Community engagement and interactive displays of forecast and observed air-quality data, via the soft-launched BasinWx.com website, will improve communication on various levels of complexity appropriate for stakeholder needs
- The existing ubair.usu.edu website will be decommissioned as part of the BasinWx.com project.

7.2. Initial Challenge

7.2.1. Winter Ozone Behavior

After snowfall and increasing surface pressure in Utah's Uinta Basin, ground-level wintertime ozone can spike to unhealthy levels, sometimes exceeding national air quality standards. This happens when four specific weather conditions align (Mansfield, 2018; Lyman et al., 2024a):

1. **Fresh snow cover** creates a highly reflective surface that bounces sunlight back into the atmosphere, increasing solar energy available for reactions that create ozone.
2. **High atmospheric pressure** allows quiet meteorological conditions that allow cold air to settle in the Basin and form a pool of stable, dense, cold air trapped near the ground.

3. **Calm winds** prevent this cold air and ozone precursors from oil and gas operations from mixing away or moving out of the Basin. This forms a temperature inversion where it becomes warmer with height: an “upside-down” configuration that is stubborn to clear from the Basin.
4. **Clear skies and higher solar angle** increase the solar energy needed for ozone-forming chemical reactions.

When these conditions persist for several days or more, such as when a large-scale anticyclone weather system remains over the Intermountain West for a period, emissions from oil and gas operations (primarily nitrogen oxides and volatile organics) become trapped in the cold pool. The snow-reflected sunlight drives chemical reactions that convert these emissions into ozone, which accumulates day after day until weather patterns change and disperse the cold pool, the snow melts under persistent and sufficient insolation when temperatures are near freezing, or increasingly strong insolation in March that disrupts the cold pool through mixing (i.e., thermals of warm air that churn polluted surface air with free, cleaner air higher up).

7.2.2. The Problem with Traditional Ozone Simulations

Standard weather forecasting models that predict large-scale meteorological conditions are crucial to drive chemistry simulation models. Cumulative work from the Center has shown poor meteorology modeling hamstrings ozone-forecast quality more than chemistry modeling (Lyman et al., 2024b). Traditional grid-based numerical weather prediction models often perform poorly in mountainous regions due to two major obstacles, mainly stemming from the uncertainty of predicting a phenomenon that is sensitive to small changes in snow depth:

1. **Computational demand** required to accurately simulate the Basin’s complex terrain and shallow cold pools. The small length scale of the cold pools requires computer models to run with a grid spacing of less than 1 km. Running more than one simulation at this resolution—i.e., to estimate the variability or uncertainty of the future prediction with how different each simulation is from the others—exceeds practical resources for operational forecasting, both on a laboratory and national-center scale. However, many simulations with varying initial values are required to capture high-impact, rare events.
2. **Data scarcity** provides an obstacle to identifying the "tipping point" between conditions that do or do not support persistent temperature inversions. The formation of the cold pools is sensitive to small changes in snow cover, pressure, and wind, so small forecast errors in these inputs can lead to completely missed events or too many false alarms. It further restricts the ability of machine-learning methods to “train” Clyfar to produce better forecasts in future seasons. More of this discussion can be found in Davies et al. (2025).

7.2.3. Deliverables for Stakeholders

Effective decision-making requires forecasts that:

- Provide advance warning at lead times of up to 15 days; beyond this, there is no benefit in any meteorological forecasting models due to the rapid growth of errors over time.
- Communicate confidence alongside predictions, i.e., distinguishing "highly likely" from "possibly, but uncertain"

- Run efficiently enough to run four times daily throughout each winter with many parallel simulations to better capture rare events that are highly sensitive to changes in snowstorm tracks, for instance
- Remain transparent to researchers and users so all parties understand what drives forecast changes, and to build trust in the prediction model (i.e., reduce the perception that Ozone Alert forecasters do not understand a “black box” and cannot trust when forecasts are useful or not)

These needs motivate continued development of Clyfar. Version 0.9, the development version at the time of writing, is documented technically in an upcoming report (*CLYFAR v0.9 Research to Operations: Wintertime Ozone Forecasts for Utah’s Uinta Basin*, John R. Lawson, in preparation).

7.3. Solution: Combining Expert Knowledge with Computer Predictions

7.3.1. Prediction System (Clyfar) Overview

Clyfar combines expert meteorological knowledge with ensemble weather forecasts to predict daily maximum ozone concentrations 1–15 days ahead. Rather than simulating chemical reactions at, say, kilometer-scale resolution, Clyfar asks a simpler question: *Given what we know about how weather drives ozone in the Uinta Basin, how plausible is an elevated ozone event under these forecast conditions*?

The system operates through six stages:

1. Download ensemble weather data from NOAA's Global Ensemble Forecast System (GEFS)—31 different forecast scenarios run four times daily (Zhou et al., 2022)
2. Process meteorological inputs to extract Basin-wide representative values for snow depth, pressure, wind, and solar radiation
3. Evaluate *fuzzy logic* rules that encode expert knowledge about how these weather conditions relate to ozone production (Dubois and Prade, 1988)
4. Generate possibility values representing the plausibility of four ozone categories: background (approx. <40 ppb), moderate (40–60 ppb), elevated (60–80 ppb), and extreme (>80 ppb)
5. Join various statistics to quantify forecast uncertainty (confidence) arising from different weather scenarios that the forecasters have in hand
6. Produce visualization products, including heatmaps and meteograms, for the Ozone Alert program and BasinWx.com website

7.3.2. Communication of Risk

Traditional forecasts provide a single number: "Tomorrow's maximum ozone will be 58 ppb" or "There's a 40% chance of exceeding 70 ppb." The Ozone Alert program also issues outlooks with these forecast amounts in mind. However, these statements hide important information about confidence. A 40% probability derived from reliable data with known uncertainties is fundamentally different from a 40% guess when the model has never seen similar conditions (Lawson 2024).

Clyfar uses possibility theory, which is a mathematical framework for analyzing a system with incomplete knowledge. It is useful when we have so little data in our archives that percentages are

unreliable. To make these distinctions explicit, and instead of forcing everything into probabilities that must sum to 100%, possibility theory asks two separate questions:

- How plausible is this outcome? (Possibility: 0 = impossible, 1 = completely consistent with current knowledge)
- How inevitable is this outcome? (Necessity: 0 = many alternatives remain viable, 1 = this must happen)

Crucially, when the system encounters meteorological conditions outside its knowledge base—for example, conflicting inputs where snow is present but solar insolation is strong (i.e., snow should melt)—it may signal this explicitly as *ignorance* rather than arbitrarily assigning probabilities.

7.4. How It Works: From Weather Data to Ozone Forecast

7.4.1. Step 1: Representative Weather Values

GEFS provides grid-level forecasts across the Basin every 3 hours for 16 days. Clyfar collapses this spatial information into single representative values for the Basin, rather than fine-gridded values that cannot be validated in the real world. Our aggregation choices reflect physical understanding: ozone production is driven by widespread (not localized) snow cover, a more “peaked” pressure (not simply a daily average), and a representative value for incoming solar radiation.

7.4.2. Step 2: Fuzzy Membership Functions

Meteorological values get translated into degrees of "truthiness" for linguistic categories (Lawson and Lyman, 2024). For example:

- Wind of 1 m/s is "completely calm" (membership = 1.0)
- Wind of 3 m/s is "somewhat calm, somewhat breezy" (membership = 0.5 for each)
- Wind of 5 m/s is "completely breezy" (membership = 1.0)

These smooth transitions encode threshold uncertainty. This is intuitive: there is no sharp cutoff where "calm" becomes "breezy" (Zadeh, 1996). The transition widths and positions come from observational case studies of historical ozone events and are continuously used to calibrate these functions.

7.4.3. Step 3: Fuzzy Rule Evaluation

Six expert-derived rules link weather conditions to ozone outcomes. For example:

Rule 4: IF snow is sufficient AND wind is calm AND pressure is strong AND solar is high THEN ozone is extreme

Each rule's "activation level" equals the minimum membership across its conditions—the weakest link in the chain. All activated rules for a given ozone category combine using the OR operation (taking the maximum). This multi-rule structure allows different weather pathways to produce similar ozone outcomes, can cope with conflicting evidence, and is honest about this ignorance.

7.4.4. Step 4: Possibility Distribution and Scalar Forecasts

The combined rule activations create plausibility values of each ozone category between 0 and 1. This distribution can have multiple high-possibility categories simultaneously—for example, "moderate" and "elevated" might both be fully possible when conditions are marginal. For stakeholders who need single-number forecasts, Clyfar "defuzzifies" by taking, e.g., the 90th percentile of the possibility curve. We may also generate probability calculations: "*22 out of 31 Clyfar members show elevated ozone, so there is 71% probability of exceeding 60 ppb*."

7.4.5. Step 5: Three-Component Uncertainty Communication

Clyfar's key innovation lies in communicating three aspects of uncertainty:

- Possibility: How plausible is elevated ozone given current knowledge? (Upper bound on probability)
- Ignorance: How much do we not know? (Gap between maximum possibility and 1.0)
- Conditional Necessity: If we assume the model knows everything relevant, how inevitable is elevated ozone?

This framework gives risk-averse users actionable information: if extreme is *plausible* at a 7-day lead time, protective actions may be warranted even if we cannot assign a precise probability. The possibility bounds the worst case; ignorance reveals whether that bound is trustworthy; necessity gives the more certain prediction.

7.5. Winter 2024-25: Quasi-Operational

7.5.1. Deployment

Clyfar v0.9 operated quasi-operationally throughout winter 2024-25 in support of the Uinta Basin Ozone Alert program. The system ran intermittently from late December through March, with intensive coverage during periods of elevated ozone risk. In total, 162 forecast runs generated GEFS (meteorological) meteograms, Clyfar ozone-possibility heatmaps, and Ozone Alert text outlooks that were delivered via email. These products will continue to be sent via email in 2025-26, and will be duplicated on the BasinWx.com website (albeit with the site subject to intermittent technical issues on a new supercomputer server).

7.5.2. Late January 2025 Exceedance Event

The winter season was characterized by relatively benign ozone conditions through early January, with snow cover arriving later in January (Figure 7-1). While ozone increased above background levels at many sites, the only site with ozone above the EPA ozone standard of 70 ppb (for an 8-hour average) was Castle Peak. Clyfar successfully provided advance warning of elevated ozone risk during this period, but ended the window of high ozone too early. Forecasters during this event recall the debate over whether snow would persist or melt, showing the difficulty of identifying a “tipping point” in snow depth.

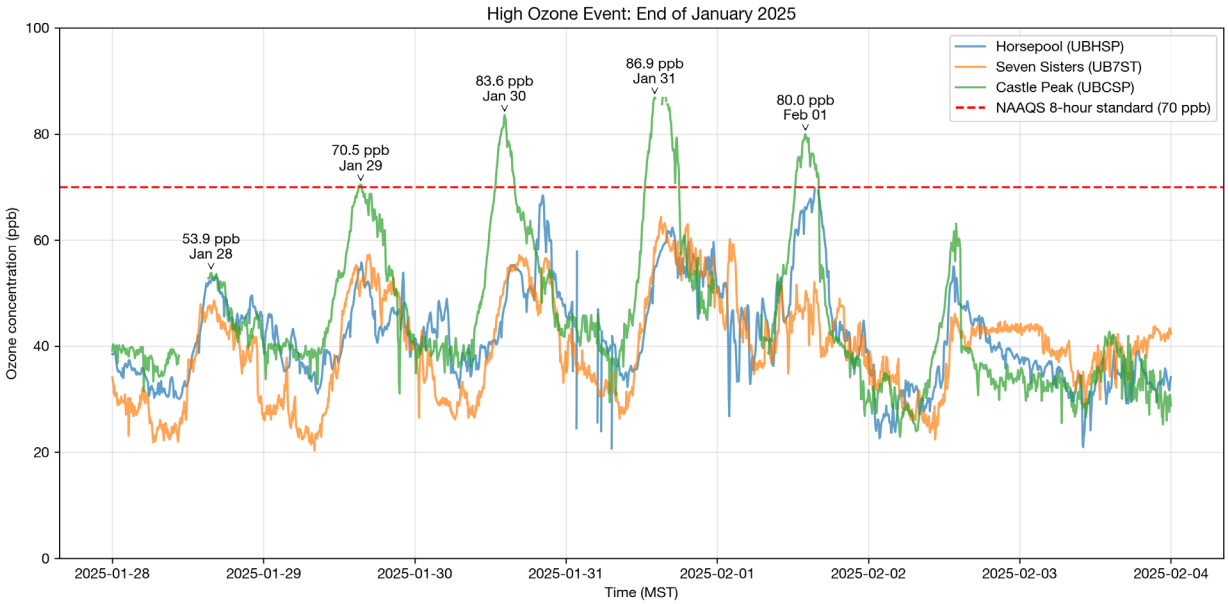

Figure 7-1: 5-minute average ozone from 28 January through 4 February 2025, as sampled by USU-operated air quality stations. Mild filtering is applied to remove noise; otherwise, these are uncorrected data.

Analysis revealed a systematic bias in snow depth estimates during this event (Figure 7-2), traced to an elevation masking bug in v0.9.0. The elevation weighting function incorrectly assigned high weights to Basin-rim cells above 2,500 m elevation, where snow accumulates but doesn't affect ground-level ozone production. This led to overestimation of representative snow depth, producing some false-alarm forecasts when rim snow persisted, but Basin-floor snow had melted. Of course, this would not have helped the case discussed here.

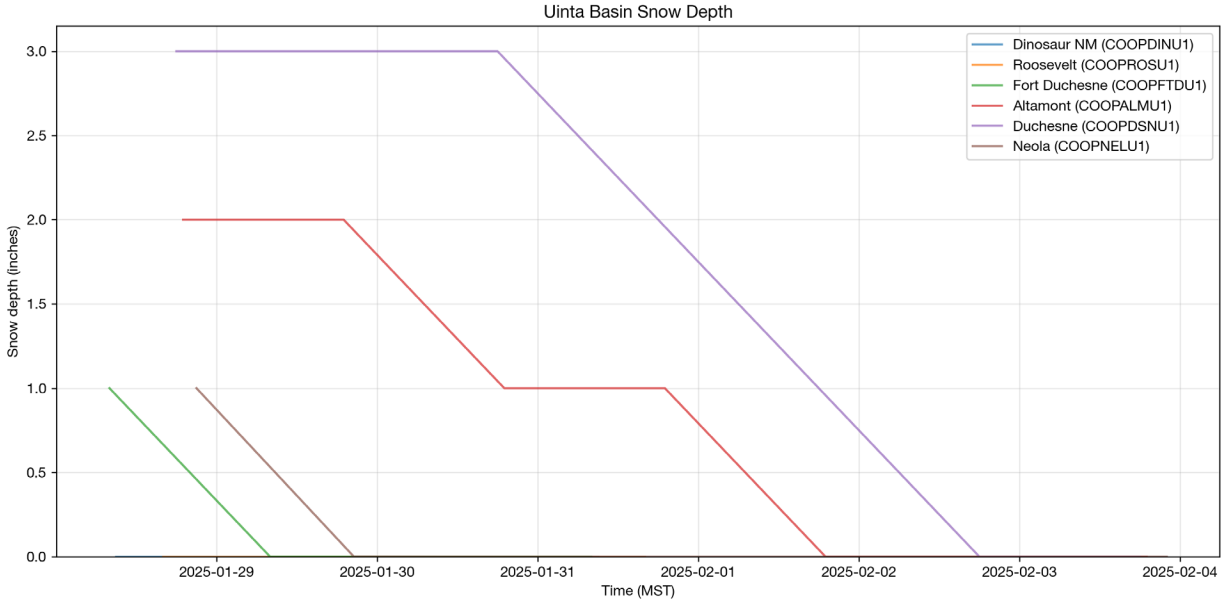

Figure 7-2: Observed snow depth at Basin stations.

The missed case (Figure 7-3; starting at the same time as in the above figures) shows that Clyfar has the capacity to capture high-ozone events, but is at the mercy of numerical weather prediction accuracy

unless we correct for consistent errors. In this case, our input weather data was not aware of snow lying across the Basin. This is fixed in version 1.0 by taking observed snow-depth and nudging the forecast snow depth up or down accordingly to make the value representative of actual conditions.

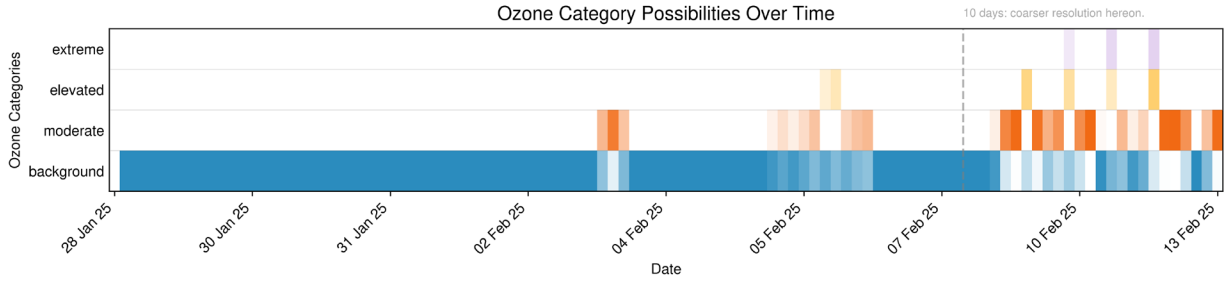

Figure 7-3: Clyfar possibility output initialised at sunrise, 28 January 2025, while snow was observed on the ground but not in the weather models that Clyfar uses as input. Darker colors indicate a greater chance of seeing the indicated ozone categories.

Nonetheless, this failure exemplifies the value of Clyfar's transparency and hands-on expert-rule system. The error source is quickly identified in a post-mortem by examining membership function inputs, allowing rapid diagnosis and correction during ongoing development. Version 0.9.3 (hotfixes) corrected the elevation mask implementation.

7.5.3. Next Steps

Reforecasts (i.e., re-running old forecasts with a fixed but old version) are underway. Also, the Center aims to publish the results of Clyfar's first "version 1.0" winter after the ozone season ends in March 2026. Version 1.0 will run beginning 1 December 2025 every six hours (times may vary due to dependence of Clyfar on receiving GEFS data from federal servers). Summaries will be created by large language models and placed on www.basinwx.com, but this is highly experimental, and Ozone Alert users will be directed to text in emails primarily.

7.6. Acknowledgements

This work was primarily funded by Uintah Special Service District 1 and the Utah Legislature. Some student wages for the project were paid by an endowment from Anadarko Petroleum and the Bingham Family Foundation.

8. BasinWx: A New Website for Air-Quality and Weather

Authors: John R. Lawson, Michael J. Davies, Elspeth C. Montague, Luke Neilson

8.1. Summary

The Bingham Research Center's existing air quality data website at ubair.usu.edu was designed to give real-time air quality data to stakeholders and the public. Simply due to the march of technology, the site, which uses old, proprietary software, has become outdated and is no longer the most effective way to disseminate this information. For instance, the data do not go automatically to a central repository for use by the public as part of a nationwide observational network. Hence, there was a need for a new site to best serve our stakeholders. A prototype was completed last winter, but insurmountable issues with security ports on university servers precluded public release. Instead, the group released Ozone Alert texts in the same way as previous seasons: solely by email. Output from graphics created to visualize ozone forecasts was pasted into email. The main lesson was to move the website to a third-party, cloud-based server, including branding via the domain name of www.basinwx.com. Initially, the goal was simply to recreate the original static map on the old site, improving it with modern web languages. For instance, instead of a flat, static map, the user would be able to pan or zoom, similar to the experience of using Google Maps. Over the past year, we have added a number of additional features to the site.

8.2. Initial Development

8.2.1. Proof-of-Concept: Running Privately During 2024-25

The blueprint and first version of the website were running by early January, but we could not make the site accessible publicly due to security limitations of the university's web server. This did not affect the ubair.usu.edu website or the Ozone Alert program. Likewise, development continued internally during this time. The original websites will continue as a failsafe for at least the next season as a failsafe.

8.2.2. Moving to Cloud Server with New BasinWx Domain

Akamai (Linode) offered a free month on their cloud-based web server to test deployment. With help from our research assistants and cutting-edge artificial intelligence (AI) software, we quickly iterated over the blueprint. We avoided the downtime experienced worldwide by those who chose Amazon Web Services for their cloud computing, as an example of the resilience and value-for-money of the Linode server (mid-level, European-based, twice-used video-call customer support at no charge).

8.2.3. Public Archive

All website code and versions are archived on GitHub, allowing for full transparency and reproducibility. More in-depth outreach about the site and its functionality will be disseminated via www.jrl.ac.

8.3. Functionality Walkthrough

8.3.1. Air Quality

8.3.1.1. Live Monitoring and Data Archive

This is the main drive of funded research (Figure 8-1). We send live data from our air quality measurement stations to an online repository, https://synopticdata.com/, in a mutually beneficial arrangement. Not only do we obtain access to others' data for private research use and display on our website, but we also have a publicly-accessible, maintained archive with near-instant logging of our data, which we then download back to our web server when needed, along with many other available datasets. This keeps all our codebase functions and databases as one object.

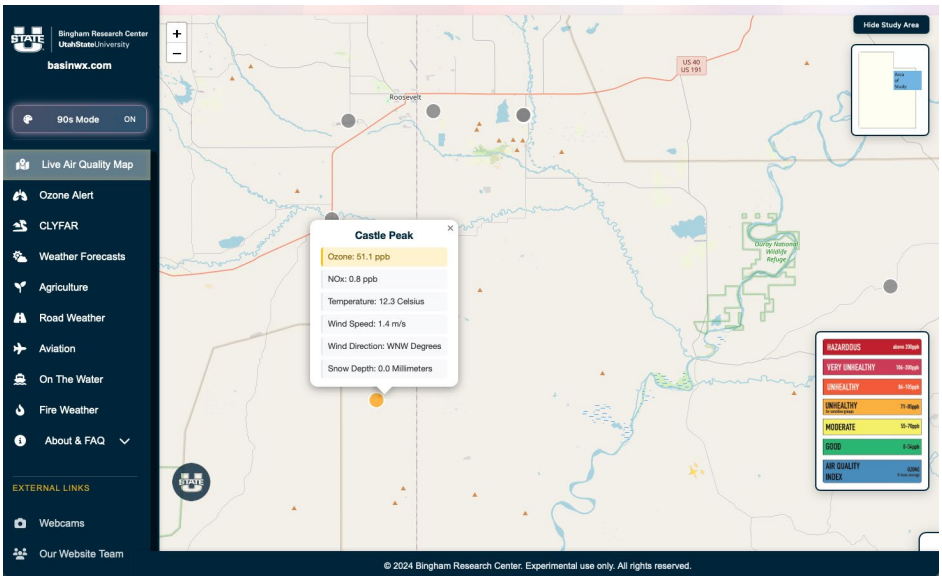

Figure 8-1. Air quality test page for real-time data.

8.3.1.2. Forecasts (Clyfar)

See the previous section for more information. We show Clyfar forecast output as static heatmaps at present (Figure 7-3) and are working on making Clyfar output user-interactive. Stretch goals include foundations for more research (e.g., deducing snowfall from webcams, greatly increasing snow-related datapoints around the Basin), and proofs-of-concept for research funding proposals to support air-quality prediction, local airports, road safety, etc.

8.3.2. General Weather and Recreation

We are implementing pages for general weather, as well as recreation or tourism topics such as "on the water" for fishing and boating.

8.3.3. Aviation

We are implementing a page specific to aviation weather needs. This will include maps of airports with the probability of crosswinds from thunderstorms, for example. This, along with a 3D map of weather data, should serve travelers to and from the Uinta Basin via improved flight planning when utilizing local airports.

8.3.4. Road Weather

The is great demand on local social media for information about mountain passes, and we address this with an interactive map of open-sourced fair-usage data from the Utah Department of Transportation that shows webcams, snow-plows, accidents, and so on (Figure 8-2). This also allows for future development of algorithms that, for example, estimate snowfall from white pixels in a webcam. Traffic reports will be displayed as colored warnings and points.

Figure 8-2. Road conditions test page, using live data from the Utah Department of Transportation within fair-use limits.

8.3.5. AI summaries

AI summaries of graphical/text forecasts (Lawson, 2024) allow informed, concise, plain-language overviews of general weather, air quality forecasts (Clyfar), live air-quality data, risk communication via Ozone Alert, etc., especially when constrained to use language appropriate for the user. We are testing the implementation of these features (Figure 8-3).

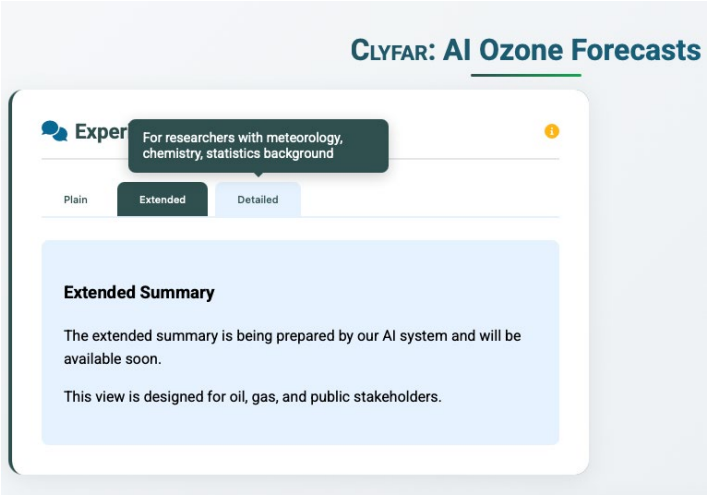

Figure 8-3. A tabbed placeholder for AI overviews at different complexity levels for various stakeholders

8.4. Roadmap

8.4.1. Stability Testing (Nov 2025)

This is a soft launch, which will involve posting on social media and taking comments from the public and key stakeholders. Our aim is for a low number of reliable features at this stage due to ongoing stability tests and occasional, inevitable downtime due to bugs.

8.4.2. Full Launch (Dec 2025)

Our goal is for a full launch by 1 December to support Ozone Alert with deeper dives into future and past events to support emails sent as part of the program. This will be done in tandem with social outreach videos related to Ozone Alert.

8.4.3. Continuing Feedback from Stakeholders

During and after the full launch, we welcome feedback that allows us to learn stakeholder needs. The team uses a codebase versioning system and modern best practices, so a parallel website could be launched if necessary to trial or roll back changes. The team can also internally tweak a development for intermediate feedback during development. This can be done publicly for further comment by more technologically-minded users.

8.5. Comment on student involvement

Due to the rapid development of AI "agents" that assist coding development, onboarding of our current group of high-school student researchers has been easier, given that website development partly became coding as natural language (we call that "CANAL") through AI tools. Initial student-written proof-of-concept code was iterated: research has shown this vastly improves our team's performance. Hence, not only have we lowered the bar for a fast return-on-investment for students such as Michael Davies, an undergraduate who published a first-author research paper this year (Davies et al., 2025), we

have also improved preparation for the next-generation cutting-edge workforce, whether it be here in the Uinta Basin, in Logan, or beyond. We train our students in the ethical, efficient use of AI.

8.6. Acknowledgements

This work was primarily funded by Uintah Special Service District 1 and the Utah Legislature. Some student wages for the project were paid by an endowment from Anadarko Petroleum and the Bingham Family Foundation.

9. Uinta Basin Snow Shadow: Impact of Snow-Depth Variation on Winter Ozone Formation

Author: Michael Davies

9.1. Introduction

The Uinta Basin in eastern Utah, USA, is subject to intermittent, yet severe, episodes of elevated surface ozone concentrations during winter, a phenomenon distinct from typical summertime ozone problems. This air quality issue arises when specific meteorological and geographic conditions coincide. Following heavy snowfall, cold, dense air flows drain into the Basin, forming a persistent cold-air pool characterized by a temperature inversion. This inversion effectively traps ozone precursors—primarily volatile organic compounds and nitrogen oxides (NO_x)—which are emitted mostly by local oil and gas industry operations.

Snowfall is paramount to this system. The high reflectivity, or albedo, of the snowpack reflects incoming solar radiation, significantly increasing the amount of energy available for the atmospheric chemistry that leads to ozone formation. This feedback loop can result in ozone that exceeds the U.S. National Ambient Air Quality Standards (NAAQS) threshold of 70 ppb. Days with snow cover throughout the Uinta Basin can lead to unhealthy levels of ozone, while days with little snow cover never lead to high ozone.

The Basin's location leeward (downwind) of the Wasatch Mountains suggests the potential existence of a precipitation shadow or snow shadow—a region of sharply reduced precipitation caused by subsiding, drier air. This study was undertaken to gauge evidence for this snow shadow effect and determine if spatial variations in snow depth across the Basin floor impact ozone levels.

The following is a summary of the study. Full results from the study are available as a peer-reviewed publication, (Davies et al., 2025).

9.2. Background

The mechanism of a precipitation shadow involves moist flow rising over high terrain (in this case, the Wasatch Range), causing cooling and condensation, with precipitation occurring predominantly on the windward side. The resulting drier air then descends on the leeward side (the Uinta Basin), warming adiabatically and suppressing precipitation. This would hypothetically lead to less snow cover in the western Basin compared to the eastern portions.

For winter ozone to occur, several factors must align: the location must be equatorward enough for sufficient sunlight but poleward enough (and/or at high enough elevation) to preserve the snowpack; it must possess complex terrain to facilitate cold-pool formation; and there must be precursor emissions that allow for ozone formation chemistry.

The schematic representation of the Basin's winter-ozone formation (Figure 9-1) shows the critical role of the persistent cold pool over snow, which increases the photolytic pathway to wintertime ozone.

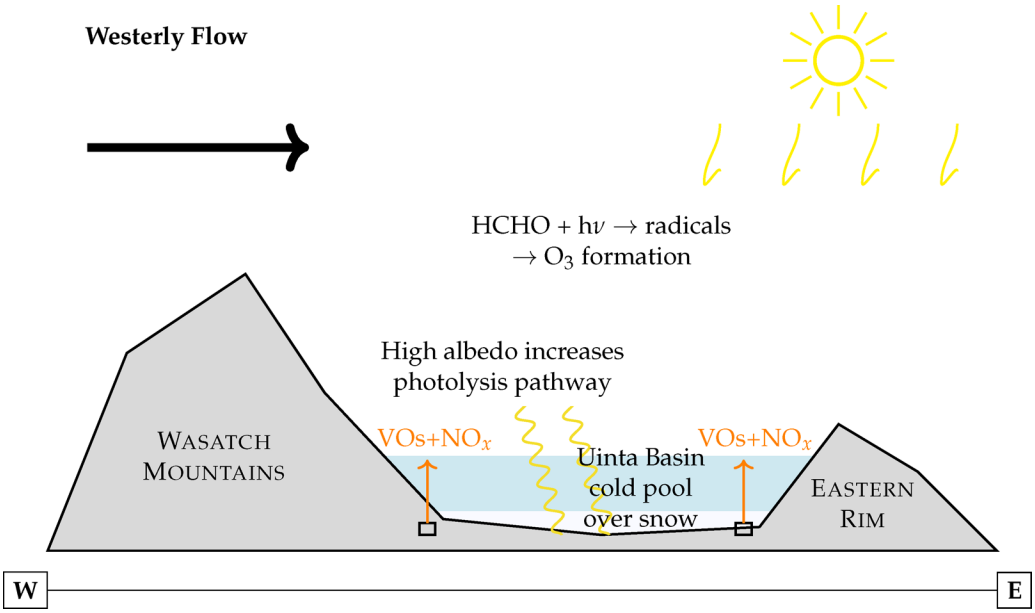

Figure 9-1. Schematic representation of winter ozone formation in the Uinta Basin. Westerly flow creates a precipitation shadow leeward of the Wasatch Mountains. The persistent cold pool over snow increases photochemistry, with high albedo enhancing photochemical reactions that lead to ozone production from trapped volatile organics (VOs) and nitrogen oxides (NO_x).

9.3. Data and Methods

The study analyzed multiple years of ground-based snow depth measurements, surface ozone data, and meteorological observations from sources including the Synoptic Weather repository and the Bingham Research Center's own air quality network. However, diagnosing the snow shadow and its fine-scale impact on ozone proved challenging due to pervasive data uncertainty in the rural, complex terrain.

9.3.1. Key Data Challenges

Three primary data challenges limited the analysis:

Radar Beam Blocking: The Uinta Basin is located far from national NEXRAD sites that provide radar information about precipitation. The high terrain surrounding the Basin blocks the radar beam, causing the beam to overshoot shallow winter cold pools (100-500 m), resulting in systematic underestimation of snowfall and conspicuous "radar holes" in gridded precipitation products (Figure 9-2).

Data Sparsity: In situ meteorological and chemistry sensor data are sparse compared to urban regions, inadequately sampling the spatial gradients of snow depth and ozone. The few NOAA Cooperative Stations that exist in the Uinta Basin, for instance, report snow depth manually only once daily and with coarse precision (to the nearest 1 inch, or 2.5 cm).

Model Inadequacy: Traditional Numerical Weather Prediction (NWP) systems, such as the 13 km Air Quality Model (AQM), are often mathematically incapable of resolving the small-scale mountain cold pools critical for ozone formation in the Uinta Basin, leading to missed high-ozone events. The Real-Time Mesoscale Analysis (RTMA) system, which incorporates radar, also struggles in this region due to the poor radar coverage and sparse surface observations.

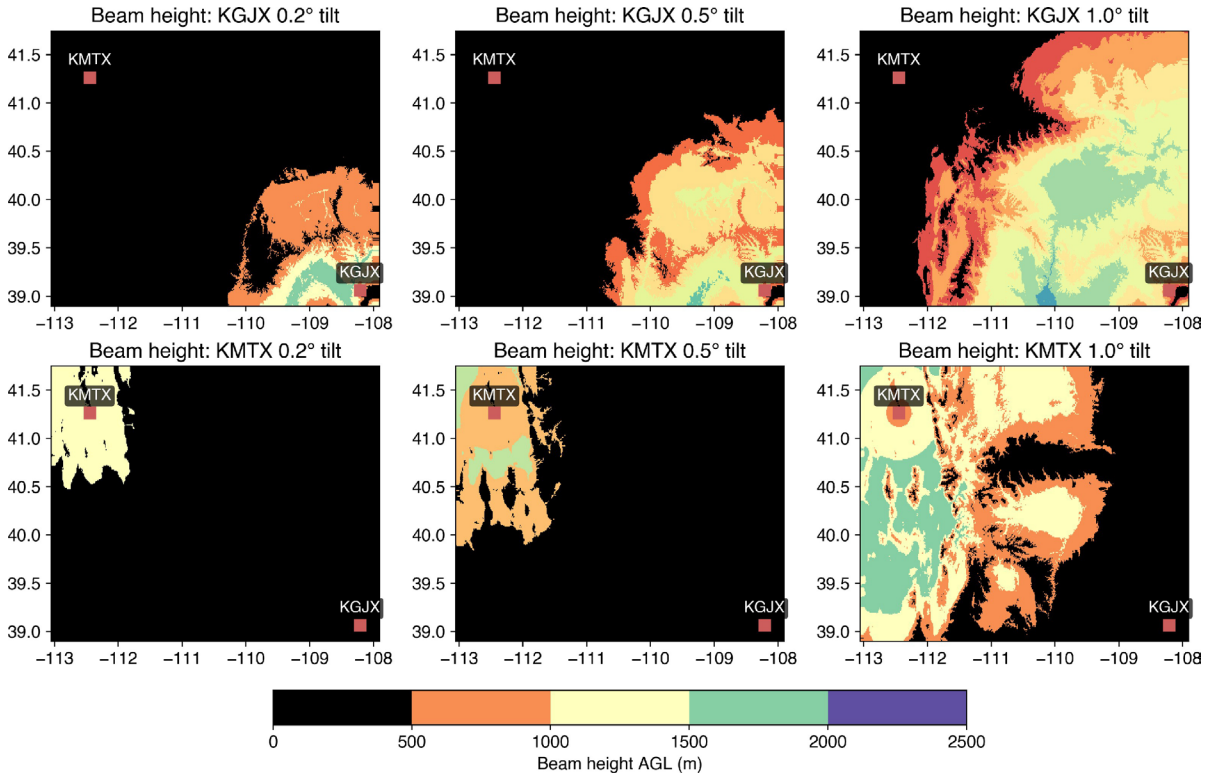

Figure 9-2. Radar beam height above ground level (AGL) from KGJX and KMTX NEXRAD sites at different tilt angles (0.2°, 0.5°, 1.0°). Black areas indicate regions where the radar beam is blocked by terrain, creating significant data gaps in the Uinta Basin. The shallow winter cold pools (~100 m) are often below the radar beam, leading to systematic underestimation of precipitation.

9.4. Results

The analysis of case studies confirmed the established link between snow and ozone: Basin stations frequently reported daily maximum ozone exceeding 70 ppb when widespread snow cover was present, a pattern absent along the windward Wasatch Front. This corroborates the understanding that snow cover is a critical factor for elevated winter ozone episodes (Figure 9-3).

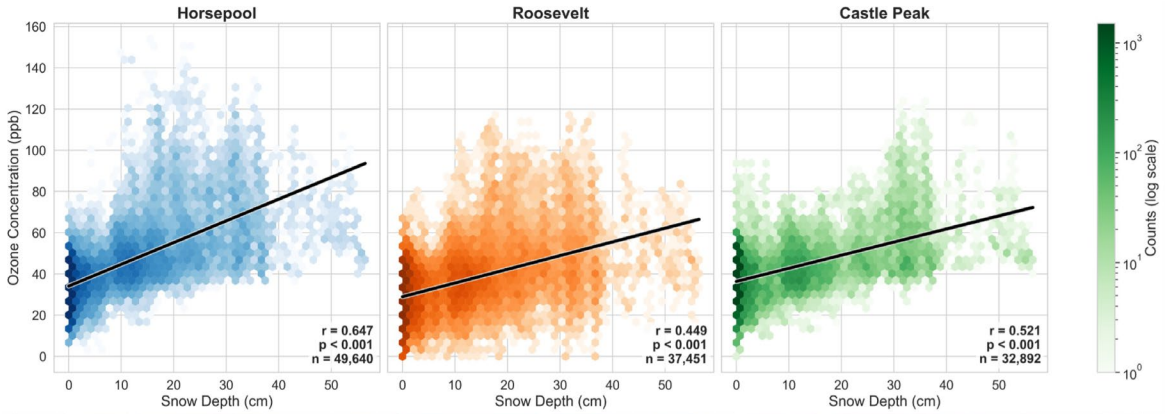

Figure 9-3. Relationship between snow depth and ozone concentration at three Uinta Basin monitoring stations. Scatter plots show positive correlations at all sites (Horsepool: *r* = 0.647, Roosevelt: *r* = 0.449, Castle Peak: *r* = 0.521; all *p* < 0.001). Colors represent data density on a logarithmic scale. The black lines indicate linear regression fits.

However, the hypothesis regarding the fine-scale impact of the snow shadow could not be definitively confirmed. The quantitative precipitation estimates (QPE) derived from RTMA data frequently showed near-zero accumulation in the Basin during observed snowfall events (Figure 9-4 and Figure 9-5). This apparent lack of precipitation, which might superficially resemble a snow shadow, is instead likely an artifact of radar beam blocking and undersampling. While some visual evidence suggested a west-to-east snow depth gradient consistent with a snow shadow, the severe data quality issues prevented robust spatial analysis linking precipitation gradients to ozone concentration patterns.

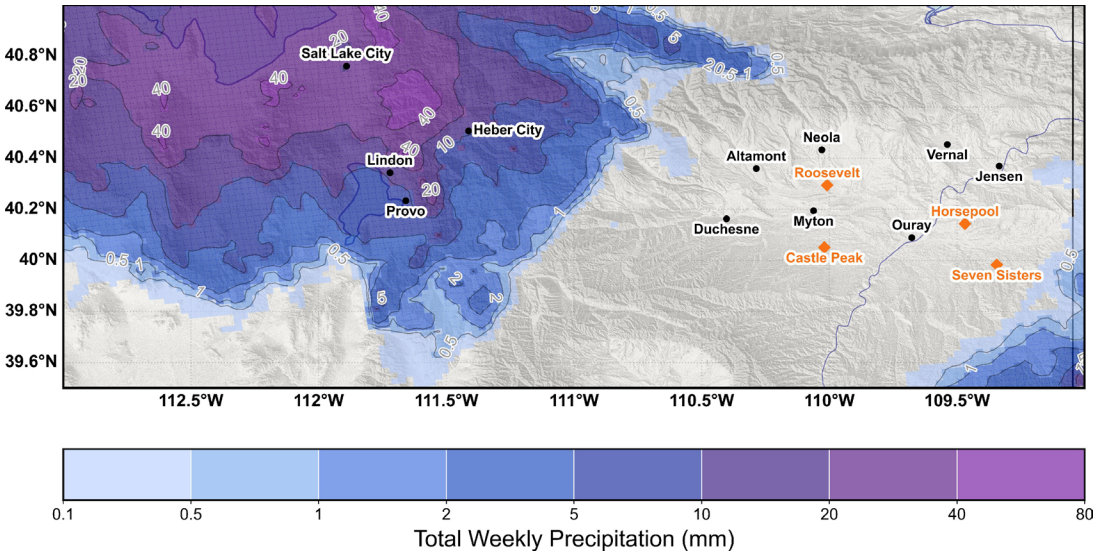

Figure 9-4. Total weekly precipitation (mm) across the Uinta Basin region, showing potential evidence of a precipitation shadow effect leeward of the Wasatch Mountains. Orange markers indicate monitoring stations within the Basin (Horsepool, Roosevelt, Castle Peak, Seven Sisters) while black markers show reference stations in surrounding areas. The reduced precipitation in the western Basin relative to the Wasatch Front suggests orographic effects.

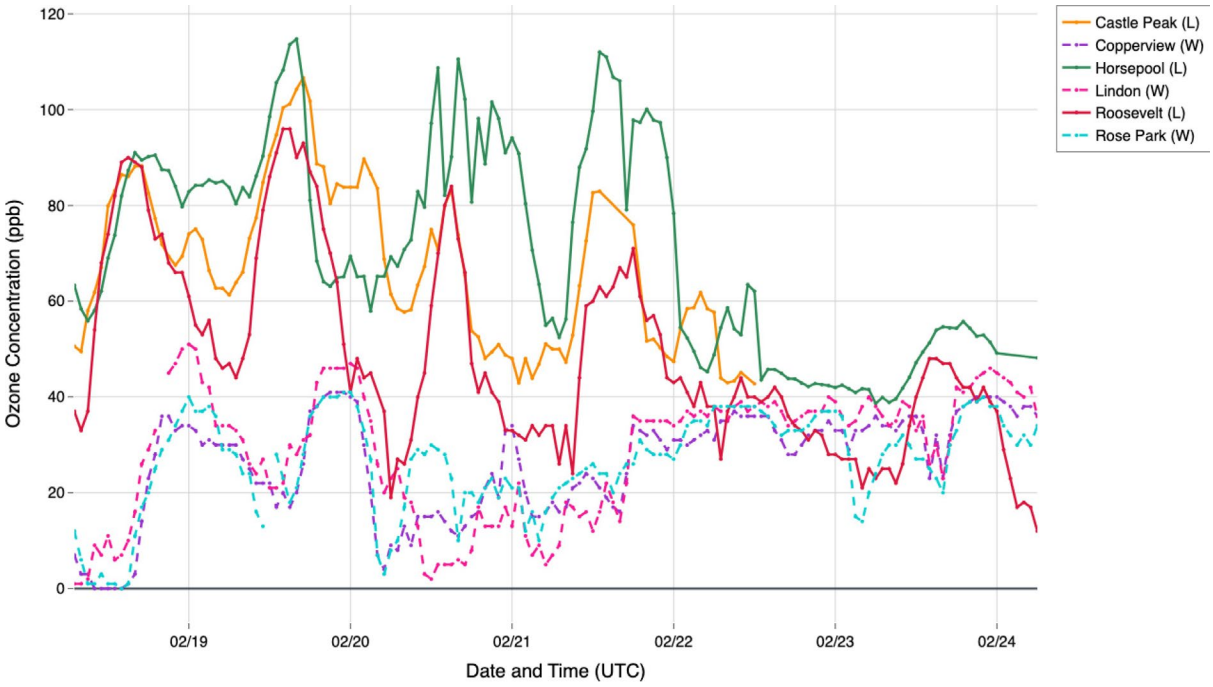

Figure 9-5. Time series of ozone concentrations (ppb) during February 2023 at Uinta Basin stations (marked L for leeward) and windward reference stations (marked W). Leeward stations (Horsepool, Roosevelt, Castle Peak) show sustained elevated ozone episodes exceeding 70 ppb, while windward stations (Orem, Provo, Rose Park, Lindon, Copperview) maintain lower background levels, demonstrating the localized nature of winter ozone formation in the Basin.

9.5. Conclusions

The study acknowledges the existence of regional wisdom suggesting a Uinta Basin snow shadow, conceptually supported by evidence of lower humidity and snowfall leeward of the Wasatch Mountains. Nonetheless, data-quality limitations are substantial, hindering robust confirmation of the phenomenon and its fine-scale impact on ozone production. High uncertainty stemming from radar gaps, sparse surface networks, and inherent model limitations reduces predictive and diagnostic capability.

To enhance operational forecasting, protect public health, and ensure industry regulatory compliance, future work must focus on mitigating these data deficiencies. Proposed steps include deploying low-cost snow-depth sensors that report live onto national networks and identifying new observation sites to better capture the spatial gradients in this complex terrain.

9.6. Acknowledgements

This work was primarily funded by Uintah Special Service District 1 and the Utah Legislature. Some student wages for the project were paid by an endowment from Anadarko Petroleum.

10. Understanding the Role of Organic Compounds in Winter Ozone Formation

Authors: Loknath Dhar and Seth Lyman

10.1. Introduction

Elevated ground-level ozone has become a concern due to its harmful effects on human health, vegetation, and climate (Soares and Silva, 2022; Filippidou and Koukouliata, 2011). While ozone pollution is usually a summertime problem, high ozone levels have been observed during winter in several regions, including Utah's Uinta Basin (Mansfield and Lyman, 2021). These events occur when emissions from oil and gas operations are trapped under strong temperature inversions and react in sunlight to form ozone. Snow cover enhances this process by reflecting more sunlight and strengthening the inversion (Edwards et al., 2014). Non-methane organic compounds (NMOC) and nitrogen oxides (NO_x) released due to oil and gas activities undergo photochemical reaction to produce ozone. However, the detailed chemistry of NMOC involved in winter ozone formation has not been thoroughly investigated yet. Box models can be useful to understand the chemistry of winter ozone formation because they allow modification and adjustment of inputs like emission rates and help to isolate key chemical pathways that drive ozone production.

The following is a summary of a completed study that is under review for publication in *Atmospheric Chemistry and Physics*, a peer-reviewed journal.

10.2. Methods

In this study, we used the Framework for 0-D Atmospheric Modeling (F0AM) box model to better understand the chemistry behind winter ozone formation in the Uinta Basin. The model was run with four chemical mechanisms to (a) identify which carbonyl compounds are most important for ozone production and how they form, (b) estimate emission factors for those compounds, (c) evaluate their potential to produce ozone, and (d) test how different hydrocarbon groups such as alkanes, alkenes, alkynes, alcohols, and aromatics influence the formation of carbonyls and ozone. To ensure the simulations reflected real winter conditions, we used measured concentrations of ozone precursors collected at the Horsepool monitoring site as model inputs. A subset of the Master Chemical Mechanism version 3.3.1 (MCMv331; Saunders et al. (2003)) served as the base chemical mechanism. Results from MCMv331 were compared with three simplified, or "lumped," mechanisms, including Regional Atmospheric Chemistry Mechanism version 2 (RACM2; Goliff et al. (2013)), Statewide Air Pollution Research Center Chemical Mechanism version 07 (SAPRC07; Carter (2010)), and Carbon Bond Chemical Mechanism version 6 (CB6; Yarwood et al. (2010)). We also included reactions that happen on particle surfaces (i.e., heterogeneous chemistry) to see if they change ozone levels under winter conditions. Emission factors were adjusted until modeled carbonyl levels matched measurements collected at the Horsepool monitoring site. The final emission factors were at or near zero for most compounds, suggesting that most carbonyls were secondary pollutants that formed through chemical reactions in the atmosphere, rather than being directly emitted. The simulations covered 24–27 February 2019, a strong inversion period with high ozone, using measured meteorological and chemical data as inputs for each model day.

10.3. Results

During the simulation period, the measured daily maximum 8-hour average ozone level reached 94 ppb, exceeding the U.S. EPA standard of 70 ppb, and had a peak hourly average value of 102 ppb. The F0AM box model using the detailed MCMv3.3.1 mechanism successfully reproduced these high values, estimating a maximum of 107 ppb (1-hour average) on the fourth day. Among the simplified mechanisms, SAPRC07 predicted 111 ppb, RACM2 predicted 100 ppb, and CB6 predicted 122 ppb, showing that all mechanisms captured the observed ozone buildup during strong winter inversions.

As shown in Figure 10-1, model simulations with MCMv3.3.1 showed that formaldehyde was the dominant contributor to winter ozone production, accounting for nearly 50% of the total ozone formed from carbonyl compounds. Acetaldehyde was the second most important contributor, with an impact of 0.06 ppb/h on the ozone production rate. In contrast, benzaldehyde reduced ozone formation, acting as a compound that slows down the process. The MCMv3.3.1, SAPRC07, and RACM2 mechanisms displayed similar behavior, consistently identifying formaldehyde and acetaldehyde as the most influential carbonyls in winter ozone chemistry. The CB6 mechanism, however, grouped most carbonyls into a generic class called “ketones,” leading to higher estimated contributions from this category.

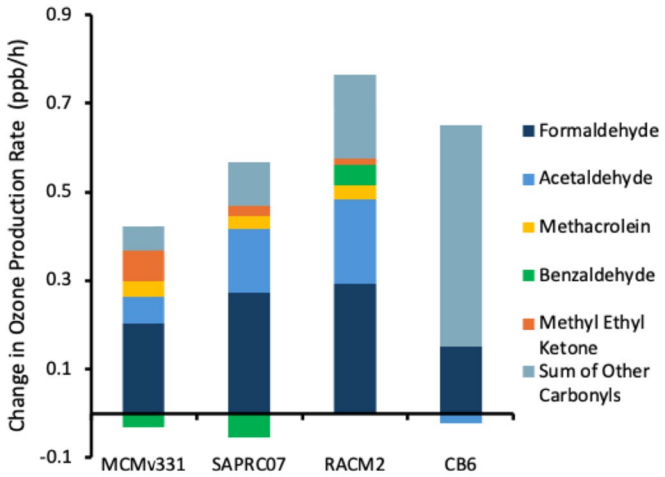

Figure 10-1. Impact of different carbonyl compounds on ozone production rate.

All chemical mechanisms also identified alkanes as the main precursors for forming most carbonyl compounds, such as acetaldehyde, methacrolein, and benzaldehyde. However, the formation of formaldehyde was influenced by multiple groups of organic compounds. Overall, hydrocarbons from oil and gas activities, especially light alkanes, play a key role in producing carbonyls that contribute to winter ozone formation.

Consistent across all mechanisms, alkanes were found to be the most influential hydrocarbons driving winter ozone formation (Figure 10-2). In MCMv3.3.1, increasing alkane levels by 50% raised the ozone production rate by about 0.3 ppb/h on average. Aromatics were the second most important group, followed by alkenes and alkynes. Although light alkanes react more slowly than these other hydrocarbon groups, they dominate emissions from oil and gas operations in the Uinta Basin and account for most of the chemical reactions that generate ozone and its precursors.

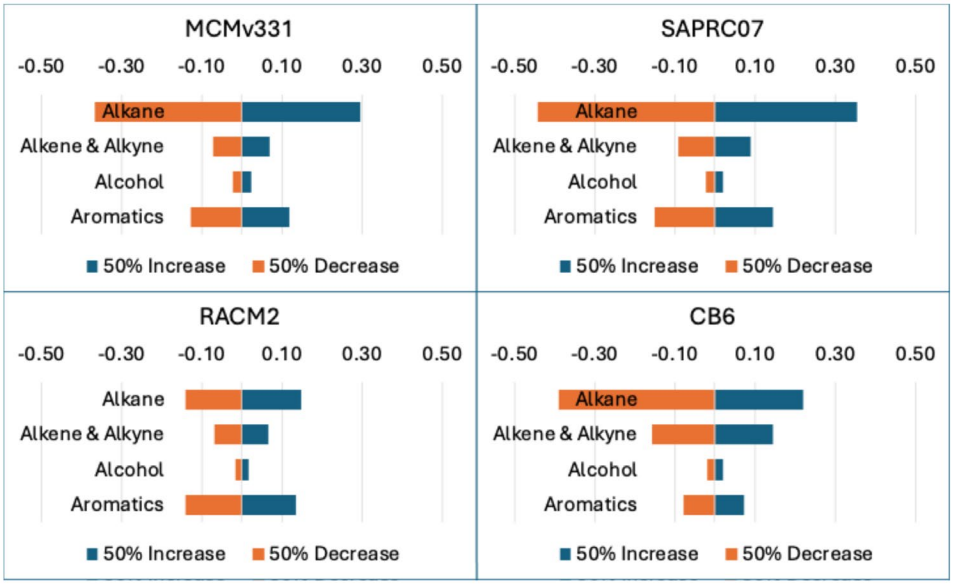

Figure 10-2: Sensitivity of primarily-emitted organic compound groups to the ozone production rate.

10.4. Conclusion

This study identified formaldehyde as the most important carbonyl compound driving winter ozone production in the Uinta Basin, followed by acetaldehyde. Alkanes were found to be the main precursors to the formation of both carbonyl compounds and ozone, with aromatics also contributing significantly. Among the tested mechanisms, SAPRC07 performed the most similarly to MCMV331 in representing winter ozone chemistry, while CB6 was the least similar. These findings emphasize the role of emissions from oil and gas activities in winter ozone formation.

10.5. Current and Future Work

Currently, we are working on a project that aims to improve understanding of winter ozone formation in the Uinta Basin by replicating much of the work described above with CMAQ, a 3D photochemical model. The goal of this work is to simulate the period of February 2013 using CMAQ, along with emission outputs from the SMOKE emissions model, with previous WRF meteorological inputs that include vertical nudging to better capture inversion strength and stability. So far, we have completed the setup of SMOKE and CMAQ, generated emission outputs for different sectors, and merged them into a CMAQ-ready input file. For this project, we are using RACM2 as the base chemical mechanism. The next step is to run the CMAQ model with these emissions and compare the simulated results with observations, followed by targeted modifications and refinements based on the model's performance.

In the future, we plan to test different chemical mechanisms and assess how well each represents wintertime chemistry and ozone production in the Basin. We are also planning to perform sensitivity analysis of carbonyls and ozone to changes in various organic compound groups, following a similar approach to our completed F0AM study, to observe how these changes affect ozone and key carbonyls. We will also explore NO_x versus NMOC sensitivity to better understand how precursor emissions control winter ozone formation. This future work will provide a broader chemical perspective and help refine strategies for improving air quality in the Uinta Basin.

11. Investigation of Organic Compound Fluxes at the Air-Snow Interface

Authors: KarLee Zager and Seth Lyman

11.1. Introduction

In cold regions like the Uinta Basin, snowpacks do much more than simply store water. They host a range of physical and chemical processes that can influence the composition of the surrounding air (Grannas et al., 2007). Under certain conditions, snowpacks can both absorb and release organic compounds into the atmosphere. The Uinta Basin's bowl-shaped topography makes it prone to wintertime inversions, during which stagnant air traps emissions and leads to high levels of ozone that can affect local air quality and public health. Carbonyl compounds, in particular, are important because they act as radical precursors that help drive ozone formation during these events (Edwards et al., 2014).

The goal of this project was to build on our previous work and increase our understanding of the organic compound fluxes occurring at the snow–air interface. This work contributes to a broader understanding of the chemical and physical processes that drive ozone formation during wintertime inversion events in the Uinta Basin, directly supporting the Bingham Research Center's mission to monitor and understand wintertime ozone formation in the Uinta Basin. We have previously shown, through both laboratory (Lyman et al., 2020) and field (Lyman et al., 2019) studies, that organic compounds—particularly carbonyls such as acetaldehyde—can be emitted from snowpacks in the presence of sunlight. Background information about these processes was presented in our 2019 Annual Report (Lyman et al., 2019).

To further explore these findings, we designed and built a custom two-chamber system that allowed us to observe emissions of organic compounds from snow samples under controlled conditions. All aspects of this research project were conducted by the Bingham Research Center at Utah State University's Uinta Basin Campus.

11.2. Methods

We conducted controlled experiments to investigate organic compound fluxes at the snow–air interface. Although designed as a laboratory study, tests were performed outdoors to use ambient air and natural sunlight. The experimental system was mounted on a cart, allowing us to move it outside for runs and inside for storage.

11.2.1. Chamber System Design

We built a two-chamber system (Figure 11-1) that allowed two tests under different conditions simultaneously. A chest freezer was divided into two sections to form the chambers. The freezer lid above each chamber was replaced with ultraviolet (UV)-transparent acrylic panes to allow sunlight to enter. Snow samples were sealed inside PTFE bags (90% UV-transparent) connected by PFA tubing to external pumps, which circulated air, refilled the bags with ambient air, and assisted with sample

collection. A septum in the tubing allowed injection of additional organic compounds to test how added vapors interacted with the snow–air interface. Figure 11-2 illustrates the key components of the two-chamber system and how air circulation and sunlight exposure were managed during each run.

Figure 11-1. Photograph of the snow chamber system.

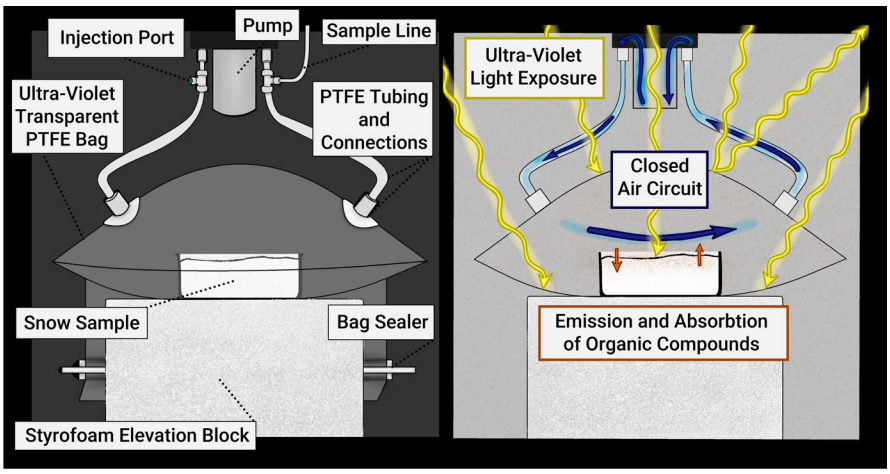

Figure 11-2. Schematic of the snow chamber system showing its key components, air circulation pathways, and exposure of snow samples to natural sunlight.

11.2.2. Environmental Control

Temperature was regulated by a liquid nitrogen delivery system connected through copper tubing and controlled with separate Auber temperature controllers for each chamber. Thermocouples monitored each chamber, and liquid nitrogen was automatically delivered when temperatures rose above set points. UV intensity was measured continuously using UVA and UVB sensors attached to the inside of the freezer lid. Cardboard coverings provided dark conditions when needed.

11.2.3. Sample Collection and Preparation

Snow samples were collected in 2021 and stored in a laboratory freezer. *Clean snow* was collected in Dry Fork, Utah (40.5653, -109.6915), away from urban and industrial sources, and *dirty snow* at the Horsepool air quality monitoring station (40.1433, -109.4680), an area of intensive oil and natural gas production. Snow samples were collected with nitrile gloves and stored in Liquinox-washed HDPE containers until use. During analysis in the chambers, snow was transferred to PFA trays, and the trays were placed inside the PTFE bags. Depending on test objectives, snow depth and surface area were varied by adjusting tray fill levels or using one versus two containers per chamber.

11.2.4. Injection of Additional Organic Compounds

For some tests with clean snow, we injected a suite of gas-phase organic compounds into a chamber as it was being filled with air to determine whether additional organic compounds in the air impacted interactions of organic compounds with snow. The organic compounds added were in a similar proportion to ambient air found in oil and gas-producing areas of the Uinta Basin.

11.2.5. Sampling and Analysis

Air samples were collected from each chamber using evacuated whole-air canisters and 2,4-dinitrophenylhydrazine (DNPH) cartridges. Gas canister samples were analyzed by gas chromatography–mass spectrometry (GC-MS) to quantify 54 non-methane organic compounds, and DNPH samples were analyzed by high-performance liquid chromatography (HPLC) to quantify 13 carbonyl compounds. These were grouped and summarized into 6 cumulative organic classes for a more condensed comparison. Details about the methods used for analyzing these samples are presented in the section of this technical report that deals with air quality results for winter 2024-25.

Temperature was recorded every 30 minutes, and UV intensity every 30 seconds. Each run lasted for between two and three hours. DNPH and canister samples were collected from ambient air just before the bags were filled and from the bags at the end of each run. Early tests required separate sampling for gas canisters and DNPH cartridges, but later runs used larger chamber bags that allowed simultaneous collection.

11.2.6. Data Processing and Quality Control

For each run, recorded temperature and UV data were averaged to obtain representative conditions over the entire run. Average UVA and UVB values were combined to produce a total UV value. Fluxes of individual organic compounds at the snow-air interface ($\mu g\ m^{-2}\ h^{-1}$) were calculated from measured concentrations, snow–air interface area, and exposure duration. Mass accumulation was first determined for the total air volume inside each chamber, and the appropriate surface area of snow (for one or two containers) was used to calculate flux at the snow surface. Exposure start and end times were used to determine run duration.

Ambient air samples collected concurrently with each test were used to correct measured concentrations so that reported values represented the change in organic compound levels relative to background conditions. Blank runs with empty containers were used to identify and correct for background contamination from the chamber system, and their averaged results were subtracted from

sample data. Replicate tests were conducted, and chamber conditions were alternated between runs to verify reproducibility.

11.3. Results

Fluxes varied among compound classes and experimental conditions (Table 11-1). UV exposure produced the strongest overall correlations with emission rates. For alkene fluxes, UV intensity showed a strong *positive* relationship under clean-snow conditions ($r^2 = 0.86$) and a weaker one under dirty-snow conditions ($r^2 = 0.33$), indicating that increased sunlight enhances alkene emissions from snow (Figure 11-3). In contrast, carbonyl emissions decreased as UV intensity increased, with moderate to strong *negative* correlations ($r^2 = 0.64$ for clean snow; $r^2 = 0.56$ for dirty snow), suggesting photochemical depletion rather than production (Figure 11-4).

Table 11-1. Matrix of correlation coefficients (r^2) for organic summary classes—by snow type (clean or dirty) and test variable (temperature, UV exposure, depth/surface area, ambient air/organic injection).

Organic Summary Classes	Temp. (clean)	Temp. (dirty)	UV (clean)	UV (dirty)	Depth/ Surface Area (clean)	Depth/ Surface Area (dirty)	Ambient/ Injection (clean)
All Alkanes	<0.01	0.11	0.33	0.15	0.07	<0.01	0.09
All Alkenes	<0.01	0.05	0.86	0.33	0.26	<0.01	0.65
All Aromatics	<0.01	<0.01	0.43	0.08	0.07	0.11	0.01
All Alcohols	0.23	<0.01	0.01	0.02	0.21	<0.01	<0.01
All Carbonyls	0.28	0.03	0.64	0.56	<0.01	0.04	0.34
All Hydrocarbons	<0.01	0.11	0.34	0.12	<0.01	<0.01	0.09

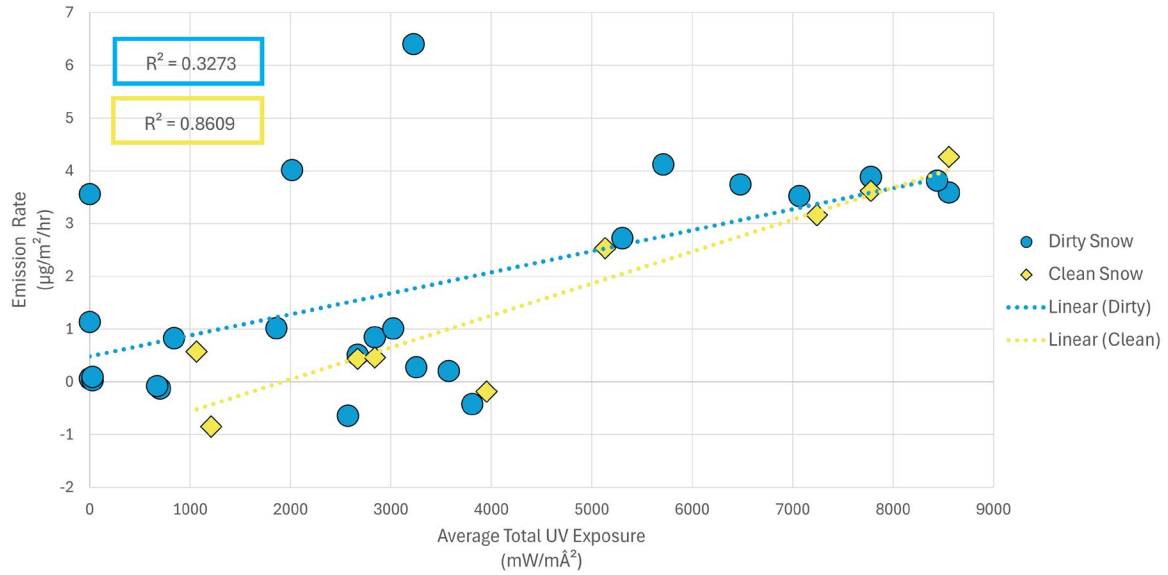

Figure 11-3. Relationship between ultraviolet (UV) intensity and total alkene fluxes for clean and dirty snow.

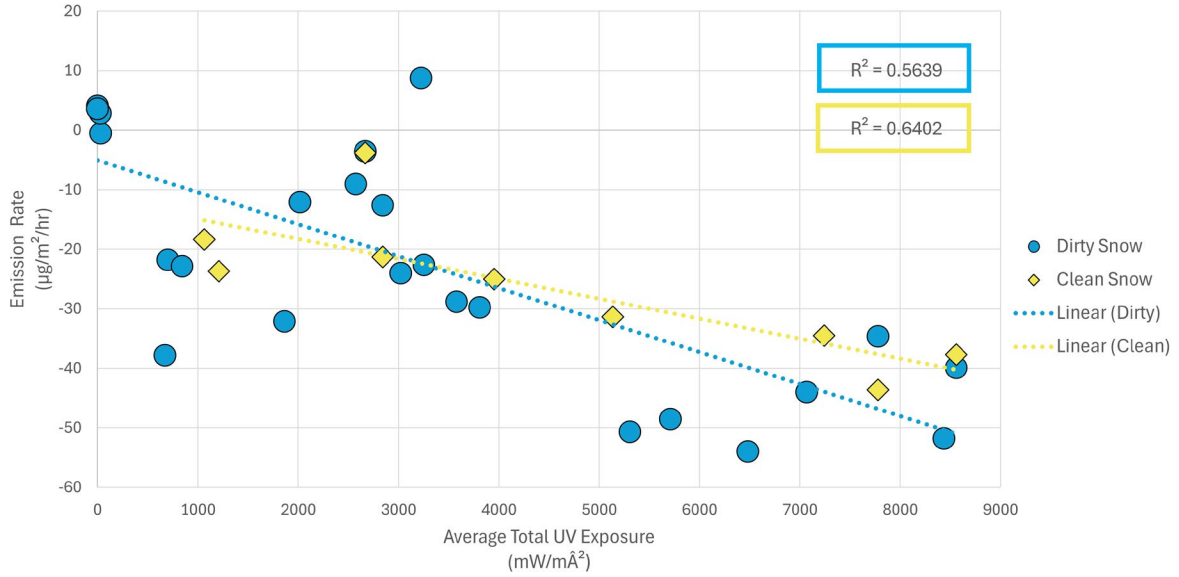

Figure 11-4. Relationship between ultraviolet (UV) intensity and total carbonyl fluxes for clean and dirty snow.

Temperature had smaller effects, with moderate correlations for carbonyls ($r^2 = 0.28$) and alcohols ($r^2 = 0.23$) in clean snow and minimal relationships for dirty snow ($r^2 < 0.03$). Depth and surface-area variations produced negligible responses across all compound classes ($r^2 < 0.27$). In comparisons of ambient air versus air with additional volatile organic compounds added, alkenes ($r^2 = 0.65$) and carbonyls ($r^2 = 0.34$) showed modest differences, suggesting that the introduction of additional organic vapors slightly influenced exchange at the snow–air interface. Overall, UV exposure exerted the dominant control on organic emissions, with smaller secondary effects from temperature and air composition.

11.4. Discussion

Alkenes showed strong positive correlations with UV exposure ($r^2 = 0.86$ clean; 0.33 dirty), indicating sunlight-driven production or release, while carbonyls showed strong negative correlations ($r^2 = 0.64$ clean; 0.56 dirty), suggesting photochemical loss. Temperature and snow-structure effects were minor, and organic vapor additions produced limited responses. Overall, the results show that sunlight controls both the production and removal of organic compounds that influence winter ozone formation in the Uinta Basin.

Some data variability likely resulted from experimental constraints, including occasional system leaks, pinholes in PTFE bags, timing differences between gas canister and DNPH phases, and the use of several-year-old snow samples. Even with these challenges, consistent patterns across compound classes confirm that photochemical processes dominate snowpack emissions.

Together, these findings advance our understanding of how sunlight-driven processes in Uinta Basin snowpacks influence winter ozone formation and provide a foundation for future investigations under real-world atmospheric conditions.

12. Drone-based Measurement of Emissions from Oil and Gas Sources

Authors: Colleen Jones and Shalyn Drake

12.1. Background

Methane is a potent greenhouse gas released during oil and gas extraction, processing, and transportation (Alvarez et al., 2018). Accurate measurement of these emissions is essential for regulatory compliance, environmental protection, and climate change mitigation (Moreno et al., 1996). Traditional ground-based methods, though effective, are often limited by time, spatial coverage, and accessibility, particularly in remote or hazardous locations (Casagli et al., 2017).

Drone-based methane measurement systems offer a transformative solution (Fosco et al., 2025). Equipped with high-resolution sensors, drones can access difficult terrain, collect real-time data, and map emissions over large areas at lower cost and higher efficiency than traditional methods. Advances in sensor technology and data analytics continue to improve the precision, speed, and visualization of methane measurements, making drone-based monitoring increasingly viable for industrial and environmental applications (Fu et al., 2023).

This project aims to design, build, and validate a drone-based methane emission monitoring system that integrates a methane analyzer, meteorological sensors, and real-time data processing software. The project is conducted through collaboration between the Bingham Research Center and USU Eastern's Unmanned Aircraft Systems (UAS) Certificate Program, providing students with applied research and technical experience in environmental monitoring and drone operations (Figure 12-1).

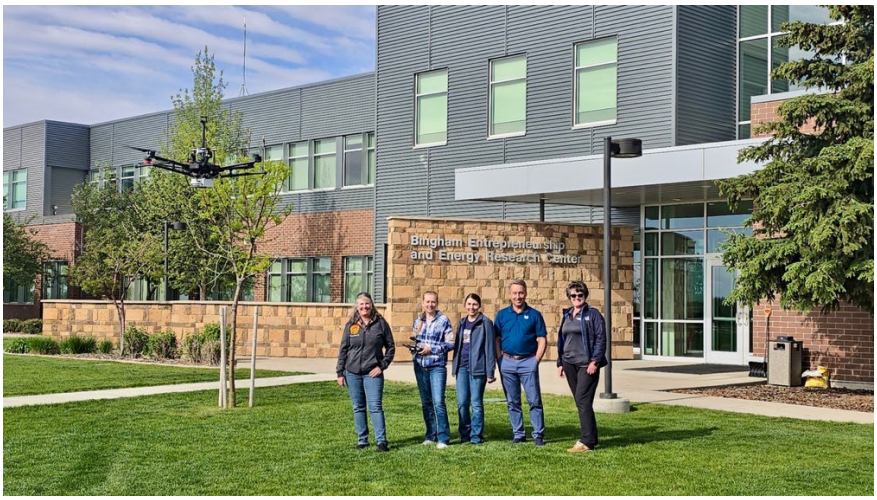

Figure 12-1. The Bingham Research Center's methane emissions measurement drone in flight (upper left), with staff involved in measurement (from left to right: Colleen Jones, Ambria Migliori, Cheyenne Reid, Bob Peterson, and Shalyn Drake).

12.2. Project Impacts

During this reporting period, major progress was made in system programming, SOP development, and testing. Key accomplishments include:

- Programming and SOP development: USU Eastern student Ambria Migliori finalized the programming workflow and authored Standard Operating Procedures (SOPs) for setup, calibration, and field operations.

- Drone downwash testing: Completed controlled “smoke test” flights to evaluate how drone propeller downwash affects methane plume movement and measurement accuracy.

- Data visualization development: Began developing a real-time visualization system for mapping methane concentrations during flight and post-flight 3D rendering of emission data.

- Student engagement and training: Three student pilots from the UAS program participated in system programming, integration, and testing, gaining hands-on experience in environmental drone applications. A new student drone pilot was hired to support upcoming field campaigns (Students included Sam Dupiax, Ambria Migliori, and James Peterson).

These accomplishments have laid the foundation for a reliable, field-deployable methane monitoring platform (Figure 12-2) that enhances data accuracy and operational efficiency. The project also supports student learning and workforce development in drone-based environmental monitoring technologies (Figure 12-3).

Figure 12-2. Bingham Research Center’s methane emissions measurement drone, which was designed and built by students.

Figure 12-3. Dr. Seth Lyman and student KarLee Zager assessing the Sensit methane analyzer's inlet port after a smoke bomb down-wash test.

12.3. Manual Flight Skills and Pattern Testing

Manual flight skills played a critical role in the development and testing phases of the methane monitoring system. Using the DJI Matrice 600 platform, our team conducted a series of Visual Line of Sight (VLOS) flights to evaluate plume detection accuracy across various flight patterns. These included parallel transects, orbital flights, and expanding square patterns at altitudes ranging from 20 to 50 feet Above Ground Level (AGL). Each pattern was manually flown to simulate real-world conditions and assess the drone's responsiveness, plume effects, and sensor stability. These manual operations allow for real-time adjustments based on plume behavior and terrain variability, as well as on crew expertise. The expanding square pattern emerged as the most effective for capturing methane concentrations around emission sources, offering spatial coverage, repeatability, and even scalability.

These manual flight tests were informed by training protocols from Utah State University's Unmanned Aircraft Systems (UAS) Program, which emphasizes hands-on flight experience. Students in the program learn to manually pilot drones through structured labs that include both fixed-wing and multirotor situations in a variety of applications. The curriculum prioritizes manual flight proficiency to prepare students for dynamic field conditions and directly supported our project, as student pilots applied their skills to execute precise flight paths and adapt to plume movement during testing.

By integrating manual flight expertise with sensor technology, the project not only advanced methane detection capabilities but also provided valuable experiential learning for student researchers. These skills will be critical as the system moves into field deployment phases across active oil and gas sites.

12.4. Future Work

The next phase of the project will focus on calibration, validation, and field deployment:

- Calibration and validation: Finalize testing using certified calibration gases and a mass flow controller to simulate controlled emission rates. We will release methane at known rates from

UBTech's non-functional oil and gas equipment to simulate emissions from actual oil and gas equipment, assessing system accuracy across multiple emission points.

- Software and real-time processing: Complete programming of a data processing system capable of integrating GPS, meteorological, and chemical data to calculate emission fluxes using the mass balance method outlined by Gålfalk et al. (2021).

- Field deployments: Establish collaborations with regional energy companies to conduct on-site methane emission measurements from active oil and gas facilities.

- Visualization and reporting: Finalize the 3D visualization and post-flight analysis tools to support data interpretation and reporting for regulatory and research use.

The project remains on track to complete system validation and begin operational field measurements within early 2026. Once fully implemented, this drone-based methane monitoring system will provide an efficient, scalable, and cost-effective approach to emissions detection—advancing both scientific research and practical environmental management.

12.5. Acknowledgements

This project was funded by the Utah Legislature and Uintah Special Service District 1.

13. Satellite-based Remote Sensing and Interactive Modeling of Emissions

Authors: Colleen Jones and Gus Williams (BYU)

13.1. Background

Satellite-based remote sensing offers a powerful, scalable means of quantifying greenhouse gas emissions and detecting spatial patterns of atmospheric methane, carbon dioxide, and related pollutants over large geographic areas (Wilson et al., 2025). Unlike ground- or drone-based systems, satellite observations enable consistent temporal and spatial monitoring across entire energy basins, providing critical data for emissions assessment, regulatory compliance, and environmental policy development (Haske et al., 2024).

Recent advances in cloud-based platforms such as Google Earth Engine (GEE) have transformed the way scientists process and analyze large-scale geospatial data (Vijayakumar et al., 2024). GEE integrates global satellite archives with advanced computing power and coding tools, enabling automated workflows for image processing, classification, and trend analysis (Rahimoon et al., 2025). These capabilities allow researchers to visualize emission sources, quantify changes through time, and correlate emissions with industrial activity, meteorological patterns, and land use characteristics (Liu et al., 2023).

This project builds upon the Bingham Research Center's drone-based monitoring program by extending its spatial and temporal reach through satellite-based analysis. Conducted in collaboration with Dr. Gus Williams of Brigham Young University's Civil and Environmental Engineering Department, the project integrates engineering modeling with satellite data analytics to advance emission quantification and visualization.

Specifically, it aims to develop an interactive, web-based modeling tool that integrates satellite data, emission rate estimation algorithms, and meteorological data. The tool will be built using GEE, Python, and web-based dashboards to support stakeholders, researchers, and policy makers in tracking emissions and evaluating mitigation strategies.

13.2. Project Impacts

During this reporting period, significant progress was made in data acquisition, coding workflow development, and interactive model design. Key accomplishments include:

- Satellite data integration: Established a cloud-based data repository within GEE, incorporating Sentinel-5P (TROPOMI), Landsat 8–9, and MODIS datasets for methane (CH_4), nitrogen dioxide (NO_2), carbon dioxide (CO_2), and ozone (O_3) detection. Baseline data layers for Uinta Basin oil and gas wells were compiled and spatially aligned with existing drone and ground measurements.
- Algorithm and code development: Developed initial Python and JavaScript scripts within the GEE platform to detect emission hotspots, calculate plume dispersion indices, and perform time-

series analyses of methane concentrations. These scripts enable automated data processing and visualization directly within the GEE interface.

- Prototype interactive app: Designed a web-based application framework that allows users to explore emission data through an intuitive dashboard. The prototype integrates satellite imagery, emission rate estimates, and ground validation datasets from USU Eastern's drone campaigns.
- Student involvement and training: One student from BYU's Data Science program contributed to coding, data management, and app interface design. Their work provided valuable hands-on experience in remote sensing analytics, environmental modeling, and cloud computing.
- Cross-Scale Integration: The project established a data fusion workflow linking drone-derived methane measurements with satellite-based concentration maps, creating a multi-resolution monitoring system for validating and refining emission estimates.

These achievements mark a critical step toward developing a comprehensive, scalable emission monitoring system that merges field data and satellite analytics, strengthening Utah's leadership in applied environmental technology.

13.3. Future Work

Next steps will expand data integration, strengthen collaborations, and advance methane measurement standardization.

- Integrated modeling: Combine drone, ground, and satellite observations to validate emission estimates for methane (CH_4), nitrogen dioxide (NO_2), carbon dioxide (CO_2), and ozone (O_3). Advanced dispersion algorithms developed in Google Earth Engine (GEE) and Python will improve emission mapping and temporal trend analysis.
- Interactive dashboard: Deploy a stakeholder-accessible dashboard visualizing satellite and UAS data for emission tracking, regulatory compliance, and mitigation planning.
- Partnership expansion: Continue collaboration with Dr. Gus Williams (BYU Civil Engineering) to integrate engineering-based atmospheric dispersion models with remote sensing data, enhancing emission accuracy and student research opportunities.
- IEEE methane standard development: Conduct field tests at the USU Bingham Research Center to evaluate GETBag® calibration targets for quantitative methane measurement. These tests—conducted with the IEEE GRSS Methane Working Group (USU, BYU, and Condor Calibration Services)—will provide foundational data toward establishing an IEEE Standard for airborne and spaceborne methane sensor calibration.

This phase will deliver an integrated satellite–drone emission monitoring framework, support IEEE standardization for methane quantification, and provide hands-on training for USU and BYU students in advanced remote sensing and atmospheric monitoring.

13.4. Acknowledgements

Time spent by Bingham Research Center staff on this project is funded by the Utah Legislature, Uintah Special Service District 1, and IEEE GRSS.

14. Public Lands Initiative – Cost-Benefit Analysis of Cattail Control at Stewart Lake

Authors: Colleen Jones and Lisa Boyd

14.1. Background

Cattails (*Typha* spp.) can dominate wetland ecosystems, reducing biodiversity and altering habitat structure (Apfelbaum, 1985). Effective management is needed to maintain a balance between cattail cover and open water to support overall wetland ecosystem health (Ball, 1990). Traditional herbicide treatments, while effective, are costly and non-selective, potentially impacting non-target species. Alternative methods, such as controlled burns or grazing by goats, may offer more sustainable and cost-efficient options (Wwa, 2018).

As part of her doctoral dissertation research at Utah State University, Lisa Boyd is evaluating and comparing cattail management strategies using small experimental plots distributed throughout a wetland (Figure 14-1). Treatments include controlled burns, herbicide applications, goat grazing, and combinations of these approaches. The study tests the hypothesis that spring treatments, applied prior to flooding, are as effective as fall treatments following lake drainage. Remote sensing technologies, including multispectral satellite and drone imagery, are used to monitor cattail canopy cover and open water extent.

This 18-month project is scheduled to conclude in December 2025. All data collection has been completed, and data analysis is underway. Findings from this work will form one chapter of Lisa Boyd's dissertation and be submitted for peer-reviewed publication. Dr. Doug Ramsey (Logan Campus) and Dr. Colleen Jones (Vernal Campus, Bingham Research Center) provide mentorship and expertise in remote sensing and data analysis for the project, and an undergraduate research assistant supported field data collection.

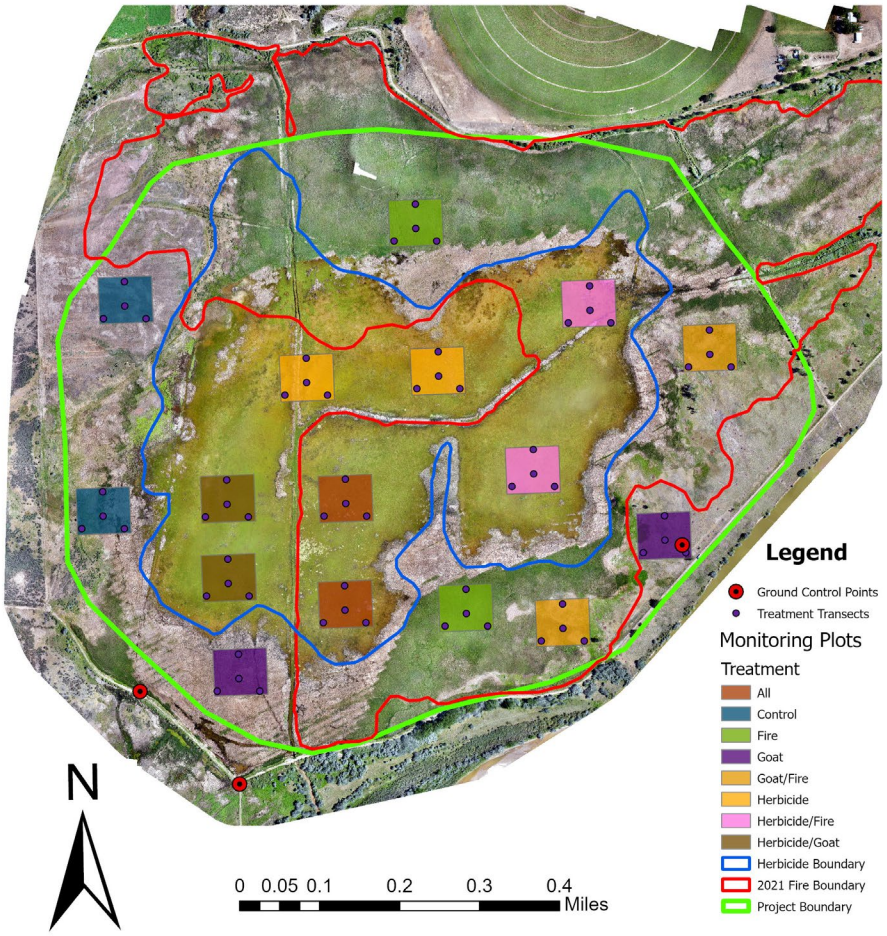

Figure 14-1. Project map.

14.2. Project Impacts

This project advances sustainable wetland management by evaluating cost-effective and environmentally responsible methods to control cattail populations while maintaining biodiversity and open water habitat. By reducing reliance on non-selective herbicides, the project minimizes ecological and financial impacts, contributing to healthier wetland ecosystems. The integration of controlled burns, grazing, herbicide application, and combinations of these methods provides land managers with practical tools to balance vegetation control with ecological preservation. In addition to ecological benefits, the project fosters the training and mentorship of students in applied research, wetland management, field techniques, and remote sensing technologies. The findings will inform broader wetland management strategies, support peer-reviewed publications, and contribute a chapter to Lisa Boyd's doctoral dissertation, ensuring that the knowledge generated is accessible to both the scientific community and natural resource managers.

14.3. Future Work

Results from this project will inform broader wetland management strategies and may be expanded to control other invasive wetland species. Data will support publications to guide managers in sustainable cattail control and may lead to additional studies on long-term impacts of combined treatments under varying hydrological and ecological conditions. Ongoing collaborations stemming from this project will continue to provide mentorship, student training, and integration of remote sensing techniques into applied ecological research.

14.4. Acknowledgements

This project is funded by the Utah Public Lands Initiative.

15. Public Lands Initiative – Precision Spray Drone for Invasive Plant Species at Stewart Lake

Authors: Colleen Jones, Shalyn Drake, and Lisa Boyd

15.1. Background

Stewart Lake is a critical wetland complex located near the Green River in Uintah County, Utah, supporting diverse wildlife and providing vital spawning and rearing habitat for two federally endangered fish species—the razorback sucker (*Xyrauchen texanus*) and bonytail chub (*Gila elegans*) (Modde and Irving, 1998). The ecological integrity of this system depends on maintaining a mosaic of open water and emergent vegetation, particularly cattails (*Typha spp.*), which offer essential cover but can become overly dominant when unmanaged (Webber, 2013). Encroachment by cattails and other invasive plants—such as Canada thistle (*Cirsium arvense*), Russian knapweed (*Rhaponticum repens*), and whitetop (*Lepidium draba*)—has reduced open-water habitat, restricted water flow, and degraded native biodiversity at Stewart Lake.

Traditional control methods have relied heavily on broadcast herbicide applications using glyphosate and similar compounds (Solberg and Higgins, 1993). While effective in reducing biomass, these approaches are costly, non-selective, and pose ecological risks through chemical runoff, impacts to non-target vegetation, and potential long-term environmental persistence (Riaz et al., 2021). Mechanical control methods, such as mowing or excavation, are limited by accessibility and labor intensity. Consequently, managers have sought a more sustainable, targeted, and data-driven approach to restore and maintain habitat balance at Stewart Lake.

To address these challenges, a two-year research and management project (2024–2025) was implemented using precision spray drones to manage invasive species across approximately 100 acres of the Stewart Lake wetland complex (Figure 15-1). Drones equipped with RTK-GPS guidance, variable nozzle systems, and advanced sensors enabled highly targeted herbicide applications to dense cattail stands and patches of secondary invasives. Pre- and post-treatment monitoring included aerial multispectral imagery, vegetation density assessments, and habitat condition mapping. Treatments were evaluated for both effectiveness and ecological response, including open-water recovery, vegetative diversity, and habitat quality for aquatic species.

This project complements an ongoing cost-benefit analysis of cattail control strategies and provides an important applied research component for adaptive wetland management. The work contributes directly to Lisa Boyd's PhD dissertation, forming two dissertation chapters and supporting at least two peer-reviewed publications focused on precision herbicide application and wetland restoration outcomes.

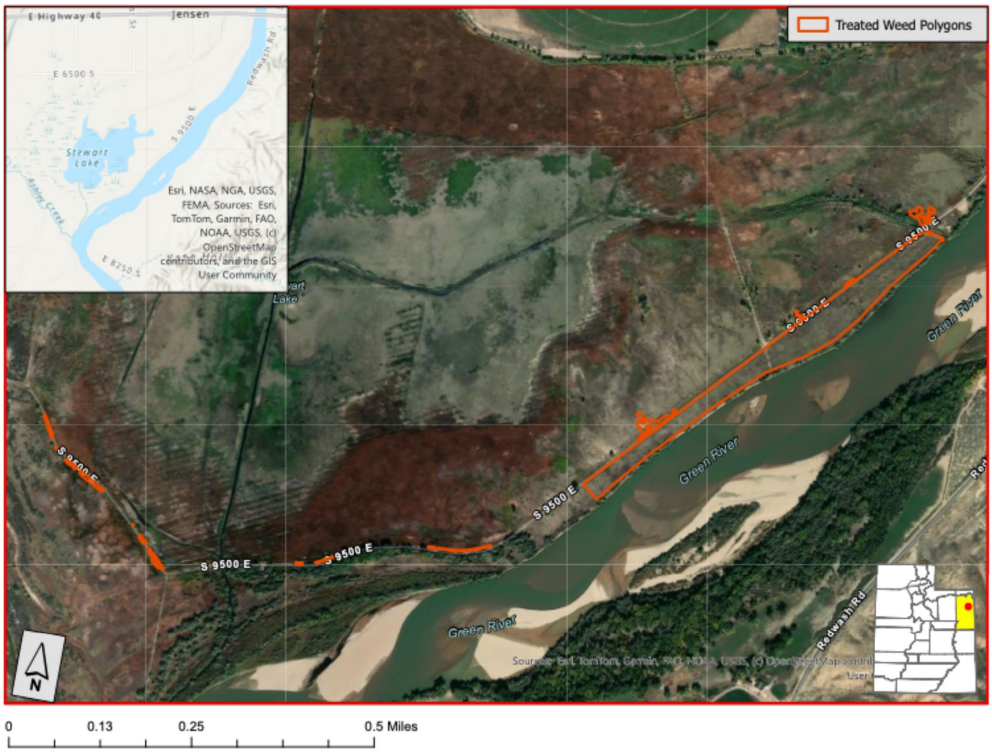

Figure 15-1. Map of Aerial Spray Treatment Polygons completed on 27 September 2025 at Stewart Lake.

15.2. Monitoring and Data Collection

Monitoring was designed to evaluate treatment effectiveness and ecological response using a combination of drone-based remote sensing and field-based assessments.

- Aerial imagery and analysis: A complete multispectral prescription flight was conducted on 15 September 2025, generating maps for targeted herbicide application and vegetation analysis using an eBeeX fixed-wing drone with dual multispectral and RGB cameras. Imagery was processed in Pix4Dfields to generate NDVI and vegetation classification maps that quantified changes in cattail coverage, open-water area, and invasive species distribution using the workflow in Figure 15-3.
- Herbicide application data: On 27 September 2025, drones treated 13 acres of noxious weeds, applying precision-targeted herbicide to minimize non-target exposure.
- Field day workshop and training: On 27 September 2025, in partnership with USU Extension and WildAss Aerial, a hands-on field day was held to train six participants in drone operation, data capture, and mapping workflows. Participants gained experience with flight planning, imagery collection, and basic analysis for agricultural and environmental applications (Figure 15-2).
- Ground and habitat validation: Field surveys at fixed plots measured percent cover of noxious weeds and native vegetation to validate drone imagery and train AI models for automated vegetation classification. These data were combined with observations of water quality, hydrologic connectivity, and vegetation regrowth to assess overall habitat health and conditions supporting endangered fish species.

Figure 15-2. Field Day Workshop and Train at Stewart Lake, 27 September 2025, in partnership with USU Extension and Wild ASS Aerial and six participants.

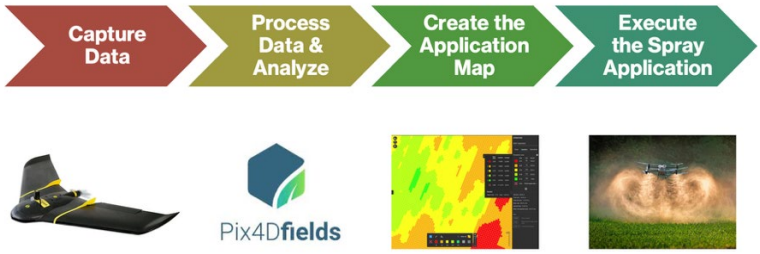

Figure 15-3. Workflow overview for precision drone spray projects.

15.3. Project Impacts

This project has enhanced public lands management by demonstrating the feasibility and effectiveness of precision spray drones for invasive species control in sensitive wetland environments. The approach reduced total herbicide volume, minimized overspray and chemical runoff, and protected non-target vegetation and aquatic habitats. Ecological monitoring confirmed improved wetland structure and greater open-water connectivity—critical for endangered fish recruitment and broader ecosystem health.

The project also facilitated hands-on outreach and training: six participants attended a field day on 27 September 2025, gaining practical experience with drone operations, precision herbicide application, and wetland monitoring techniques.

The work generated valuable data on drone nozzle performance, droplet size calibration, and variable-rate application efficacy, informing statewide protocols for aerial herbicide use in conservation areas. Collaboration among Utah State University-Eastern, USU Extension, the Utah Division of Wildlife Resources, and Wild ASS Precision Drone Company fostered applied research training, technical skill development, and integration of emerging technologies into field-based management. Collectively,

these efforts have created a scalable, cost-effective, and environmentally responsible model for wetland restoration and invasive species control across Utah's public lands.

15.4. Future Work

Building on the success of this project so far, future efforts will refine drone treatment protocols through expanded testing of nozzle configurations, herbicide formulations, and application timing to optimize efficiency and ecological outcomes. Long-term monitoring will continue to assess vegetation recovery, hydrologic function, and habitat suitability for aquatic species.

The team also plans to scale the precision drone management framework to additional wetland complexes throughout the Uinta Basin, integrating remote sensing and machine learning tools for automated vegetation classification and treatment mapping. Findings will inform best management practices and guide policy development to support the adoption of sustainable, technology-driven invasive species management methods across Utah. Continued collaboration with state and federal partners will ensure long-term ecological resilience and protection for endangered species dependent on healthy wetland ecosystems.

15.5. Acknowledgements

This project is funded by the Utah Public Lands Initiative and the Utah Department of Natural Resources.

16. Post-wildfire Vegetation and Soil Stability Monitoring Assessment

Authors: Colleen Jones and Justin Allred

16.1. Background

Wildfires cause extensive ecological disruption, including vegetation loss, soil destabilization, and water quality degradation, while imposing high economic and social costs (Bowman et al., 2017; Szpakowski and Jensen, 2019). In 2024, the U.S. Congress allocated $7 billion toward wildfire preparedness, suppression, and restoration (Riddle, 2024). Climate change and prolonged drought are projected to increase wildfire-prone days by 20–50%, highlighting the need for effective post-fire restoration strategies (Bowman et al., 2017).

Current post-fire recovery practices focus on erosion control through seeding, mulching, and channel treatments, but challenges such as poor seed establishment and invasive species introduction remain (Wohlgemuth et al., 2009). Burned Area Emergency Response (BAER) teams address immediate stabilization needs, while long-term ecological restoration occurs over subsequent years (Robichaud et al., 2009).

Remote sensing technologies, particularly multispectral imaging, offer efficient and repeatable methods to monitor post-fire vegetation recovery and soil stability (Szpakowski and Jensen, 2019). At Utah State University's Bingham Research Center, multispectral imagery has been used in a two-year project to evaluate wildfire management practices and ecosystem responses at the Snake John, Richard Mountain, and Bear Fire sites (Figure 16-1). This work serves as the basis for Justin Allred's Ph.D. dissertation (completion scheduled for spring 2026) and is expected to result in three peer-reviewed publications.

Figure 16-1. Justin Allred preparing to launch the Bingham Research Center's eBeeX fixed-wing drone with dual multispectral and RGB cameras.

16.2. Project Impacts

This research advances post-wildfire restoration science by integrating multispectral remote sensing with field-based monitoring to quantify vegetation recovery and soil stabilization over time. The findings will improve the understanding of how management interventions influence ecosystem resilience and guide best practices for state and federal land managers. The results will directly improve adaptive management strategies, enhance the efficiency of restoration investments, and support data-driven decision-making in wildfire recovery planning across the Intermountain West.

16.3. Future Work

Future efforts will expand multispectral and drone-based monitoring across additional fire sites in Utah and neighboring states to build long-term datasets on post-fire vegetation recovery and soil stability. Collaboration with federal and state land management agencies will continue to refine restoration techniques and validate remote sensing models. The project team also plans to integrate thermal and hyperspectral imaging to improve detection of invasive species and soil moisture variability, supporting scalable, technology-driven wildfire restoration practices throughout the region.

16.4. Acknowledgements

This project was funded by the Utah Watershed Restoration Initiative and the Bureau of Land Management.

17. Stochastic Population Model for *Penstemon flowersii*

Authors: Colleen Jones and Lisa Boyd

17.1. Background

Penstemon, or beardtongue, is a perennial genus nearly endemic to North and Central America, comprising roughly 280 species organized into six subgenera (Morin et al., 2015). Many species are restricted to specific habitats with narrow ecological ranges, and the center of diversity occurs in the Intermountain West—Utah alone hosts approximately 73 taxa. Numerous Penstemon species are adapted to highly specific substrates, including deep sand, limestone, oil-shale barrens, and volcanic soils, and many bloom in late spring to early summer (May–June), with flower colors ranging from red through pink and purple to blue, cream, and white (https://www.wildflower.org/plants/result.php?id_plant=PEST2).

In the Uinta Basin, four rare endemic *species occur: Goodrich's penstemon* (*Penstemon goodrichii*), *Graham's beardtongue* (*Penstemon grahamii*), *White River beardtongue* (*Penstemon scariosus var. albifluvis*), and *Flowers penstemon* (*Penstemon flowersii*). These species are limited to narrow bands of unique geologic formations, including the Duchesne, Green River, and Uinta Formations (https://www.federalregister.gov/documents/2011/02/23/2011-3675/endangered-and-threatened-wildlife-and-plants-12-month-finding-on-a-petition-to-list-astragalus).

P. flowersii was petitioned for listing under the Endangered Species Act in 2010, but the U.S. Fish and Wildlife Service determined listing was not warranted because of insufficient evidence of population decline or threats. Monitoring was conducted from 2015 to 2019 and again in 2023–2024, focusing on survival, recruitment, health, life-stage, and population abundance. The species grows on clay slopes in shadscale communities, averaging 8–25 cm in height with pink flowers blooming from May to early June. Seeds require cold stratification for germination, with an average of 19.6 seeds per capsule. Two populations were monitored on the Collier (The Nature Conservancy) and Dude Young (Bureau of Reclamation) sites.

17.2. Project Impacts

Monitoring data indicate a decline in *P. flowersii* populations, though the timeframe for maintaining a viable population remains uncertain. Major threats include oil and gas development and changing weather patterns. The development of a habitat model in ArcGIS Pro will identify critical habitat areas for focused protection. Although most populations occur on private or Tribal lands, federal permitting by the Bureau of Land Management must consider listed plants. Defining critical habitat will help document plant loss and guide avoidance during new well pad, road, and utility corridor development.

17.3. Future Work

Future work will focus on conducting a population viability analysis (PVA) using the collected monitoring data to model the long-term persistence of *P. flowersii* under current and projected threats. Critical habitat maps will be refined to guide land management and federal permitting decisions, ensuring that

development activities minimize impacts on known populations. Management strategies will be evaluated to mitigate the effects of oil, gas, and infrastructure development, while continued long-term monitoring will track trends in survival, recruitment, and overall population health. Additionally, collaboration with private and Tribal landowners will be pursued to implement avoidance measures and support targeted conservation actions across the species' range. This work is being conducted in collaboration with Dr. Loreen Allphin-Flinders and her graduate student at Brigham Young University, with the resulting analyses and findings to be prepared for peer-reviewed publication to provide formal documentation of population trends and habitat requirements, supporting conservation and protection efforts for *P. flowersii*.

17.4. Acknowledgements

This project was funded by The Nature Conservancy.

18. Verification of Atmospheric Mercury Redox Rates

Authors: Colleen Jones and Seth Lyman

18.1. Background/Goals

This four-year project investigates how mercury in the atmosphere changes form and moves through the environment. The research focuses on improving our understanding of how mercury is oxidized—transformed into species that can deposit more easily into ecosystems. The project brings together four universities to develop new tools, collect high-quality data, and improve global models that predict mercury movement and deposition (Selin et al., 2007; Lyman and Jaffe, 2012; Elgiar et al., 2025; Shah et al., 2021).

18.2. Project Accomplishments

We have completed the following tasks for the project:

- Built and tested a large (35 m^3) environmental chamber to study mercury chemical reactions under controlled conditions.
- Upgraded instruments for precise measurement of different forms of mercury.
- Began computer modeling to help interpret experimental results and guide next steps.
- Coordinated research plans across collaborating universities.
- Trained six students (four undergraduates and two PhD candidates) in experimental design, data collection, and modeling.

18.3. Dissemination

Three abstracts were submitted for presentation at the 2025 AGU Fall Meeting in New Orleans, highlighting early findings from the collaborative chamber studies.

1. Jones, C. P., & Lyman, S. N. Collaborative Chamber Study of Mercury Redox Chemistry Involving Br, O_3, NO_x, OH, and CH_4.
2. Haskins, J., Coley, J., Lyman, S. N., & Jones, C. P. Novel Mechanistic Insights from a Mercury Oxidation Chamber Experiment.
3. Harper, A., Flowerday, C., Giauque, Z., Lowe, L., & Hansen, J. Quantifying the Role of Atmospheric Oxidants (OH, O, Br) in Mercury Oxidation Using an Environmental Chamber.

18.4. Future Work

Future work includes:

- Integrate new, validated chemical data into the GEOS-Chem global model to improve mercury forecasts.
- Continue experiments and student mentoring across institutions.
- Publish results and share findings at national conferences.

18.5. Acknowledgements

This project is funded by the U.S. National Science Foundation (award #2321378).

19. References

Alvarez, R. A., Zavala-Araiza, D., Lyon, D. R., Allen, D. T., Barkley, Z. R., Brandt, A. R., Davis, K. J., Herndon, S. C., Jacob, D. J., and Karion, A.: Assessment of methane emissions from the US oil and gas supply chain, Science, 361, 186-188, 2018.

Anneken, D., Striebich, R., DeWitt, M. J., Klingshirn, C., and Corporan, E.: Development of methodologies for identification and quantification of hazardous air pollutants from turbine engine emissions, J. Air Waste Manag. Assoc., 65, 336-346, 2015.

Apfelbaum, S. I.: Cattail (Typha spp.) management, Natural Areas Journal, 9-17, 1985.

Ball, J. P.: Influence of subsequent flooding depth on cattail control by burning and mowing, Journal of Aquatic Plant Management, 28, 32-36, 1990.

Bowman, D. M., Williamson, G. J., Abatzoglou, J. T., Kolden, C. A., Cochrane, M. A., and Smith, A. M.: Human exposure and sensitivity to globally extreme wildfire events, Nature ecology & evolution, 1, 0058, 2017.

Carter, W. P.: Development of the SAPRC-07 chemical mechanism, Atmos. Environ., 44, 5324-5335, 2010.

Casagli, N., Frodella, W., Morelli, S., Tofani, V., Ciampalini, A., Intrieri, E., Raspini, F., Rossi, G., Tanteri, L., and Lu, P.: Spaceborne, UAV and ground-based remote sensing techniques for landslide mapping, monitoring and early warning, Geoenvironmental Disasters, 4, 9, 2017.

Davies, M. J., Lawson, J. R., O'Neil, T., Lyman, S. N., Zager, K., and Coxson, T. D.: Uinta Basin Snow Shadow: Impact of Snow-Depth Variation on Winter Ozone Formation, Air, 3, 22, 2025.

Dubois, D. and Prade, H.: Representation and combination of uncertainty with belief functions and possibility measures, Computational intelligence, 4, 244-264, 1988.

Edwards, P. M., Brown, S. S., Roberts, J. M., Ahmadov, R., Banta, R. M., deGouw, J. A., Dube, W. P., Field, R. A., Flynn, J. H., Gilman, J. B., Graus, M., Helmig, D., Koss, A., Langford, A. O., Lefer, B. L., Lerner, B. M., Li, R., Li, S.-M., McKeen, S. A., Murphy, S. M., Parrish, D. D., Senff, C. J., Soltis, J., Stutz, J., Sweeney, C., Thompson, C. R., Trainer, M. K., Tsai, C., Veres, P. R., Washenfelder, R. A., Warneke, C., Wild, R. J., Young, C. J., Yuan, B., and Zamora, R.: High winter ozone pollution from carbonyl photolysis in an oil and gas basin, Nature, 514, 351-354, 10.1038/nature13767, 2014.

Elgiar, T. R., Gratz, L., Hallar, A. G., Volkamer, R., and Lyman, S. N.: Underestimation of atmospheric oxidized mercury at a mountaintop site by the GEOS-Chem chemical transport model, EGUsphere, 2025, 1-23, 10.5194/egusphere-2025-977, 2025.

EPA, U.: Compendium Method TO-11A, U.S. Environmental Protection Agency, Research Triangle Park, North Carolina, 1999.

EPA, U. S.: Technical Assistance Document for Sampling and Analysis of Ozone Precursors, United States Environmental Protection Agency, Research Triangle Park, North Carolina, 1998.

Filippidou, E. and Koukouliata, A.: Ozone effects on the respiratory system, Prog Health Sci, 1, 144-155, 2011.

Fosco, D., De Molfetta, M., Renzulli, P., Notarnicola, B., Carella, C., and Fedele, G.: Innovative drone-based methodology for quantifying methane emissions from landfills, Waste Management, 195, 79-91, 2025.

Fu, L., You, S., Li, G., and Fan, Z.: Enhancing methane sensing with NDIR technology: Current trends and future prospects, Reviews in Analytical Chemistry, 42, 20230062, 2023.

Gålfalk, M., Nilsson Påledal, S. r., and Bastviken, D.: Sensitive drone mapping of methane emissions without the need for supplementary ground-based measurements, ACS Earth and Space Chemistry, 5, 2668-2676, 2021.

Goliff, W., Stockwell, W., and Lawson, C.: The regional atmospheric chemistry mechanism, version 2, Atmos. Envirion., 68, 174–185, 2013.

Grannas, A., Jones, A. E., Dibb, J., Ammann, M., Anastasio, C., Beine, H., Bergin, M., Bottenheim, J., Boxe, C., and Carver, G.: An overview of snow photochemistry: evidence, mechanisms and impacts, Atmos. Chem. Phys., 7, 4329-4373, 2007.

Haske, B., Rudolph, T., Bernsdorf, B., and Pawlik, M.: Innovative environmental monitoring methods using multispectral UAV and satellite data, First Break, 42, 41-47, 2024.

Jung, J., Lee, J., Kim, B., and Oh, S.: Seasonal variations in the NO2 artifact from chemiluminescence measurements with a molybdenum converter at a suburban site in Korea (downwind of the Asian continental outflow) during 2015–2016, Atmos. Environ., 165, 290-300, 2017.

Karion, A., Sweeney, C., Petron, G., Frost, G., Hardesty, R. M., Kofler, J., Miller, B. R., Newberger, T., Wolter, S., Banta, R., Brewer, A., Dlugokencky, E., Lang, P., Montzka, S. A., Schnell, R., Tans, P., Trainer, M., Zamora, R., and Conley, S.: Methane emissions estimate from airborne measurements over a western United States natural gas field, Geophys. Res. Lett., 40, 4393-4397, 10.1002/grl.50811, 2013.

Lawson, J. R.: Communicating risk with possibility, not probability, arXiv preprint arXiv:2410.21664, 2024.

Lawson, J. R. and Lyman, S. N.: A Preliminary Fuzzy Inference System for Predicting Atmospheric Ozone in an Intermountain Basin, Air, 2, 337-361, 2024.

Lin, J. C., Bares, R., Fasoli, B., Garcia, M., Crosman, E., and Lyman, S.: Declining methane emissions and steady, high leakage rates observed over multiple years in a western US oil/gas production basin, Sci. Rep., 11, 1-12, 2021.

Liu, M., Chen, Y., Chen, K., and Chen, Y.: Progress and hotspots of research on land-use carbon emissions: A global perspective, Sustainability, 15, 7245, 2023.

Lyman, S., jones, c., Lawson, J. R., O'Neil, T., and gardner, P.: Bingham Research Center: 2024 Annual Report, Utah State University, Vernal, Utah, 2024a.

Lyman, S., Mansfield, M. L., Tran, H., Tran, T., and Holmes, M.: 2019 Annual Report: Uinta Basin Air Quality Research, Utah State University, Vernal, Utah, 2019.

Lyman, S., Mansfield, M. L., Tran, H., Tran, T., Holmes, M., and O'Neil, T.: 2020 Annual Report: Uinta Basin Air Quality Research, Utah State University, Vernal, Utah, 2020.

Lyman, S. N. and Jaffe, D. A.: Formation and fate of oxidized mercury in the upper troposphere and lower stratosphere, Nature Geoscience, 5, 114-117, 10.1038/ngeo1353, 2012.

Lyman, S. N., Lin, C. J., and Tran, H.: Top-down Estimates of Emissions from Oil and Gas Production in the Uinta Basin: Final Project Report, Utah State University, Vernal, Utah, 2024b.

Lyman, S. N., Holmes, M., Tran, H., Tran, T., and O'Neil, T.: High ethylene and propylene in an area dominated by oil production, Atmos., *12*, 1, 2021.

Lyman, S. N., Mansfield, M. L., Tran, H. N., Evans, J. D., Jones, C., O'Neil, T., Bowers, R., Smith, A., and Keslar, C.: Emissions of organic compounds from produced water ponds I: Characteristics and speciation, Sci. Tot. Environ., 619, 896-905, 2018.

Mansfield, M. L.: Statistical analysis of winter ozone exceedances in the Uintah Basin, Utah, USA, J. Air Waste Manag. Assoc., 68, 403-414, 2018.

Mansfield, M. L. and Lyman, S. N.: Winter ozone pollution in Utah's Uinta Basin is attenuating, Atmos., *12*, 4, 2021.

Modde, T. and Irving, D. B.: Use of multiple spawning sites and seasonal movement by razorback suckers in the middle Green River, Utah, North American Journal of Fisheries Management, 18, 318-326, 1998.

Moreno, R., Baron, R., Bohm, P., Chandler, W., Cole, V., Davidson, O., Dutt, G., Haites, E., Ishitani, H., and Kruger, D.: Technologies, policies, and measures for mitigating climate change, Intergovernmental Panel on Climate Change1996.

Morin, N. R., Brouillet, L., and Levin, G. A.: Flora of North America North of Mexico, Rodriguésia, 66, 973-981, 2015.

Oltmans, S., Schnell, R., Johnson, B., Pétron, G., Mefford, T., and Neely III, R.: Anatomy of wintertime ozone associated with oil and natural gas extraction activity in Wyoming and Utah, Elem. Sci. Anth., 2, 000024, 2014.

Rahimoon, S. U. D., Yamamoto, K., Ghafar, M. A., Anwar, M. M., Majeed, M., Khattak, W. A., and Muhammad, M.: Exploration of science of remote sensing and GIS with GEE, in: Google Earth Engine and Artificial Intelligence for Earth Observation, Elsevier, 49-76, 2025.

Restek: Improve Analysis of Aldehydes and Ketones in Air Samples with Faster, More Accurate Methodology, Restek, Bellefonte, Pennsylvania, 2018.

Riaz, U., Rafi, F., Naveed, M., Mehdi, S. M., Murtaza, G., Niazi, A. G., and Mehmood, H.: Pesticide pollution in an aquatic environment, in: Freshwater Pollution and Aquatic Ecosystems, Apple Academic Press, 131-163, 2021.

Riddle, A. A.: Funding for Wildfire Management: FY2024 Appropriations for the Forest Service and the Department of the Interior, Congressional Research Service (CRS) Reports and Issue Briefs, IF 12398, 2024.

Robichaud, P. R., Lewis, S. A., Brown, R. E., and Ashmun, L. E.: Emergency post-fire rehabilitation treatment effects on burned area ecology and long-term restoration, Fire Ecology, 5, 115-128, 2009.

Saunders, S. M., Jenkin, M. E., Derwent, R., and Pilling, M.: Protocol for the development of the Master Chemical Mechanism, MCM v3 (Part A): tropospheric degradation of non-aromatic volatile organic compounds, Atmos. Chem. Phys., 3, 161-180, 2003.

Selin, N. E., Jacob, D. J., Park, R. J., Yantosca, R. M., Strode, S., Jaegle, L., and Jaffe, D.: Chemical cycling and deposition of atmospheric mercury: Global constraints from observations, J. Geophys. Res.-Atmos., 112, 14, 10.1029/2006jd007450, 2007.

Shah, V., Jacob, D. J., Thackray, C. P., Wang, X., Sunderland, E. M., Dibble, T. S., Saiz-Lopez, A., Černušák, I., Kellö, V., and Castro, P. J.: Improved mechanistic model of the atmospheric redox chemistry of mercury, Environmental Science & Technology, 55, 14445-14456, 2021.

Shimadzu: Nexera Application Data Sheet No.13: Ultrafast Analysis of Aldehydes and Ketones, Shimadzu, Tokyo, Japan, 2011.

Soares, A. R. and Silva, C.: Review of ground-level ozone impact in respiratory health deterioration for the past two decades, Atmos., 13, 434, 2022.

Solberg, K. L. and Higgins, K. F.: Effects of glyphosate herbicide on cattails, invertebrates, and waterfowl in South Dakota wetlands, Wildlife Society Bulletin (1973-2006), 21, 299-307, 1993.

Szpakowski, D. M. and Jensen, J. L.: A review of the applications of remote sensing in fire ecology, Remote sensing, 11, 2638, 2019.

Uchiyama, S., Naito, S., Matsumoto, M., Inaba, Y., and Kunugita, N.: Improved measurement of ozone and carbonyls using a dual-bed sampling cartridge containing trans-1, 2-bis (2-pyridyl) ethylene and 2, 4-dinitrophenylhydrazine-impregnated silica, Anal. Chem., 81, 6552-6557, 2009.

Data Research Center: http://oilgas.ogm.utah.gov/Data_Center/DataCenter.cfm, last access: 2023.

Varon, D. J., Jacob, D. J., Hmiel, B., Gautam, R., Lyon, D. R., Omara, M., Sulprizio, M., Shen, L., Pendergrass, D., and Nesser, H.: Continuous weekly monitoring of methane emissions from the Permian Basin by inversion of TROPOMI satellite observations, Atmos. Chem. Phys., 23, 7503-7520, 2023.

Varon, D. J., Jacob, D. J., Sulprizio, M., Estrada, L. A., Downs, W. B., Shen, L., Hancock, S. E., Nesser, H., Qu, Z., and Penn, E.: Integrated Methane Inversion (IMI 1.0): a user-friendly, cloud-based facility for

inferring high-resolution methane emissions from TROPOMI satellite observations, Geosci. Mod. Dev., 15, 5787-5805, 2022.

Vijayakumar, S., Saravanakumar, R., Arulanandam, M., and Ilakkiya, S.: Google Earth Engine: empowering developing countries with large-scale geospatial data analysis—a comprehensive review, Arabian Journal of Geosciences, 17, 139, 2024.

Wang, D. and Austin, C.: Determination of complex mixtures of volatile organic compounds in ambient air: canister methodology, Anal. Bioanal. Chem., 386, 1099-1120, 2006.

Webber, P. A.: Juvenile razorback suckers documented in wetlands in the Green River, Utah, The Southwestern Naturalist, 58, 366-368, 2013.

Wilson, D. D., Tefera, G. W., and Ray, R. L.: Application of Google Earth Engine to Monitor Greenhouse Gases: A Review, Data, 10, 8, 2025.

Wohlgemuth, P. M., Beyers, J. L., and Hubbert, K. R.: Rehabilitation strategies after fire: the California, USA experience, In: Cerdá, A.; Robichaud, PR, eds. Fire effects on soils and restoration strategies. Enfield, NH: Science Publishers. pp. 511-536, 5, 511-536, 2009.

WWA: Managing Cattails with water level control, Wisconsin Wetlands Association Wisconsin, U.S.A., 2018.

Yarwood, G., Jung, J., Whitten, G. Z., Heo, G., Mellberg, J., and Estes, M.: Updates to the Carbon Bond mechanism for version 6 (CB6), 2010 CMAS Conference, Chapel Hill, North Carolina,

Zadeh, L. A.: Fuzzy languages and their relation to human and machine intelligence, in: Fuzzy Sets, Fuzzy Logic, And Fuzzy Systems: Selected Papers by Lotfi A Zadeh, World Scientific, 148-179, 1996.

Zhou, X., Zhu, Y., Hou, D., Fu, B., Li, W., Guan, H., Sinsky, E., Kolczynski, W., Xue, X., and Luo, Y.: The development of the NCEP global ensemble forecast system version 12, Weather and Forecasting, 37, 1069-1084, 2022.